

THE FLORIDA STATE UNIVERSITY
COLLEGE OF ARTS AND SCIENCES

PDO MODIFICATION OF U.S. ENSO CLIMATE IMPACTS

By


MARK CHRISTOPHER BOVE

A Thesis submitted to the
Department of Meteorology
in partial fulfillment of the
requirements for the degree of
Master of Science

Degree Awarded:
Summer Semester, 2000

The members of the Committee approve the
thesis of Mark Christopher Bove defended on

June 27, 2000


James J. O'Brien
Professor Directing Thesis


Jon Ahlquist
Committee Member


Kwang-Yul Kim
Committee Member


Xufeng Niu
Committee Member

This thesis is dedicated to my parents and friends who always encouraged me to follow my dreams.

ACKNOWLEDGEMENTS

First, I would like to thank my committee members, Jon Ahlquist, Kwang-Yul Kim, and Xufeng Niu for taking time out of their schedule to examine my research and give constructive advice on how to proceed or improve the manuscript.

Second, I would like to thank everyone at COAPS (past and present) for their support. Individually I would like to thank Ruth Pryor, David Legler, Mark Bourassa, Shawn Smith, James Stricherz, Jiraporn Whalley, Josh Grant, and Beth McGhee for their assistance. Each of them helped make this research a reality.

Finally, I would like to thank my Major Professor, James J. O'Brien, for allowing me to undertake this exciting research. For the past five years, Dr. O'Brien has given me unique opportunities that I would never been offered anywhere else. The education and research experience I have recieved under his tutelege are one of the greatest gifts I have ever received.

The Center for Ocean-Atmospheric Prediction Studies receives its base support from the Secretary of the Navy grant to James J. O'Brien. This research was also supported by the Office of Global Programs, NOAA.

TABLE OF CONTENTS

List of Tables	vi
List of Figures	vii
Abstract	x
<u>Section</u>	<u>Page</u>
1. INTRODUCTION	1
2. DATA	4
2.a Temperature and Precipitation Data	4
2.b Sea Surface Temperature Anomaly Indices	4
3. METHODOLOGY	16
3.a ENSO and ENSO/PDO Anomaly Differences	16
3.b Statistical Significance Tests	18
3.c Probability Distribution Functions	22
4. RESULTS	24
4.a Shifts in Mean Temperature and Precipitation	24
4.b JFM Cumulative Probability Distributions	73
5. DISCUSSION	91
5.a Summary of Results	91
5.b Physical Mechanisms	95
5.c Comparison to Previous Works	96
5.d Future Applications	97
6. CONCLUSIONS	99
REFERENCES	100
o. CONCLUSIONS	99
REFERENCES	100
BIOGRAPHICAL SKETCH	104

LIST OF TABLES

<u>Table</u>	<u>Page</u>
1. Classification of ENSO years according to the JMA index	7
2. Classification of ENSO years according to the PDO Index	14
3. Combined ENSO/PDO years	15
4. ENSO seasons	17
5. Degrees of Freedom for each ENSO/PDO state, and t-scores for each confidence threshold	19
6. Example of Fisher-Irwin 2 x 2 contingency table	20

LIST OF FIGURES

<u>Figure</u>	<u>Page</u>
1. Time Series of JMA ENSO Index	6
2. Variance in Sea Surface Temperature Anomalies	10
3. Time Series of PDO SST anomalies, 1904-1992	12
4. El Niño temperature anomalies for OND	25
5. Confidence in OND El Niño temperature anomalies	27
6. El Niño precipitation anomalies for OND	28
7. Confidence in OND El Niño precipitation anomalies	30
8. El Niño temperature anomalies for JFM	31
9. Confidence in JFM El Niño temperature anomalies	33
10. El Niño precipitation anomalies for JFM	35
11. Confidence in JFM El Niño precipitation anomalies	36
12. El Niño temperature anomalies for AMJ	38
13. Confidence in AMJ El Niño temperature anomalies	40
14. El Niño precipitation anomalies for AMJ	41
15. Confidence in AMJ El Niño precipitation anomalies	43
16. El Niño temperature anomalies for JAS	44
15. Confidence in AMJ El Niño precipitation anomalies	43
16. El Niño temperature anomalies for JAS	44
17. Confidence in JAS El Niño temperature anomalies	46

18. El Niño precipitation anomalies for JAS	47
19. Confidence in JAS El Niño precipitation anomalies	49
20. La Niña temperature anomalies for OND	51
21. Confidence in OND La Niña temperature anomalies	52
22. La Niña precipitation anomalies for OND	54
23. Confidence in OND La Niña precipitation anomalies.....	55
24. La Niña temperature anomalies for JFM	56
25. Confidence in JFM La Niña temperature anomalies	58
26. La Niña precipitation anomalies for JFM	60
27. Confidence in JFM La Niña precipitation anomalies	61
28. La Niña temperature anomalies for AMJ	63
29. Confidence in AMJ La Niña temperature anomalies	65
30. La Niña precipitation anomalies for AMJ	66
31. Confidence in AMJ La Niña precipitation anomalies	68
32. La Niña temperature anomalies for JAS	69
33. Confidence in JAS La Niña temperature anomalies	71
34. La Niña precipitation anomalies for JAS	72
35. Confidence in JAS La Niña precipitation anomalies.....	74
36. Inverse cumulative probability distributions of JFM seasonal temperatures in Fort Myers, Florida	76
37. Inverse cumulative probability distributions of JFM seasonal temperatures in Fernandina Beach, Florida	76
37. Inverse cumulative probability distributions of JFM seasonal temperatures in Fernandina Beach, Florida	76

38. Inverse cumulative probability distributions of JFM seasonal temperatures in Cuyamaca, California	78
39. Inverse cumulative probability distributions of JFM seasonal temperatures in Provincetown, Massachusetts	78
40. Inverse cumulative probability distributions of JFM seasonal temperatures in Modena, Utah	79
41. Inverse cumulative probability distributions of JFM monthly precipitation in Eastman, Georgia	81
42. Inverse cumulative probability distributions of JFM monthly precipitation in Findlay, Ohio	81
43. Inverse cumulative probability distributions of JFM monthly precipitation in Purdum, Nebraska	82
44. Inverse cumulative probability distributions of JFM seasonal temperatures in Corning, Arkansas	84
45. Inverse cumulative probability distributions of JFM seasonal temperatures in Park Rapids, Minnesota	84
46. Inverse cumulative probability distributions of JFM seasonal temperatures in Pomeroy, Washington	86
47. Inverse cumulative probability distributions of JFM seasonal temperatures in Acadia National Park, Maine	86
48. Inverse cumulative probability distributions of JFM monthly precipitation in West Point, Georgia	88
49. Inverse cumulative probability distributions of JFM monthly precipitation in Warren, Ohio	88
50. Inverse cumulative probability distributions of JFM monthly precipitation in Oakdale, Nebraska	90q

ABSTRACT

North American seasonal surface temperature and precipitation anomalies associated with the like extreme phases in the El Niño-Southern Oscillation (ENSO) can vary greatly in each occurrence. The Pacific Decadal Oscillation (PDO) is considered as a potential source of the ENSO anomaly variability.

Eighty-nine years of monthly surface temperature and precipitation data are categorized as occurring during one of three ENSO phases (El Niño, neutral, La Niña) and one of three PDO states (positive, neutral, negative). Each ENSO/PDO bin is differenced from all ENSO-neutral years to highlight changes in anomaly patterns. These results are compared to anomalies seen when only investigating ENSO U.S. anomaly patterns. The anomaly patterns are then tested for statistical significance. In regions where large and significant changes are identified, cumulative probability distribution functions are created using a resampling technique to determine the underlying distribution of the data.

Key results indicate that positive PDO generally enhances expected ENSO anomaly patterns, while negative PDO interferes with the expected ENSO patterns, making anomaly patterns weaker and more incoherent. Neutral PDO, depending on the strength of the ENSO phase, can exhibit characteristics of both positive and negative PDO. These results indicate that seasonal climate forecasts based on ENSO climate anomalies can be improved by examining the current condition of the PDO.

1. INTRODUCTION

United States climate anomalies associated with extremes in the El Niño – Southern Oscillation (ENSO) are now widely accepted (Glantz 1996). Studies of ENSO extremes (i.e., El Niño, La Niña) show that eastern and central equatorial Pacific sea surface temperature (SST) anomalies influence Northern Hemisphere longwave patterns via atmospheric teleconnections (Horel and Wallace 1981). These pattern shifts create spatially coherent regions of temperature and precipitation anomalies across the United States (Sittel 1994; Gershunov 1998; Smith et al. 1998). One product from these studies are El Niño and La Niña extrema climatologies, showing the expected temperature and precipitation anomalies from an “average” ENSO event. However, individual events are hardly average, with observed anomalies varying greatly in both intensity and spatial coverage (Smith et al. 1999).

Research has shown that fluctuations of North Pacific oceanic conditions have an influence on North American Climate as well (e.g., Namias 1976). Early studies indicated that the North Pacific ocean-atmosphere system fluctuates on a scale of two to six years in response to the ENSO cycle (e.g., Bjerknes 1969; Horel and Wallace 1981; Rasmusson and Wallace 1983). More recently, the North Pacific system has been found to fluctuate on an interdecadal basis as well (e.g., Trenberth and Hurrell 1994; Nakamura et al. 1997; Zhang et al. 1997; Mantua et al. 1997; Minobe and Mantua 1999). This interdecadal fluctuation in the North Pacific has been dubbed the Pacific Decadal Oscillation (PDO) (Mantua et al. 1997). Similar to ENSO classifications, SST anomalies associated with PDO extremes have been labeled as either

positive (warm, high phase) or negative (cold, low phase) (Gershunov and Barnett 1998; Mantua 2000; JPL 2000). These SST anomalies, unlike those associated with ENSO, can persist for 20 to 30 years (Mantua 2000). Shifts in PDO regimes, like the shift from negative PDO to positive PDO in 1976, can occur rapidly and dramatically, bringing large regional climatic changes (Nakamura et al. 1997, Minobe 1997, Zhang et al. 1997). Among the climate changes witnessed after the 1976 regime shift are an intensified Aleutian low (Nakamura 1996), more cold air outbreaks in the eastern United States (Dowton and Miller 1993), and less winter precipitation in the Pacific Northwest (Chen et al. 1996). The regime shift also altered epipelagic ecosystems in the Pacific Northwest, impacting salmon catches in the region (Mantua et al. 1997). In early 2000, NASA identified a potential regime shift that would bring negative PDO conditions to the North Pacific for the first time since 1976 (Hall 2000).

Both the ENSO and PDO cycles have been shown to influence United States climate; it is likely that the climate patterns created by these two phenomena interact. Thus, it is hypothesized that different PDO states alter the temperature and precipitation anomaly patterns associated with ENSO extremes. The intent of this paper is to investigate the validity of this hypothesis.

This hypothesis deals only with the interaction of ENSO and PDO U.S. climate impacts and not the influence that ENSO and PDO SST anomalies have upon each other. The two phenomena do appear to be related. For example, the PDO has a response to ENSO extremes, with a correlation between 0.3 and 0.4 (Mantua et al. 1997). Many theories have also been offered regarding the relationship between the Northern and Tropical Pacific (e.g., Enfield and Allen 1980; Barnett et al. 1999; Schneider 1999; etc.). However, there is no consensus on the physics, causality, or Northern and Tropical Pacific (e.g., Enfield and Allen 1980; Barnett et al. 1999; Schneider 1999; etc.). However, there is no consensus on the physics, causality, or media connecting the two regions. Since the goal of this paper is to refine the abil-

ity to forecast seasonal climate anomalies over the United States, it will not debate the connections between ENSO and the PDO. Here, ENSO and PDO indices are considered independently, with the goal being to increase the predictability of the desired climate parameters.

Previous works investigating joint United States ENSO/PDO climate impacts have dealt primarily with changes in sea level pressure (SLP). Gershunov and Barnett (1998) found that during El Niño - positive PDO and La Niña - negative PDO conditions, the corresponding SLP ENSO pattern is intensified and more stable, while opposite PDO conditions are destructive to the ENSO SLP pattern. The authors note in a more recent paper that other variables, such as temperature and precipitation, are modulated as well (Gershunov et al. 1999). Higgins (2000) shows improved forecasting skill for United States temperature and precipitation when the data are regressed onto both the ENSO and PDO indices as compared to regression using only the ENSO index. The only work directly investigating precipitation changes (Dettinger et al. 1998) showed a north-south modulation of precipitation at both interannual and decadal time scales over the western United States, but it did not identify either ENSO or the PDO as a mechanism for these changes.

While other works on ENSO/PDO impacts have dealt with temperature and precipitation, no previous work has attempted to quantify the temperature and precipitation changes caused by the climate interactions of ENSO and the PDO using available data. This study will implement conditional probability analysis to determine the joint impact of ENSO/PDO extremes on United States temperature and precipitation anomalies. Key results indicate that positive PDO enhances both El Niño and La Niña, while negative PDO weakens ENSO climate anomalies.

El Niño and La Niña, while negative PDO weakens ENSO climate anomalies.

2. DATA

a. Temperature and Precipitation Data

United States temperature and precipitation data from 1903-1994 were obtained from the United States Historical Climatology Network (USHCN). The USHCN consists of 1221 observing stations, recording monthly values of maximum temperature, minimum temperature, mean temperature, and precipitation. The USHCN data have been adjusted to remove biases due to station moves, instrument changes, and urbanization effects (CDIAC 1999).

For this study, only monthly mean temperature and precipitation are used. Each station is tested for missing data values during the period of interest. Any stations with incomplete data were omitted from study. Eight hundred twenty-two stations had complete mean temperature records for the period in question, but only 190 stations had complete precipitation records.

b. Sea Surface Temperature Anomaly Indices

Sea surface temperature anomalies are used to specify extreme phases in the ENSO and the PDO cycles.

1) ENSO

1) ENSO

Classifications of extreme phases in the ENSO cycle are based on the definition

of an El Niño event as developed by the Japan Meteorological Agency (JMA Atlas 1991). This definition is preferred over the Southern Oscillation Index, which is relatively noisy (Green 1996). From 1949 onward, the JMA index is based on observed data. For earlier years, the index is based on reconstructed monthly mean SST fields (Meyers et al. 1998). The JMA index is considered suitable for quantitative studies of ENSO (Trenberth 1997).

The JMA Index defines El Niño phases based on the sea surface temperature anomalies in the region from 4°N to 4°S and from 150° to 90°W. An El Niño event is identified when the five-month running average of SST anomalies in the JMA region are greater than 0.5° C for at least six consecutive months, beginning before September and including the months of October, November, and December (Bove 1998).

We also examine the opposite extreme of the ENSO cycle, which is known as La Niña. The SST anomaly criteria for La Niña are chosen to be symmetric to that of El Niño. Thus, La Niña occurs when anomalies in the JMA region are less than -0.5°C for six consecutive months, starting before September and running through December. Years that do not meet the definition for either El Niño or La Niña are considered neutral. The time series of the JMA ENSO index is shown in Figure 1.

Extremes in the ENSO cycle typically develop during summer, peak in late fall, and decay by the following spring. Therefore we choose to define an ENSO year as running from the October of the year in which the ENSO event develops to the September of the following year. This format is selected so the effects of the ENSO event can be seen from its maturity in the fall through its dissipation the following summer. Using this format, ENSO years 1902 (October 1902 to September 1903) and 1994 (October 1994 to September 1995) are incomplete and are omitted from summer. Using this format, ENSO years 1902 (October 1902 to September 1903) and 1994 (October 1994 to September 1995) are incomplete and are omitted from this study. The classification of each ENSO year is shown in Table 1.

JMA SST Anomalies, 5 month filter

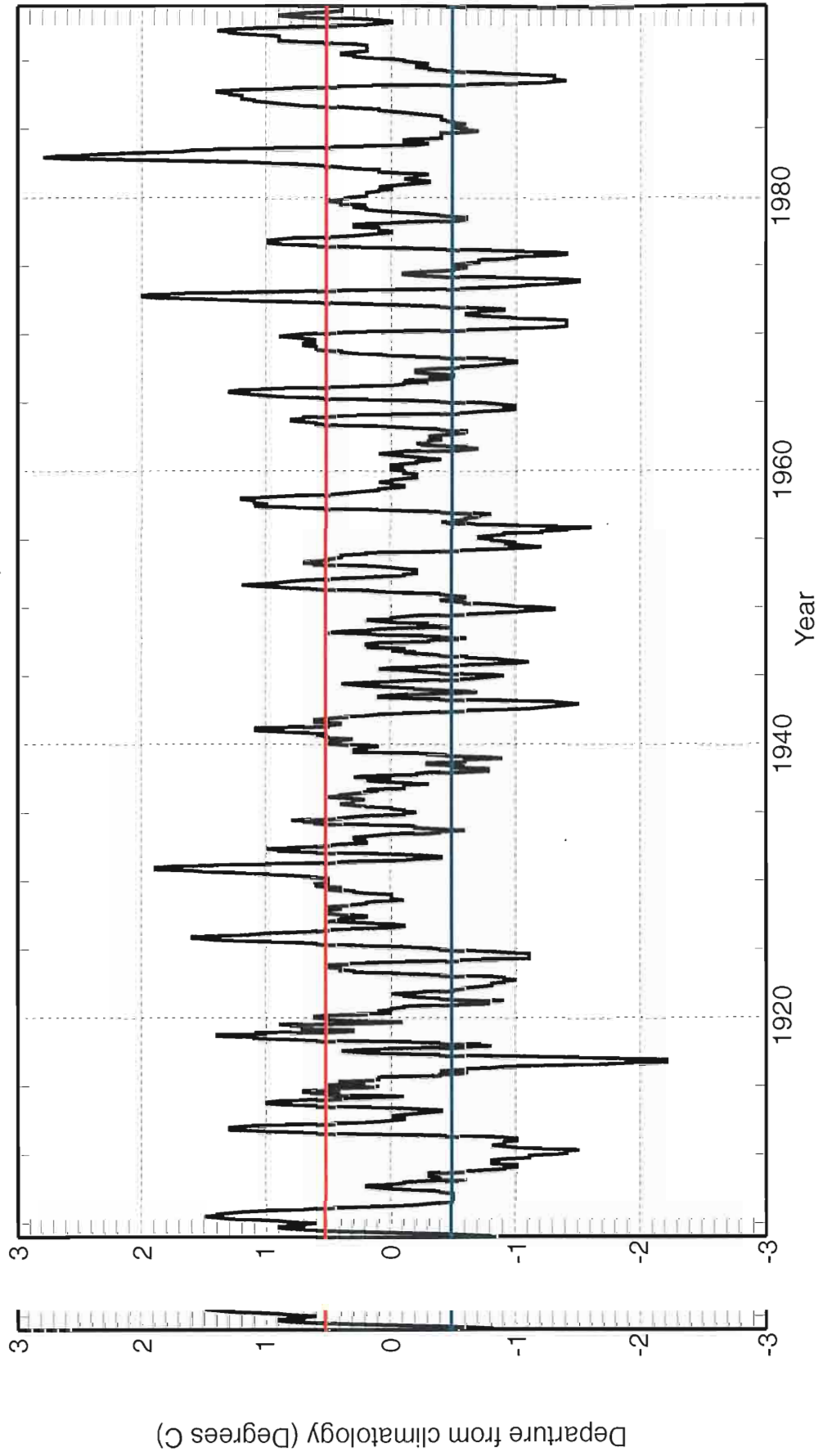


Figure 1. Time Series of JMA ENSO Index. Red and blue lines show threshold temperatures for an El Niño (La Niña) event.

Table 1. Classification of ENSO years according to the JMA index.

El Niño	1904,1905,1911,1913,1918,1925,1929,1930,1940,1951,1957,1963,1965,1969,1972,1976,1982,1986,1987,1991
Neutral	1907,1912,1914,1915,1917,1919,1920,1921,1923,1926,1927,1928,1931,1932,1933,1934,1935,1936,1937,1939,1941,1943,1945,1946,1947,1948,1950,1952,1953,1958,1959,1960,1961,1962,1966,1968,1974,1977,1978,1979,1980,1981,1983,1984,1985,1989,1990,1992
La Niña	1906,1908,1909,1910,1916,1922,1924,1938,1942,1944,1949,1954,1955,1956,1964,1967,1970,1971,1973,1975,1988

2) PDO

Sea surface temperature data for the North Pacific Ocean (north of 20° north latitude) are obtained from Version 2.2 of the Global Sea Ice and Sea Surface Temperature data set (GISST2.2) provided by the Hadley Centre for Climate Prediction and Research (Rayner et al. 1996). The data consist of monthly averaged SST values in one-degree by one-degree bins for the period 1903-1994.

The data contained in the GISST data set can be divided into three eras where different data sources or methodologies in creating the complete data record were used. The data from 1903 to 1948 are obtained from the Meteorological Office Historical SST data set (MOHSST) and are corrected for observational bias. Then an Empirical Orthogonal Function (EOF) analysis is used to interpolate the data and fill missing gaps. For 1949 to 1981, the SSTs are also from the MOHSST, which includes data in this period from the Comprehensive Ocean-Atmosphere Data Set (COADS); however, interpolation is used to fill in any missing data gaps. Finally, bias corrected satellite data are used in the modern period (Rayner et al. 1996).

If the available data are sparse, the different methods used in compiling the data set between the 1903-1948 and 1949-1981 segments can create a discontinuity in the data. Within these data-sparse regions, data prior to 1949 can average about 0.5°C colder than when data are plentiful (Rayner et al. 1996). The North Pacific is a heavily traveled region, and data are plentiful for the time period under investigation (Parker 1995).

(i) Region Selection. An SST anomaly index for North Pacific, similar to the ENSO JMA index (Section 2.b.1), is needed to identify phases in the North Pacific Oscillation. The first step in creating this index is to remove the monthly climatological means from North Pacific SST data. This is accomplished by averaging the

monthly sea surface temperatures in each one-degree bin to create an annual cycle of monthly SSTs. Subtracting individual monthly SST climatology values from the data set creates SST anomaly data. A bin is omitted if it is entirely covered by land or has spatial sea ice coverage of over 95%. This results in 3,943 SST anomaly bins, each with a time series containing 1,104 months of data.

The annual variance in SST anomalies in each bin is calculated to identify regions where SST anomalies have the widest range of fluctuation. Figure 2 indicates that the largest variance in SST anomalies occur in the Kuroshio extension region of the North Pacific, with the largest maximum east of Japan. Other local maximums in variance are seen east of the Kuroshio extension and along Baja California.

Empirical Orthogonal Functions (EOFs) are used to confirm which regions identified above show the greatest coherent variance in SST anomalies. EOFs provide a series of ranked eigenvectors, each of which contains a percentage of the temporal variability of the data (Legler 1983). The eigenvectors with the largest percentage values can usually be associated with physical processes (Servain and Legler 1986).

The first two EOF modes contain 21.% and 18.8%, respectively, of the variance in the North Pacific. (For simplicity, these EOFs are not area weighted. See Buell (1971) regarding area weighting.) Because the variances explained by EOF 1 and 2 are so similar, these modes must be considered together (North et al. 1982). Nonetheless, these EOFs confirm that the variance maximum in the western North Pacific is correlated with the maximum in the central North Pacific. Therefore, we choose an indicator region that encompasses variance maximum confirmed by EOF analysis. The geographic boundaires selected for this region are 34° to 46° north latitude and 144° to 210° east longitude (Figure 2).
analysis. The geographic boundaires selected for this region are 34° to 46° north latitude and 144° to 210° east longitude (Figure 2).

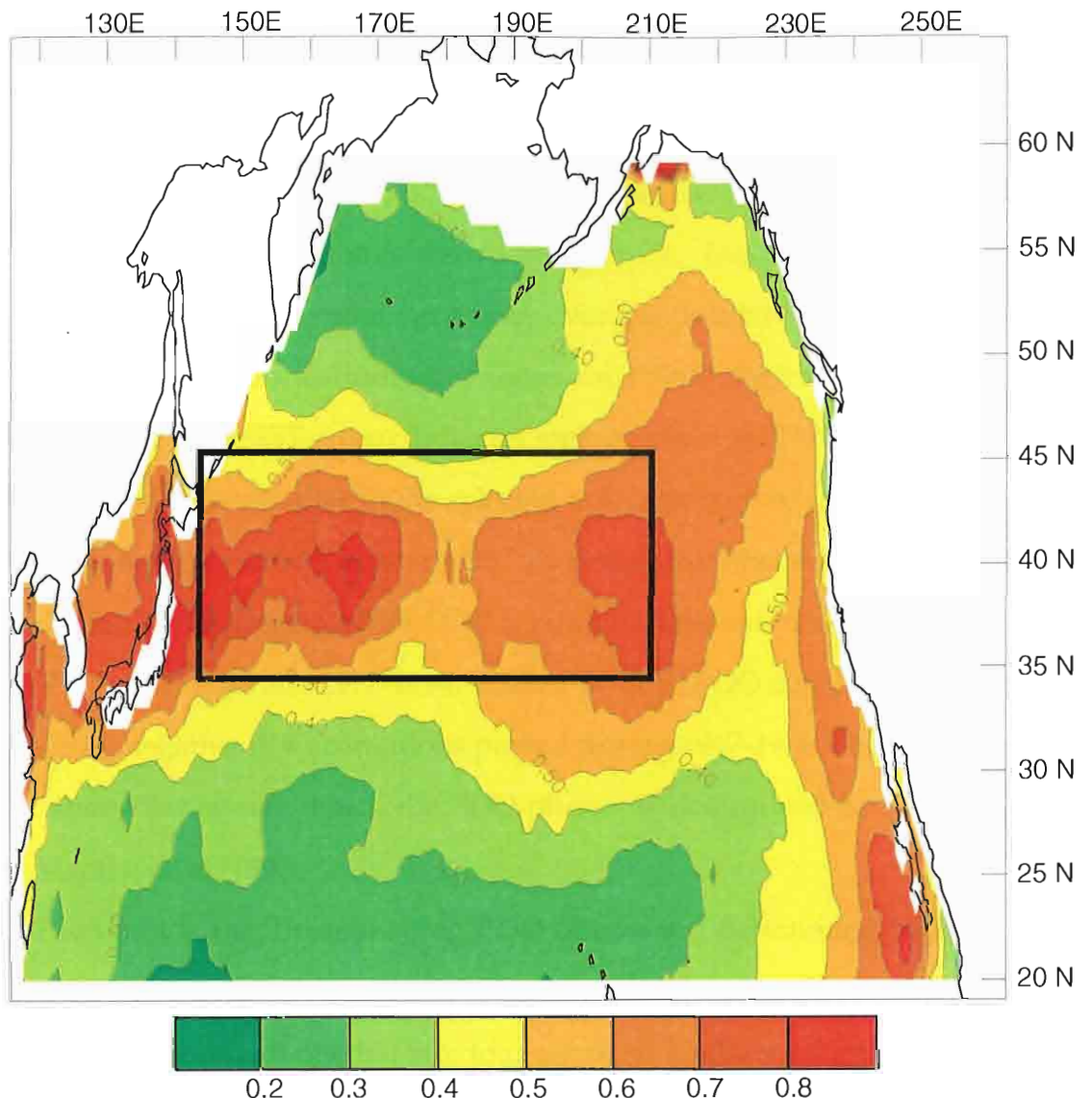


Figure 2. Annual variance of sea surface temperature anomalies in the North Pacific Ocean. PDO indicator region (black rectangle) located from 34-46 North and 144-210 East.

(ii) **PDO Event Thresholds.** The monthly anomalies within the indicator region are averaged to create a monthly anomaly time series for the entire region. A two-year centered running average is applied to the data to remove high frequency variability within the time series. The time series (1080 months) of the smoothed SST anomalies in this region is shown in Figure 3. The anomalies exhibit large interdecadal and intradecadal variability over the past 90 years. For consistency with other PDO publications that focus on ENSO regions, whose SSTs are anticorrelated to the SSTs in our indicator region,, positive PDO conditions are represented by cold anomalies in the selected indicator region, while negative PDO anomalies are associated with warm SST anomalies (Mantua et al. 1997, Gershunov and Barnett 1998). Thus, positive PDO conditions dominate the time series during 1904-1915, 1925-1946 and 1977-1994. Weaker positive PDO conditions persist from 1916-1924. negative PDO conditions prevail during 1947-1976. These periods and their anomalies closely match the PDO phases as determined by Minobe (1997) and Mantua et. al (1997).

The bounds for distinguishing PDO phases are determined based on SST anomaly quartiles. The indicator region's 1080 SST anomaly values are ranked from coldest to warmest and divided into four quarters. Ranking the data gives a lower quartile of -0.29°C , an upper quartile of 0.22°C , and a median of -0.05°C . Expectedly, the median is not equal to the mean since the 88 years of study are dominated by positive PDO. However, given a sufficient time period, the median anomaly is expected to approach zero. Applying this quartile spread to an assumed long-term median of zero and a symmetric distribution results in bounds equal to $\pm 0.25^{\circ}\text{C}$.

These limits become our thresholds for identifying extremes in the PDO. Any anomalies that are colder than (warmer than) -0.25°C (0.25°C) are considered to be

These limits become our thresholds for identifying extremes in the PDO. Any anomalies that are colder than (warmer than) -0.25°C (0.25°C) are considered to be positive (negative) PDO conditions. Thus, anomaly values contained in the coldest

PDO SST Anomalies, 2 year filter

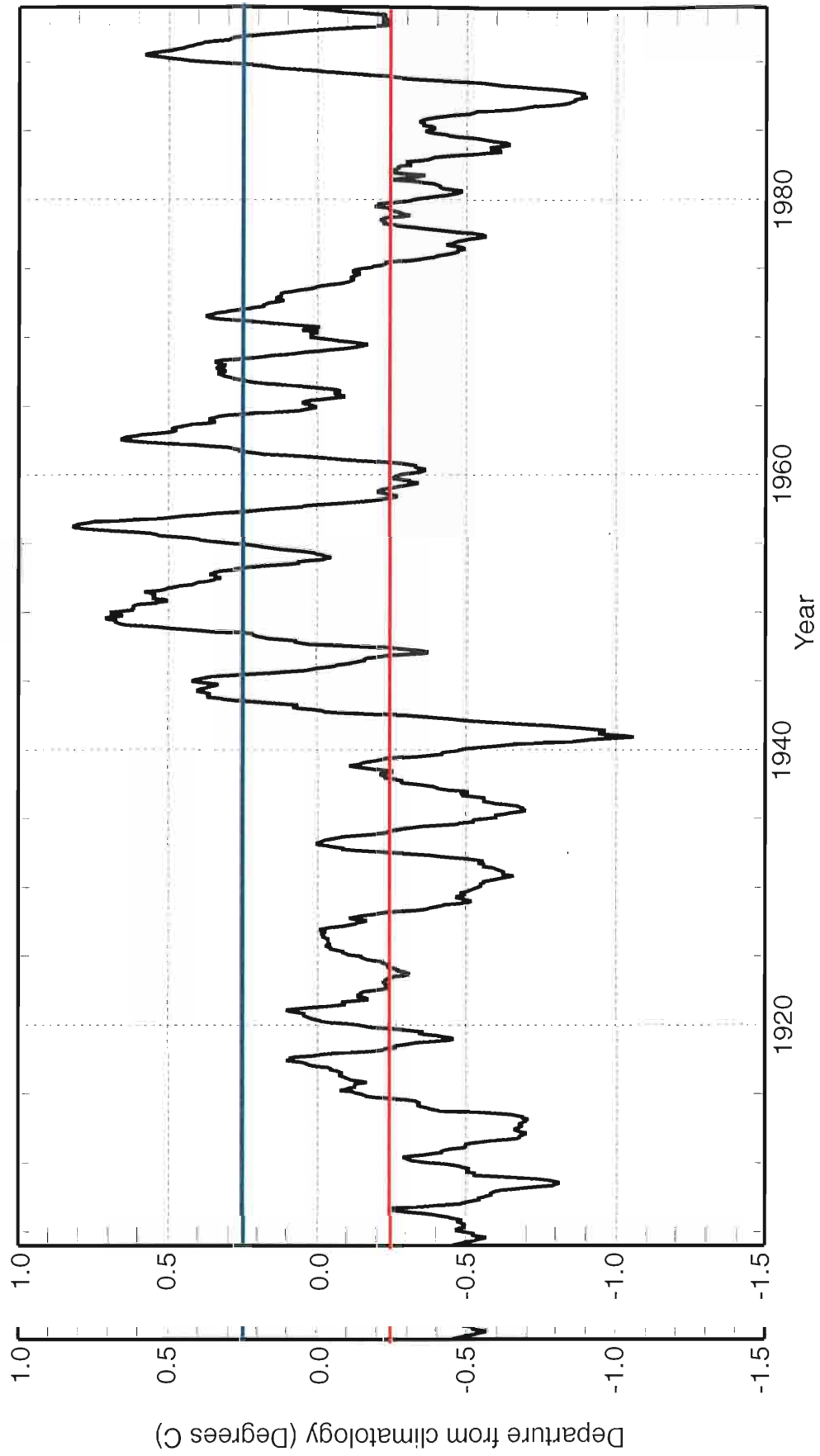


Figure 3. Time Series of PDO SST anomalies, 1904-1992. Blue and red lines indicate threshold levels for negative and positive PDO, respectively.

25% of the data are identified as positive PDO, while anomaly values contained in the warmest 25% are identified as negative PDO. The anomaly values contained in the middle two quarters are identified as neutral PDO.

We are studying impacts of PDO interaction with ENSO; therefore, we choose to investigate PDO anomalies that occur simultaneously with an ENSO extreme phase and persist during the majority of that event. A positive (negative) PDO phase is identified when the filtered SST anomaly data within the indicator region is less than (greater than) -0.25°C (0.25°C) during the period of October - March. If this criterion is not met, the PDO is considered neutral. For consistency with ENSO years, PDO phases will also run from October to September of the following year. The PDO classification of each ENSO year is listed in Table 3. During ENSO years 1904-1992, there were 19 negative PDO years, 26 neutral PDO years, and 44 positive PDO years.

This methodology to determine extremes in the PDO cycle has both similarities to and differences with the accepted PDO definition created by Mantua et. al (1996). Both methodologies identify the PDO using the first mode EOF of the Pacific Ocean north of 20°N latitude. The data used in the calculations, however, are of different resolution. Mantua et al. (1997) used from five-degree by 5-degree bins from the COADS data; this analysis uses one-degree by one-degree bins. Mantua et al. (1997) uses the entire North Pacific basin as PDO indicator region, while here we choose to use the region seeing the largest variance in SST values as our indicator region. Finally, most published papers identify the PDO as possessing only two phases, positive and negative (e.g., Mantua et. al 1996; Gershunov and Barnett 1998). Here, we assign three phases to the PDO, positive, negative, and neutral, to account for times when our indicator region is near climatology. we assign three phases to the PDO, positive, negative, and neutral, to account for times when our indicator region is near climatology.

Table 2. Classification of ENSO years according to the PDO index.

Positive PDO	1904,1905,1906,1907,1908,1909,1910,1911,1912,1913,1918,1922,1923,1928,1929,1930,1931,1933,1934,1935,1936,1937,1939,1940,1941,1945,1946,1958,1959,1975,1976,1977,1978,1979,1980,1981,1982,1983,1984,1985,1986,1987,1988,1992
Neutral PDO	1914,1915,1916,1917,1919,1920,1921,1924,1925,1926,1927,1932,1938,1942,1947,1953,1957,1960,1964,1965,1968,1969,1970,1972,1973,1974
Negative PDO	1943,1944,1948,1949,1950,1951,1952,1954,1955,1956,1961,1962,1963,1966,1967,1971,1989,1990,1991

3) COMBINED ENSO AND PDO INDICES

The application of a two-year low-pass filter on the North Pacific SST data reduces the period of study to calendar years 1904-1993. This smoothing makes ENSO years 1903 and 1993 incomplete, so they are removed from study. During the remaining 89 ENSO years, there have been 20 El Niño years, 21 La Niña years, and 48 years of neutral ENSO conditions.

ENSO and the PDO each have three oceanic states for their respective regions: warm, cold, and neutral for ENSO and positive, neutral, and negative for the PDO. Combining these conditions results in nine oceanic states for the equatorial and north central Pacific Ocean. Each year in the study period is binned accordingly (Table 4). In the text, each ENSO/PDO oceanic state will be abbreviated. Each oceanic state's abbreviation will consist of its ENSO condition (El Niño, Neutral, La Niña), and a symbol that represents its PDO condition (+ for Positive, 0 for Neutral, - for negative).

Table 3. Combined ENSO/PDO years.

ENSO State	PDO State	Years of Occurrence
El Niño	Positive	1904,1905,1911,1913,1918,1929,1930,1940,1976,1982,1986,1987
	Neutral	1925,1957,1965,1969,1972
	Negative	1951,1963,1991
Neutral	Positive	1907,1912,1923,1928,1931,1933,1934,1935,1936,1937,1939,1941,1945,1946,1958,1959,1977,1978,1979,1980,1981,1983,1984,1985,1992
	Neutral	1914,1915,1917,1919,1920,1921,1926,1927,1932,1947,1953,1960,1968,1974
	Negative	1943,1948,1950,1952,1961,1962,1966,1989,1990
La Niña	Positive	1906,1908,1909,1910,1922,1975,1988
	Neutral	1916,1924,1938,1942,1964,1970,1973
	Negative	1944,1949,1954,1955,1956,1967,1971

3. METHODOLOGY

The influence of the PDO on ENSO temperature and precipitation anomalies is examined for each ENSO/PDO subset. Each subset is then compared to its respective ENSO-only (anomalies averaged over all PDO phases) patterns. These changes are then tested for statistical significance. Finally, the temperature and precipitation probability distribution functions of each ENSO/PDO subset are examined in regions where changes have been identified.

a. ENSO and ENSO-PDO Anomaly Differences

Mean monthly temperature and precipitation data are categorized as occurring during one of three ENSO states and binned accordingly. Within each ENSO category, every month is individually averaged. These monthly averages are then used to determine seasonal (three month) means. The result is 10 three-month ENSO seasons, starting with October-November-December (OND) and running through July-August-September (JAS) (Table 5). This partitioning allows seasonal changes in temperature and precipitation patterns to be highlighted and also removes high frequency noise from the data.

Patterns of seasonal anomalies associated with ENSO extreme events over the contiguous United States are obtained by subtracting El Niño (La Niña) seasonal means from the Neutral ENSO seasonal mean at every station and plotting the differences on a map. Animations of the anomalies are created from these ten ENSO means from the Neutral ENSO seasonal mean at every station and plotting the differences on a map. Animations of the anomalies are created from these ten ENSO seasonal anomaly maps. These animations allow us to examine the temporal evo-

Table 4. ENSO Seasons.

OND	October - November - December
NDJ	November - December - January
DJF	December - January - February
JFM	January - February - March
FMA	February - March - April
MAM	March - April - May
AMJ	April - May - June
MJJ	May - June - July
JJA	June - July - August
JAS	July - August - September

lution of the magnitude and coverage of the anomalies.

ENSO/PDO temperature and precipitation anomalies are calculated in the same manner as the ENSO-only anomalies. Mean monthly temperature and precipitation data are categorized as occurring during one of the nine ENSO/PDO states and binned accordingly. Within each ENSO/PDO category, every month is individually averaged. These monthly averages are then used to determine seasonal means, created by averaging mean monthly temperature and precipitation over a three-month period for all ten ENSO seasons.

Accurate comparison of ENSO/PDO anomaly patterns to ENSO-only anomaly patterns requires a common standard from which anomalies are determined. Thus, the neutral ENSO-only seasonal mean is used in determining anomalies for the ENSO/PDO cases. The data in each ENSO/PDO state are actually subsets of their respective ENSO extremes. For example, El Niño(+) is a subset of the entire El Niño data set. Thus, by comparing the temperature and precipitation anomalies of a given subset to the corresponding ENSO data set, locations where the PDO has a visually apparent impact are identified.

apparent impact are identified.

b. Statistical Significance Tests

1) Temperature

The distribution of seasonal temperature is assumed to be approximately normal (Smith 1998). To account for the small samples available in this study, the Student's t-distribution is used to determine the statistical significance between the ENSO neutral mean and the other cases (Spiegel 1961).

Comparing the differences between two means using the Students t-test requires two independent samples of sizes N_1 and N_2 , which possess means and standard deviations given by X_1 and X_2 and s_1 and s_2 , respectively. Our null hypothesis, H_0 , is that the two samples are statistically indistinguishable from each other. To test H_0 , we use the t-score given by

$$t = \frac{(X_1 - X_2)}{\left(\sigma \sqrt{\left(\frac{1}{N_1}\right) + \left(\frac{1}{N_2}\right)} \right)} \quad (1)$$

where σ is given by

$$\sigma = \sqrt{\frac{N_1 s_1^2 + N_2 s_2^2}{v}} \quad (2)$$

where v is $(N_1 + N_2 - 2)$ degrees of freedom (Spiegel 1961). The null hypothesis is rejected if the two-tailed t-score exceeds the 90% confidence interval. If the null hypothesis is rejected, the t-score is then examined to see if it exceeds the two-tailed 95%, 97.5%, 99%, and 99.5% confidence levels, to flesh out confidence animations. The t-score threshold for each confidence level is given in Table 6. These t-tests are 95%, 97.5%, 99%, and 99.5% confidence levels, to flesh out confidence animations. The t-score threshold for each confidence level is given in Table 6. These t-tests are performed for each case in all ten ENSO seasons. Animations are available of the t-

Table 5. Degrees of Freedom for each ENSO-PDO state, and t-scores for each confidence threshold.

Pacific State	DoF	90%	95%	97.5%	99%	99.5%
El Niño	65	1.30	1.67	2.00	2.39	2.66
El Niño(+)	58	1.30	1.67	2.00	2.39	2.66
El Niño(0)	51	1.30	1.68	2.01	2.40	2.66
El Niño(-)	49	1.30	1.68	2.01	2.40	2.66
La Niña	67	1.30	1.67	2.01	2.39	2.66
La Niña(+)	53	1.30	1.67	2.01	2.39	2.66
La Niña(0)	53	1.30	1.67	2.01	2.39	2.66
La Niña(-)	53	1.30	1.67	2.01	2.39	2.66

score confidence to show the evolution and decay of regions showing statistically significant shifts in mean temperature.

2) Precipitation

Distribution of seasonal precipitation can resemble many types of distributions, including normal, log-normal, Weibull, and gamma (Sittel 1994, Smith 1999). Due to the wide possibility of precipitation distributions, we opt to utilize a non-parametric test that does not assume an underlying distribution in the data. Thus, the Fisher-Irwin exact test is implemented to determine the significance of shifts between the neutral ENSO seasonal precipitation median and the ENSO/PDO seasonal precipitation medians. The Fisher-Irwin test is an evaluation of the conditional probabilities of values in a 2 x 2 contingency table, given that the marginal

totals (details below) of the table are fixed (Bhattacharyya and Johnson 1977). In this case, we compare two samples, Y (neutral phase sample) and Z (extreme phase sample). If the medians of Y and Z are statistically indistinguishable, both Y and Z can be regarded as random samples from a single population. Using this assumption, we can combine both samples to create a population YZ.

The individual seasonal precipitation values in YZ are ranked to determine the median. Next, the number of individual seasonal precipitation values in Y and Z that are less than (greater than or equal to) the YZ median are tabulated. The total number of individual events in each sample that are less than YZ median are denoted by Y_l and Z_l , while the totals greater than or equal to the YZ median are denoted by Y_r and Z_r . These values become our 2 x 2 contingency table, and summing the columns and rows create the marginal totals (Table 7). The total number

Table 6. Example of Fisher-Irwin 2 x 2 Contingency Table.

	Number of seasons < YZ Median	Number of seasons >= YZ Median	Total
ENSO-PDO Precipitation	Z_l	Z_r	Z
Neutral ENSO Precipitation	Y_l	Y_r	Y
Total	YZ_l	YZ_r	YZ

of individual precipitation events less than the YZ median is represented by YZ_l , while the total number of events equal or greater than the YZ median is given by YZ_r .

Our null hypothesis is that the seasonal precipitation medians of Y and Z are statistically indistinguishable. If the null hypothesis is correct, Y_l , Y_r , Z_l , and Z_r are the result of a random distribution of the individual seasonal precipitation amounts (Bhattacharyya and Johnson 1977). To test this null hypothesis, a one-tailed test is constructed by determining the conditional probability the observed values of the contingency table, as well as the conditional probability of all cases that are more extreme (wetter or drier) than the observed values. The conditional probability of the observed values, via the rule of combinations, is given by

$$P_c = \frac{\binom{YZ_l}{Y_l} \binom{YZ_r}{Y_r}}{\binom{YZ}{Y}} \quad (3)$$

We finish the one-tailed test by creating table configurations that are drier (wetter). A drier (wetter) configuration would have more ENSO-PDO individual seasonal precipitation totals less than (greater than or equal to) the YZ median. For example, to calculate the condition probability of drier cases, the value Z_l is first increased by one event. Since marginal totals (Y , Z , YZ_l , YZ_r) are fixed, the values for the Z_r , Y_l , and Y_r must be modified. The conditional probability of this new, drier configuration is calculated. The process is then repeated, but with Z_l increased by two events. This incremental procedure is repeated until Z_l is equal to Z (For wet cases, Z_r becomes equal to Z), or until Z_r , Y_l , or Y_r are reduced to zero. The total conditional probabilities, P_{cd} (dry) and P_{cw} (wet), are determined by summing the conditional comes equal to Z , or until Z_r , Y_l , or Y_r are reduced to zero. The total conditional probabilities, P_{cd} (dry) and P_{cw} (wet), are determined by summing the conditional probabilities of these cases. The value of P_{cd} (P_{cw}) is a one-tail probability of the

observed conditions and its drier (wetter) cases. Confidence intervals of 80%, 90%, 95%, 97.5%, and 99% are used to determine the strength of statistical significance. If the total probability is less than 80%, we reject the null hypothesis that the two samples are randomly selected from the same population.

This test is performed for each case in all ten ENSO seasons. Animations of confidence are created to show the evolution and decay of regions showing statistically significant shifts in median precipitation.

c. Probability Distribution Functions

Anomaly patterns are visible from differencing the available data; however, the number of years in each ENSO/PDO category is insufficient to determine the actual underlying statistical distribution of seasonal temperatures and precipitation amounts. Therefore, a resampling technique based on the bootstrap method of Draconis and Efron (1983) is implemented for generating a representative probability distribution function.

The bootstrap is implemented to create three-month ENSO/PDO seasonal composites by repeated sampling of the available data with instant replacement. Monthly temperature and precipitation data are considered independent. Each individual monthly value in a composite ENSO/PDO season is chosen randomly from a list of like months that occurred during the same ENSO/PDO phases. The three randomly selected monthly values then create one composite season (Green 1996). This procedure is repeated 10,000 times.

There are some limitations to the bootstrap. While the mean of a bootstrap sample is the same as the mean of the original sample, the variance in the bootstrap sample

There are some limitations to the bootstrap. While the mean of a bootstrap sample is the same as the mean of the original sample, the variance in the bootstrap sample is conservative. Therefore, the probability distribution generated by the resampled

data is not as broad as the distribution is in nature. Also, low sample sizes allow for only a small number of unique composite seasons. This results in the probability distribution function resembling a step function instead of a smooth curve.

Only regions that exhibit changes in temperature and/or precipitation anomalies between the ENSO anomalies and the ENSO/PDO anomalies will be analyzed using the bootstrap. The resampled data are used to construct estimates of histograms showing the seasonal distribution of temperature and precipitation at each station. By summation of the histograms, cumulative probability distributions are also created. These distributions are designed to highlight changes of the seasonal temperature and precipitation distributions.

4. RESULTS

Results will be presented in two sections. The first section deals with shifts in mean temperature and precipitation for each ENSO/PDO state. The statistical significance of these shifts will also be discussed. The second section will examine spatially coherent regions that show changes in ENSO/PDO states via cumulative probability distributions.

a. Shifts in Mean Temperature and Precipitation

Due to the large amount of data analyzed, only 4 seasons (OND, JFM, AMJ, and JAS) are discussed for brevity. Results for all seasons can be seen in the anomaly and confidence animations[<http://www.coaps.fsu.edu/~bove/ENSO-PDO.shtml>].

1) El Niño OND Patterns

(i) **Temperature.** Most of the United States sees slightly cooler temperatures during El Niño OND (Figure 4a). East of the Mississippi River, the cold anomalies are small, with temperatures averaging only 0.25°C below normal. Texas and the intermountain west are colder, however, with locations in New Mexico and Colorado seeing seasonal temperatures up to 1.5°C below average. Only the high plains of North Dakota and Minnesota see a slight warming during an El Niño autumn, where seasonal temperatures can reach 1.0°C above normal. of North Dakota and Minnesota see a slight warming during an El Niño autumn, where seasonal temperatures can reach 1.0°C above normal.

El Niño(+) autumns differ little from El Niño (Figure 4b). The southwest is

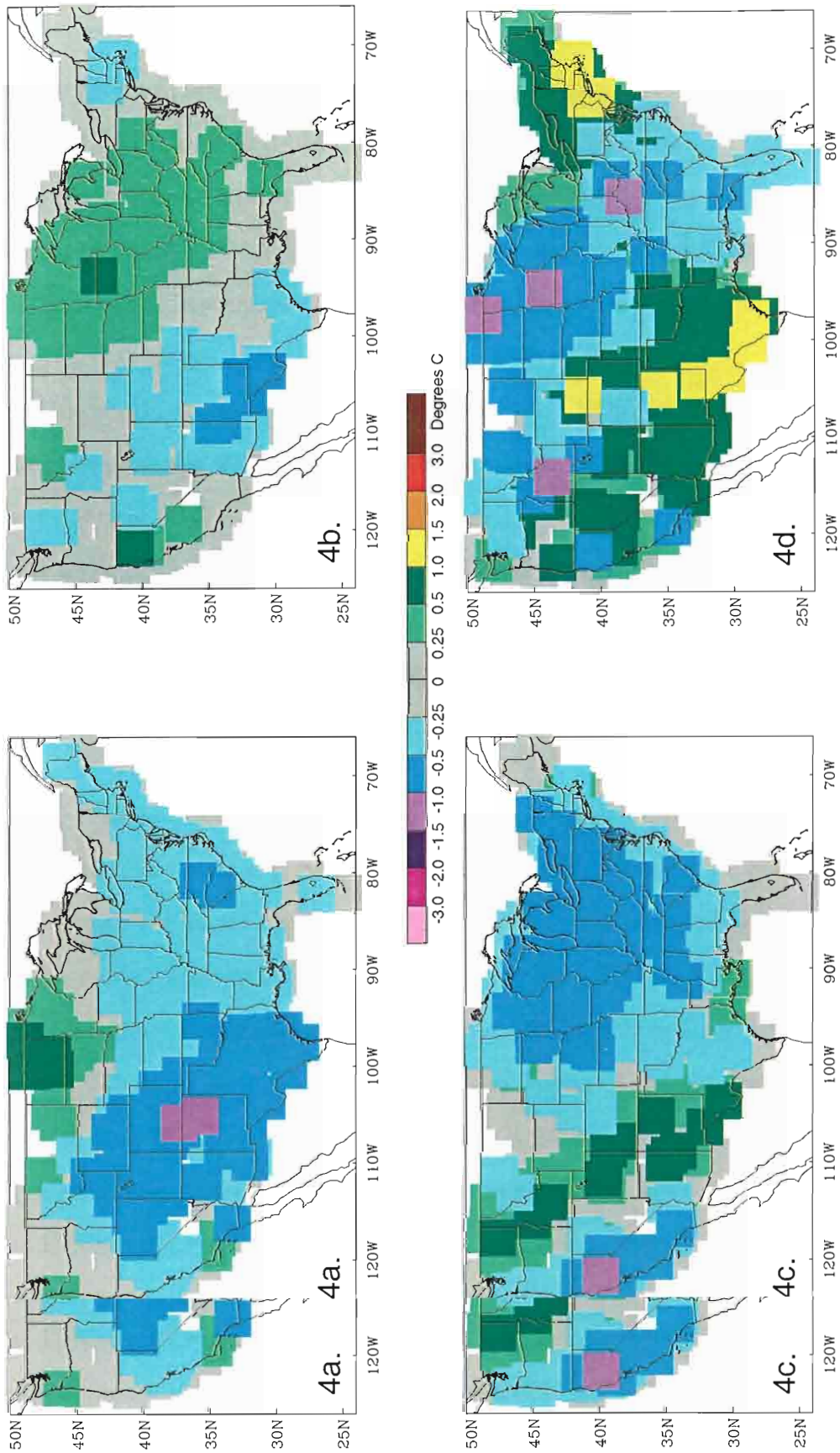


Figure 4a. El Niño temperature anomalies for OND. Difference between OND El Niño Temperature anomalies and (b) OND El Niño(0) temperature anomalies, (c) OND El Niño(-) temperature anomalies, (d) OND El Niño(-) temperature anomalies. Cool colors indicate regions of cold anomalies; warm colors indicate regions of warm anomalies.

slightly cooler, with a maximum centered in southern New Mexico. An area encompassing North Dakota and extending southeast to the Carolinas is 0.25-0.5°C warmer than El Niño. El Niño(0) OND anomalies are up to 1.5°C colder in California, while a broad area centered on the Ohio Valley is up to 1.0°C colder (4c). The El Niño(0) intermountain west is 0.25°C warmer than during El Niño. El Niño(-) is warmer than El Niño in New England, the southwest, and California, with anomalies up to 1.5°C in southwest Texas. The high plains are up to 1.5°C colder, while the southeast averages about 0.25°C cooler than El Niño.

This cooling seen in the southwest during El Niño OND shows confidence in some areas at the 99.5% level, while the warming in the northern plains has no confidence above the 90% level (Figure 5a). Confidence in the cooling in the southwest is stronger during El Niño(+) OND, with a large region showing 99.5% confidence (Figure 5b). There is little coherent confidence in the southwest anomalies during El Niño(0) OND (Figure 5c), and there are no coherent regions of confidence during El Niño(-) OND (Figure 5d).

(ii) Precipitation. El Niño OND precipitation patterns indicates wet conditions along the Gulf Coast and Nebraska, and drier conditions to the Pacific Northwest (Figure 6a). The Gulf Coast is about 20% wetter, while areas of Nebraska can be up to 50% wetter. The Pacific Northwest is about 10% drier than in neutral conditions. OND conditions in the El Niño(+) subset are 10% wetter in the south and Nebraska, and 10% drier in New England (Figure 6b). Areas of the southwest are also 20% drier during El Niño(+). El Niño(0) OND is 20-30% wetter in a band extending from Arkansas northeast to Maine (Figure 6c), a band not seen in El Niño (Figure 6a). El Niño(0) also shows 10 - 20% drier conditions in Nebraska and wetter conditions in the California and desert southwest. El Niño(-) shows dry conditions in the 6a). El Niño(0) also shows 10 - 20% drier conditions in Nebraska and wetter conditions in the California and desert southwest. El Niño(-) shows dry conditions in the

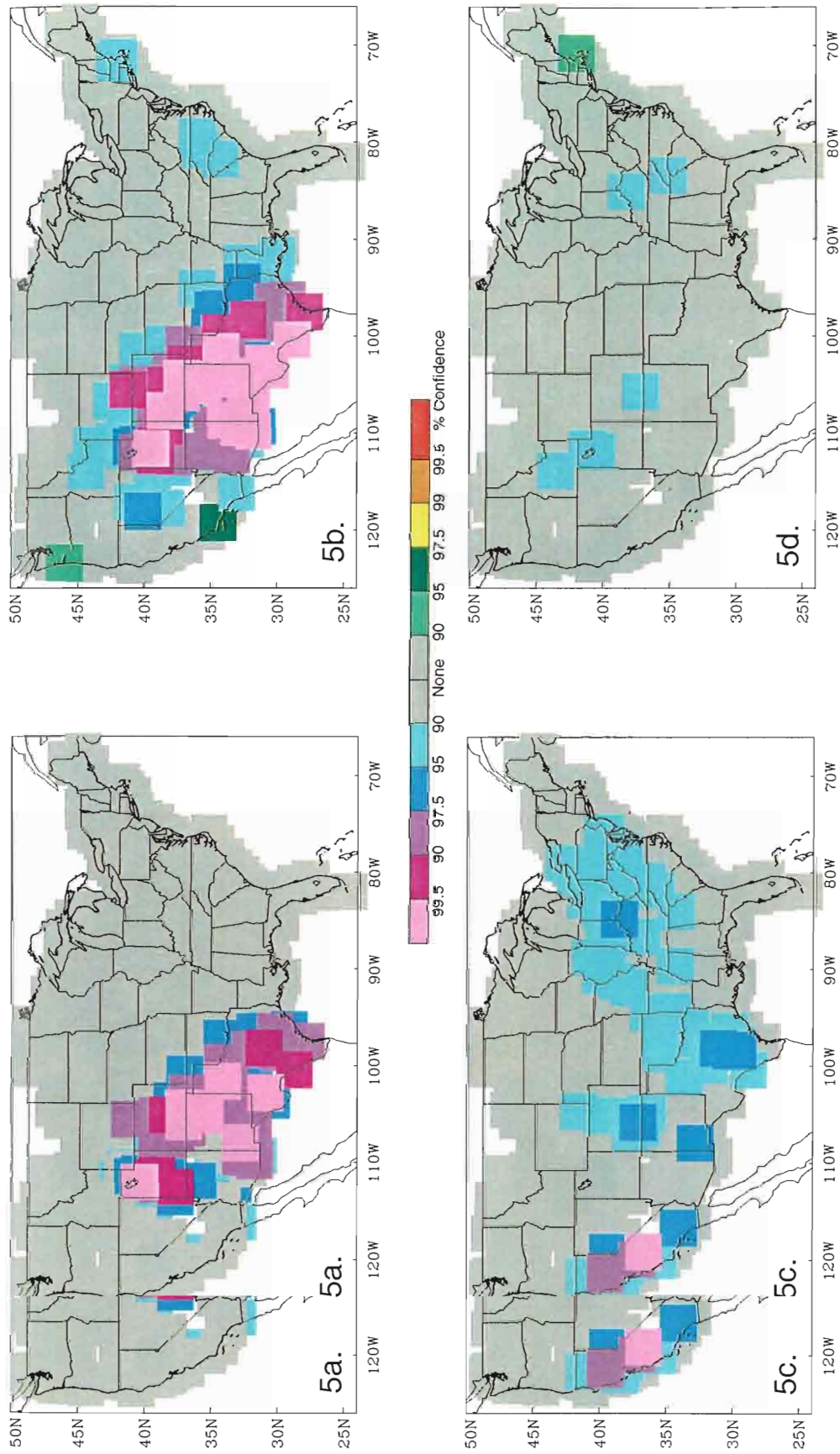


Figure 5. Confidence in (a) OND El Niño temperature anomalies, (b) OND El Niño(+) temperature anomalies, (c) OND El Niño(0) temperature anomalies, (d) OND El Niño(-) temperature anomalies. Cool colors indicate regions of cold anomaly predictability above 90%; warm colors indicate regions of warm anomaly predictability above 90%.

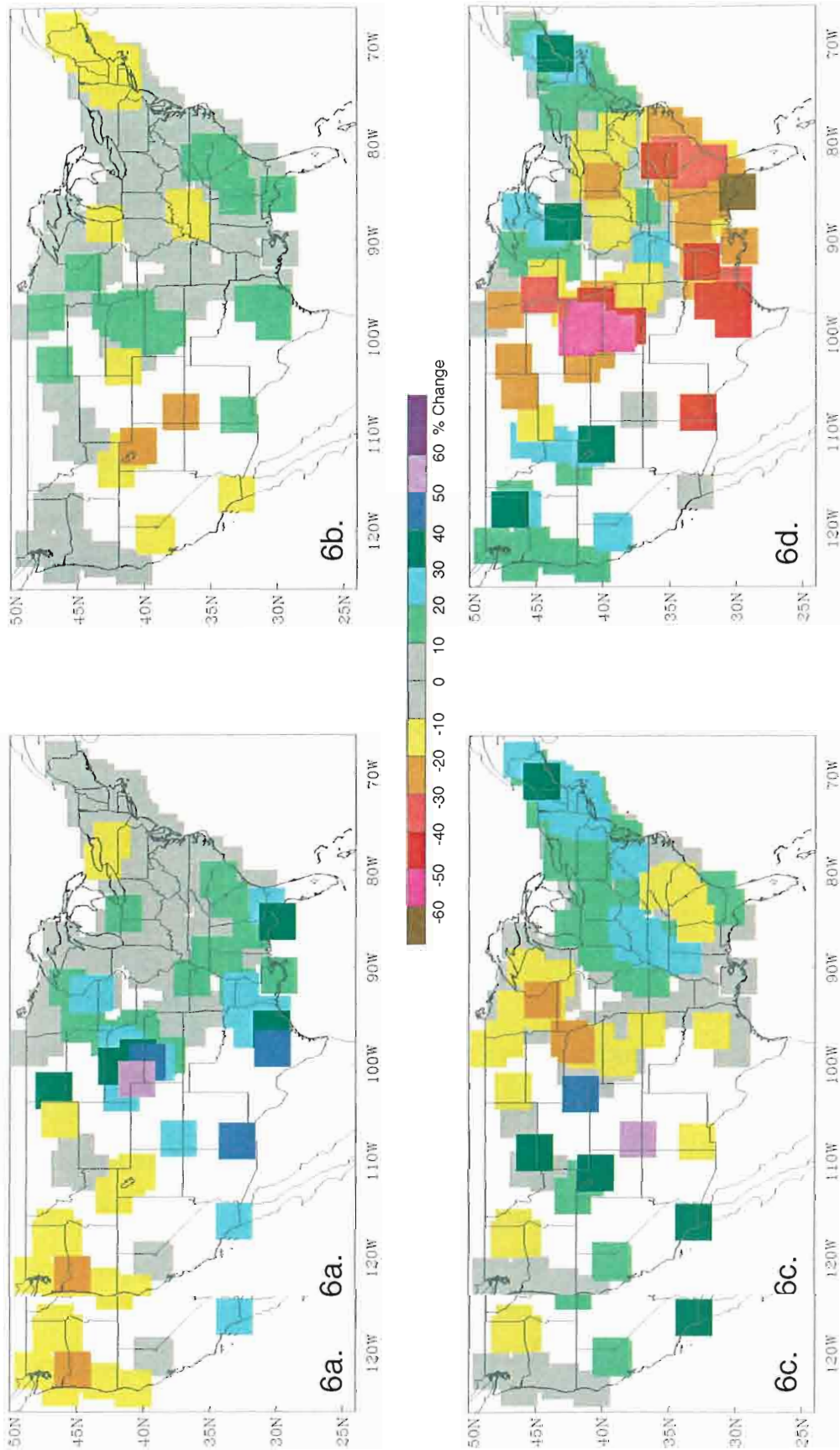


Figure 6a. El Niño precipitation anomalies for OND. Difference between OND El Niño precipitation anomalies and (b) JFM El Niño(+) Niño(+) precipitation anomalies, (c) JFM El Niño(0) precipitation anomalies, (d) JFM El Niño(-) precipitation anomalies. Cool colors indicate regions of wet anomalies; warm colors indicate regions of dry anomalies.

south and Nebraska, which negate the wet conditions seen in El Niño (Figure 6d). The Pacific Northwest during El Niño(-) is 10-20% wetter, which is shown to be dry by the same magnitude in the El Niño climatology. New England, like in El Niño(0) OND, is 20-30% wetter than El Niño.

The Pacific Northwest, Nebraska, and the south all exhibit statistical significance above the 80% level during El Niño OND (7a). Confidence can reach as high as 99% in all three locations. Pennsylvania and the surrounding states show a noisy confidence pattern, with confidence of both dry and wet seasons in the region. El Niño(+) OND has confidence patterns similar to El Niño, but confidence is lessened in the Pacific Northwest and Nebraska (Figure 7b). The Deep South shows expanded wet conditions and the northeast is significantly drier. El Niño(0) once again shows confidence in the dry conditions in Washington, but the eastern half of the United States experiences significantly wet conditions (Figure 7c). The significance of these wet conditions is relatively low, however, with confidence levels between 80 and 90 percent. El Niño(-) shows almost no regions of statistically significant precipitation shifts, partly due to low sample size (Figure 7d). Two regions which show slight significance during El Niño(-) OND are the Carolina, which are dry, and New England, which is wet.

2) El Niño JFM Patterns

(i) Temperature. The cool anomalies over the south and east intensify during JFM, with temperatures 1.5°C cooler in a extending from Texas to Florida, and north to Virginia and eastern Tennessee (Figure 8a). Weaker cool anomalies reach as far north as New England. Meanwhile, the warm anomalies in North Dakota and Minnesota deepen and expand, reaching south into Nebraska and Iowa and west to the north as New England. Meanwhile, the warm anomalies in North Dakota and Minnesota deepen and expand, reaching south into Nebraska and Iowa and west to the Pacific Northwest and California. The deepest anomalies occur over the high plains

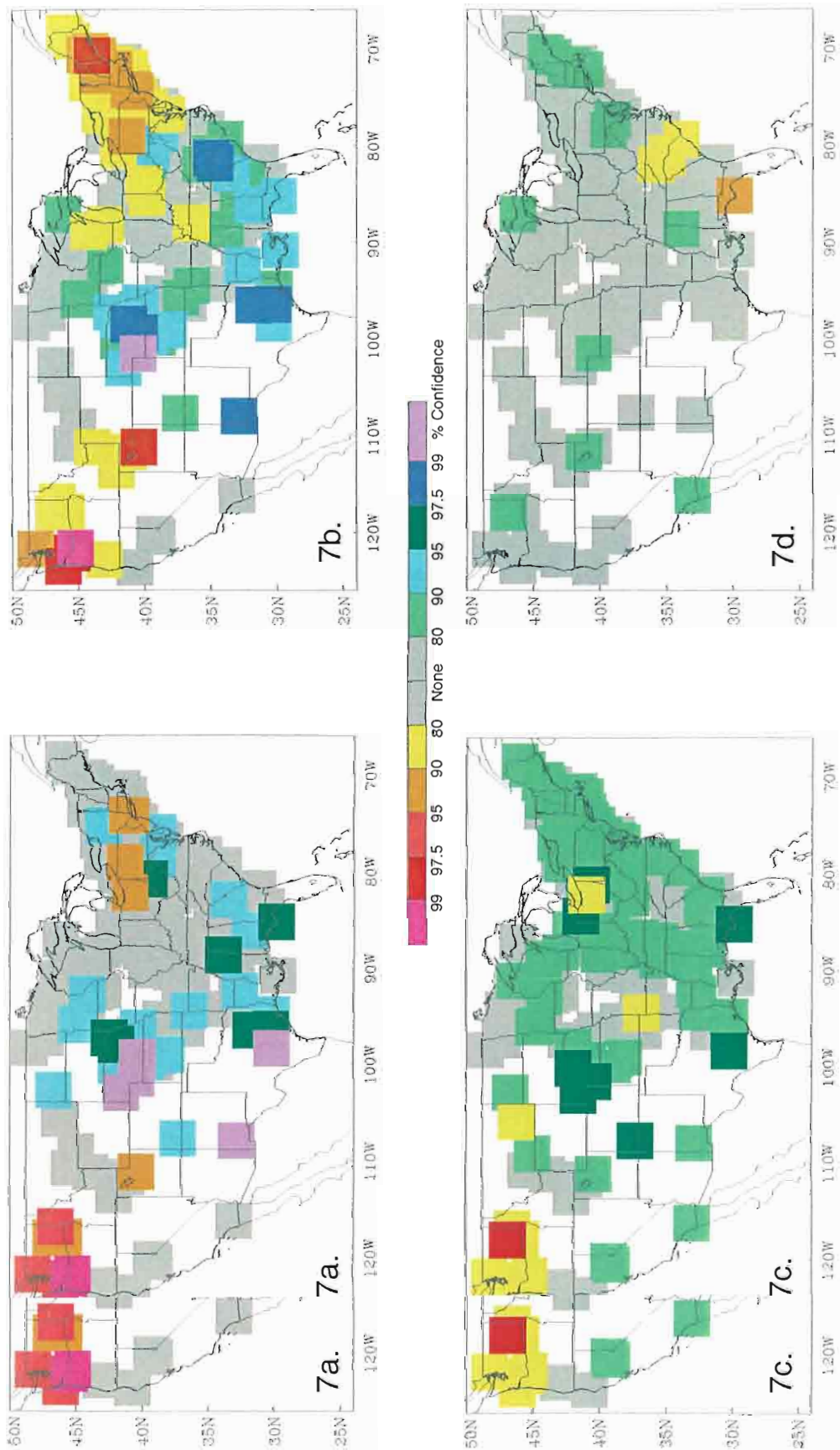


Figure 7. Confidence in (a) OND El Niño precipitation anomalies, (b) OND El Niño(+) precipitation anomalies, (c) OND El Niño(-) precipitation anomalies, (d) OND El Niño(-) precipitation anomalies. Cool colors indicate regions of statistically significant wet conditions; warm colors indicate regions of statistically significant dry conditions.

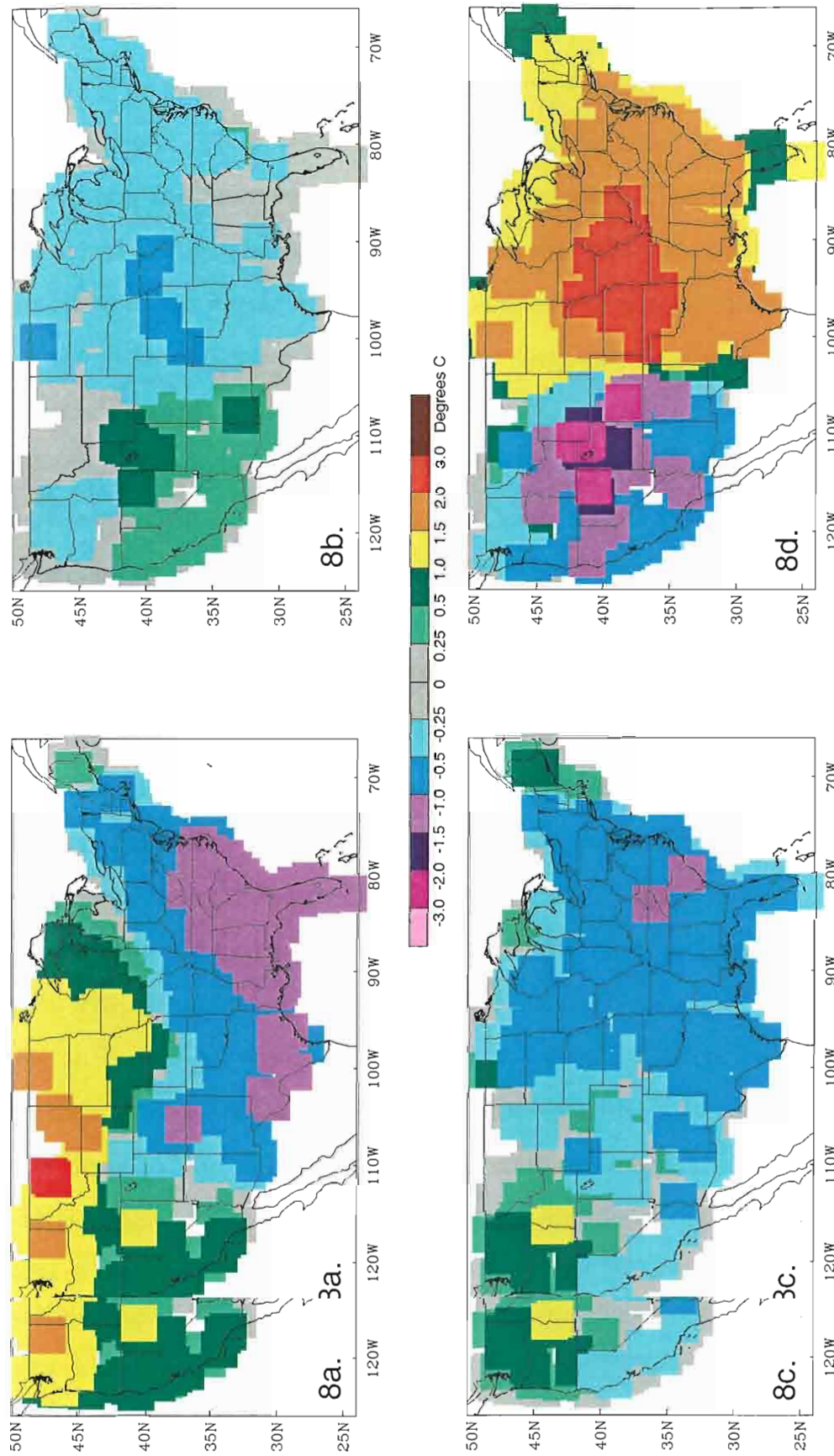


Figure 8a. El Niño temperature anomalies for JFM. Difference between JFM El Niño Temperature anomalies and (b) JFM El Niño(+) temperature anomalies, (c) JFM El Niño(0) temperature anomalies, (d) JFM El Niño(-) temperature anomalies. Cool colors indicate regions of cold anomalies; warm colors indicate regions of warm anomalies.

and Pacific Northwest, with a local maximum in Montana with seasonal temperatures up to 3.0°C above average. California and the western Great Lakes see lesser warming, on the order of 1.0°C .

Once again, El Niño(+) exhibits only minor differences from the El Niño pattern (Figure 8b). The desert southwest and California are $0.25 - 1.0^{\circ}\text{C}$ warmer, while the plains and Northeast see conditions up to 0.5 degrees cooler. El Niño(0) JFM anomalies show the southeast up to 1.5°C cooler, intensifying the already cool El Niño pattern, with maximum anomalies in the Carolinas (Figure 8c). Weaker cooling extends west to California, while the Pacific Northwest warms by up to 1.5°C . The El Niño JFM pattern is altered drastically in the El Niño(-) subset (Figure 8d). From the Rocky Mountains west to the Pacific Ocean, a region typically warm during El Niño, sees temperatures up to 3.0°C below normal. The maximum cooling is seen in the Rocky Mountains, while lesser cooling is seen in Washington and northern Idaho. Meanwhile, the states east of the Rocky Mountains are much warmer than in El Niño. Except for New England, the whole region is at least 1.0°C warmer than El Niño conditions, with a maximum of 3.0°C warmer extending from Kansas to Indiana. This warming eliminates the cooling typical in El Niño in the southeast, while intensifying the warm anomalies in the High Plains.

The warming in the Pacific Northwest and cooling in the southeast during El Niño JFM are exhibit confidence at the 99.5% level (Figure 9a). Lesser confidence is seen in Texas, California and the northern plains. Confidence is also seen in the southeastern cold anomalies during El Niño(+), with 99.5% confidence extending from Texas to North Carolina, and lesser confidence extending from New Mexico to New England (Figure 9b). Meanwhile, the confidence of warm anomalies in the west is diminished except along the Pacific coast. El Niño(0) JFM anomalies also to New England (Figure 9b). Meanwhile, the confidence of warm anomalies in the west is diminished except along the Pacific coast. El Niño(0) JFM anomalies also show statistical significance in the southeast, but with not as much confidence as in

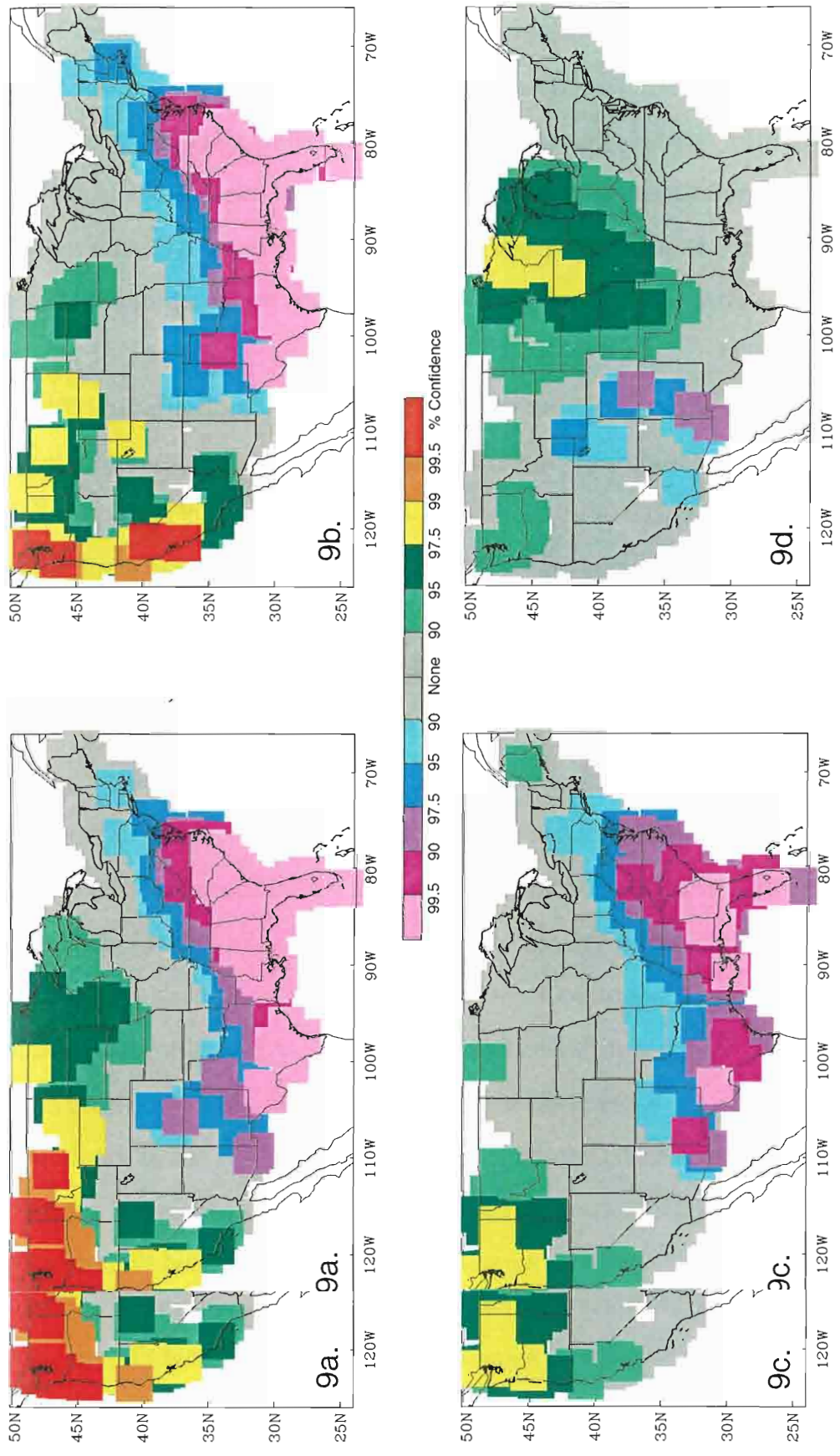


Figure 9. Confidence in (a) JFM El Niño(0) temperature anomalies, (b) JFM El Niño(+) temperature anomalies, (c) JFM El Niño(0) temperature anomalies, (d) JFM El Niño(+) temperature anomalies. Cool colors indicate regions of cold anomaly predictability above 90%; warm colors indicate regions of warm anomaly predictability above 90%.

El Niño or El Niño(+), though the spatial coverage is similar to El Niño(+) (Figure 9c). Confidence in the western warm anomalies vanishes in the northern plains and California, but some confidence remains in the Pacific Northwest. El Niño(-), which showed large differences in spatial anomaly patterns from El Niño, shows statistical significance in the warm anomalies it creates in the upper Mississippi Valley, Great Lakes, and central plains (Figure 9d). Also, the cold El Niño(-) JFM anomalies in the desert southwest show confidence above 90%.

(ii) Precipitation. JFM El Niño sees a continuation of the wet anomalies in the southeast and Nebraska, but the magnitude of the anomalies has decreased (Figure 10a). The Ohio River valley also becomes 10 - 20% drier than in neutral ENSO conditions. El Niño(+) JFM anomalies shows no coherent regions of change from the El Niño climatology (Figure 10b). El Niño(0) JFM shows the eastern seaboard 10% wetter, and Nebraska up to 40% drier, eliminating the wet conditions usually seen there during El Niño (Figure 10c). El Niño(-) is 10-30% wetter in the Ohio Valley, reversing the dry conditions typically seen there in El Niño (Figure 10d). The central plains are 10-30% drier, also a reversal of El Niño conditions.

El Niño JFM precipitation anomalies are statistically significant in the Ohio and Mississippi river valleys, where conditions are dry, and Nebraska and the southeast, where conditions are wet (Figure 11a). Confidence in all regions can reach 99%. The significant dry anomalies expand and shift eastward during El Niño(+), with local confidence maximums in eastern Ohio and Kentucky (Figure 11b). The confidence in the wet conditions along the southeastern coast diminishes, but remain in Nebraska, but at a lower confidence level. El Niño(0) exhibits a similar pattern to El Niño, but at a lower confidence interval (Figure 11c). The only location that differs is Nebraska, which does not exhibit spatially coherent statistical

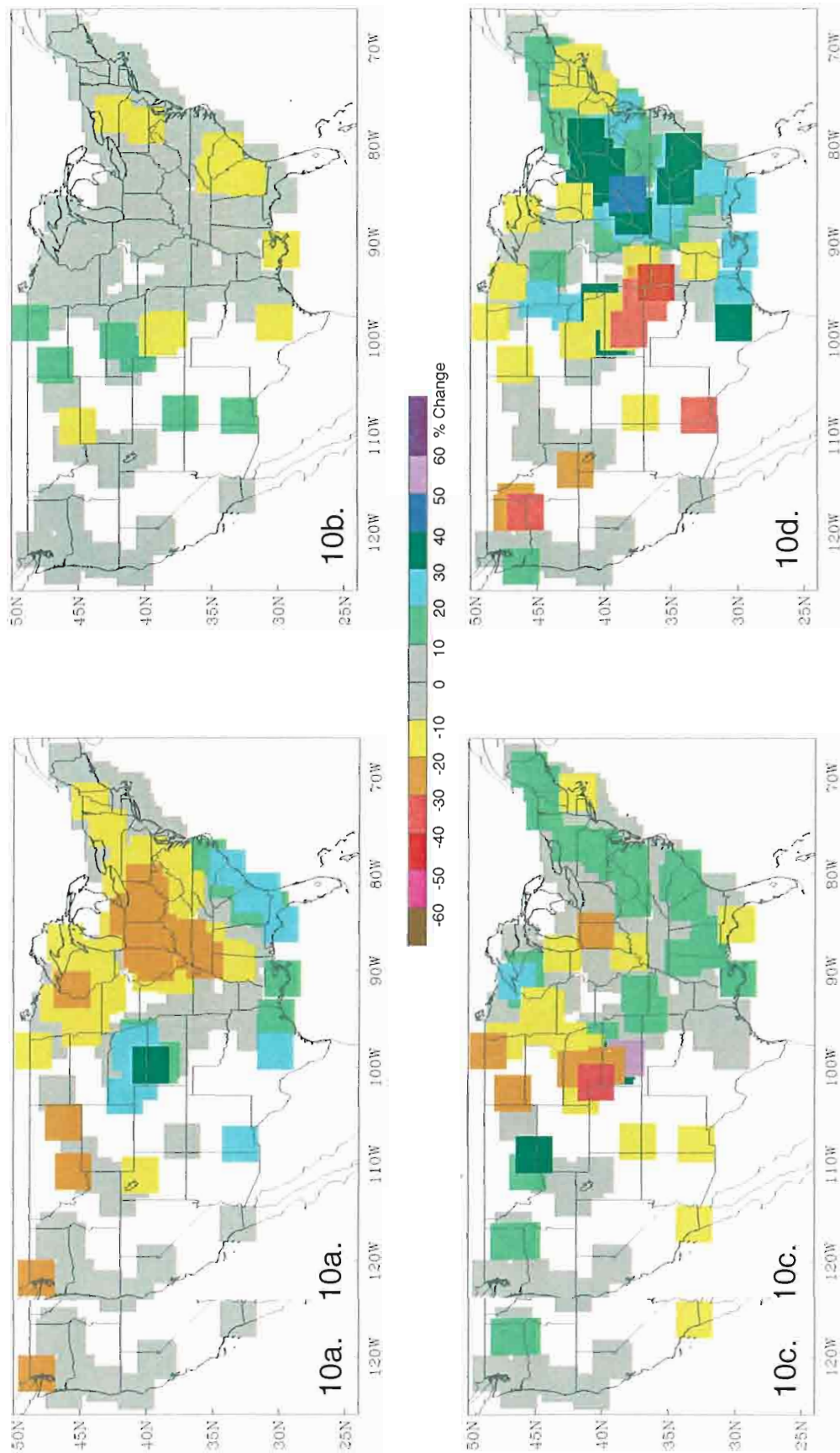


Figure 10a. El Niño precipitation anomalies for JFM. Difference between JFM El Niño precipitation anomalies and (b) JFM El Niño(+ Niño(+)) precipitation anomalies, (c) JFM El Niño(0) precipitation anomalies, (d) JFM El Niño(-) precipitation anomalies. Cool colors indicate regions of wet anomalies; warm colors indicate regions of dry anomalies.

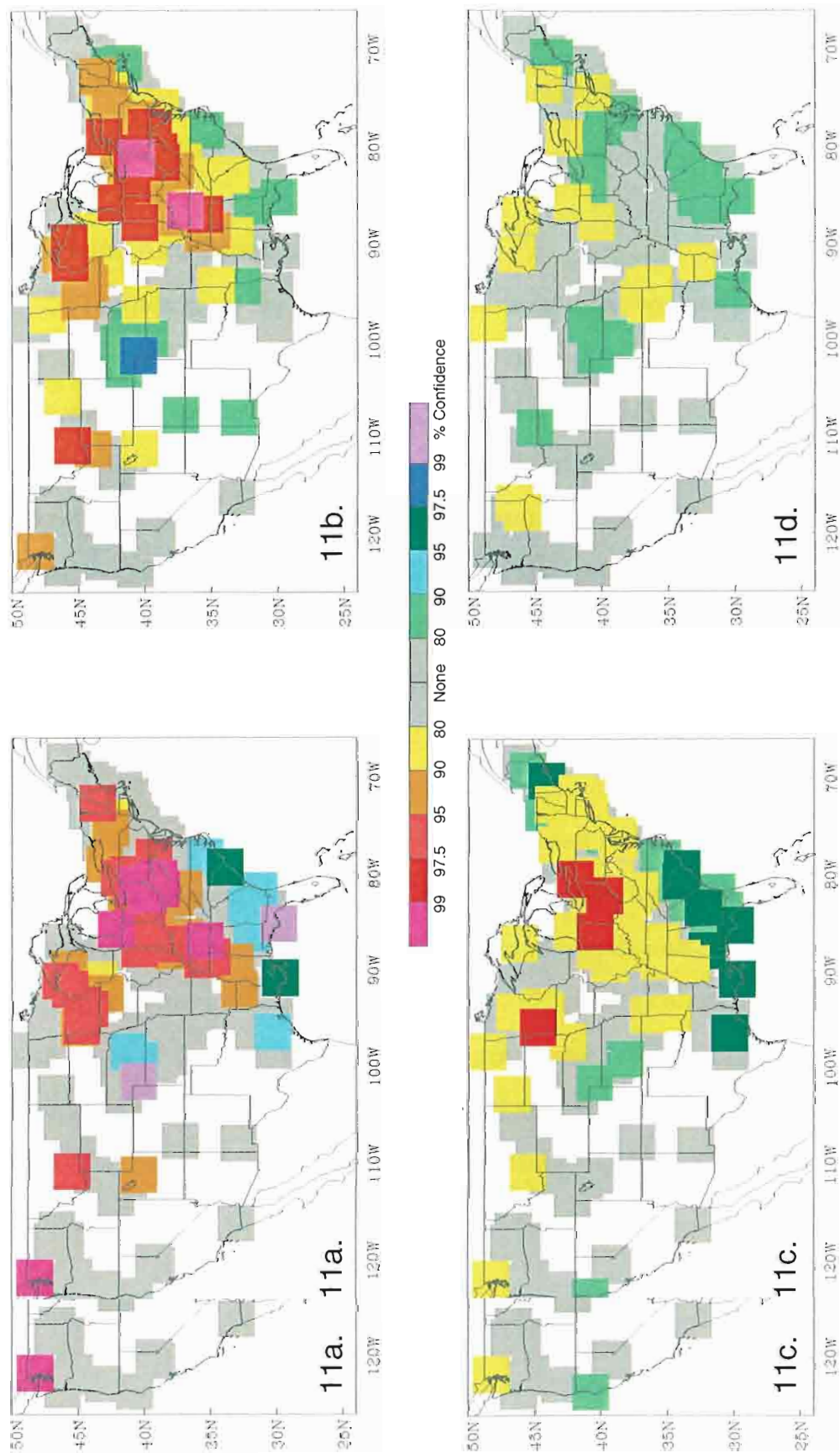


Figure 11. Confidence in (a) JFM El Niño precipitation anomalies, (b) JFM El Niño(+) precipitation anomalies, (c) JFM El Niño(0) pre>(0) precipitation anomalies, (d) JFM El Niño(-) precipitation anomalies. Cool colors indicate regions of statistically sigilly significant wet conditions; warm colors indicate regions of statistically significant dry conditions.

significance during El Niño(0). El Niño(-) once again shows only spotty significance in precipitation anomalies (Figure 11d). Areas which do exhibit confidence above 80% are the southeast and Nebraska, which are both wet. Statistically dry stations are scattered, and show no cohesion.

3) El Niño AMJ Patterns

(i) **Temperature.** The deep JFM El Niño anomalies weaken by AMJ (Figure 12a). The anomalies east of the Mississippi River weaken, with most stations showing seasonal temperatures only .25 - 0.5°C below neutral conditions. Deeper cooling persists in Texas, however, with some areas of the state remaining up to -1.5°C below neutral. The warming in the north and west also diminishes, with the maximum anomalies of 1° to 1.5°C in North Dakota.

The eastern U.S., with the exception of the immediate Gulf coast, sees conditions warmer by 0.25 - 0.5 °C during El Niño(+) AMJ (Figure 12b). Areas of the southwest are also cooler during El Niño(+), with conditions up to 1.0°C cooler in California. In contrast, El Niño(0) sees cool anomalies over the eastern two thirds of the country (Figure 12c). The cooling is greatest in a band from North Dakota to Vermont, with conditions up to 1.5°C colder than during El Niño. This cooling negates the warming seen during El Niño in the north, and intensifies the expected El Niño cooling in the south. In the west, El Niño(0) causes warmer conditions, with areas of California up to 1.5°C warmer than during El Niño. Temperature anomalies associated with El Niño(-) AMJ are generally weak and spotty (Figure 12d). The most coherent patterns are a warming of up to 1.5°C in the south central plains and a 1.0°C cooling in the Pacific Northwest.

plains and a 1.0°C cooling in the Pacific Northwest.

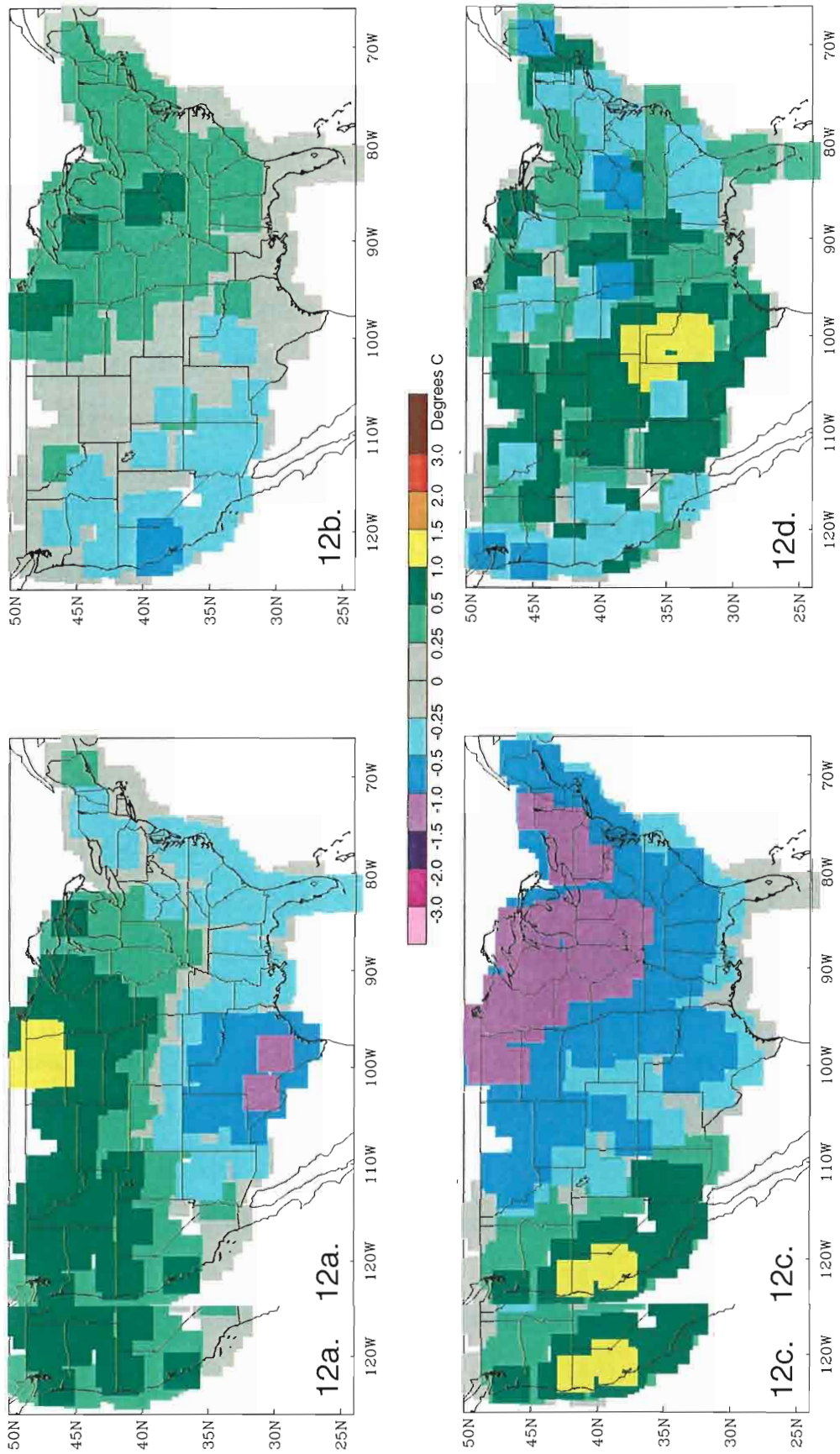


Figure 12a. El Niño temperature anomalies for AMJ. Difference between AMJ El Niño Temperature anomalies and (b) AMJ El Niño(-) Niño(+) temperature anomalies, (c) AMJ El Niño(0) temperature anomalies, (d) AMJ El Niño(-) temperature anomalies. Calies. Cool colors indicate regions of cold anomalies; warm colors indicate regions of warm anomalies.

The cool anomalies in Texas and south Florida during El Niño AMJ remain statistically significant at the 99.5% level, but the confidence in rest of the southeast diminishes (Figure 13a). The warm anomalies in the north are significant in a band from Washington to Michigan, with highest confidence centered in Montana. The confidence pattern in El Niño(+) AMJ is very similar to El Niño, with the maximum confidence of the northern warm anomalies shifted eastward into North Dakota (Figure 13b). El Niño(0) AMJ confidence patterns indicate that cool anomalies are significant above 90% over much of the eastern United States, with the highest confidence in Texas (Figure 13c). This pattern is not seen in El Niño AMJ. The warm anomalies typically seen in the northern plains during El Niño AMJ are not significant during El Niño(0), while the warm anomalies in California show increased confidence. El Niño(-) AMJ confidence patterns closely resembles those of El Niño, but are much smaller in magnitude (Figure 13d). Confidence of the warm anomalies in the high plains averages only 95%, while confidence of cool southeastern anomalies are sporadic.

(ii) Precipitation. A broad area of 10% drier weather dominates the Mississippi River valley during El Niño AMJ (Figure 14a). The only other region showing change is the desert southwest, which is 20 - 40% wetter. The El Niño(+) precipitation subset does not differ greatly from El Niño (Figure 14b). The Pacific states and Nebraska are 10% wetter, while areas of the southeast and Ohio Valley are 10% drier. El Niño(0) AMJ is 10-30% wetter in the southeast and lower Mississippi Valley, reversing of the dry conditions seen in El Niño (Figure 14c). Nebraska and Minnesota are 10-30% drier, as are the Pacific states. Most of the eastern half of the U.S. is 10-20% drier during El Niño(-) spring (Figure 14d), which intensifies the El Niño conditions. The Pacific states are also dry, with southern California up to 60% drier,

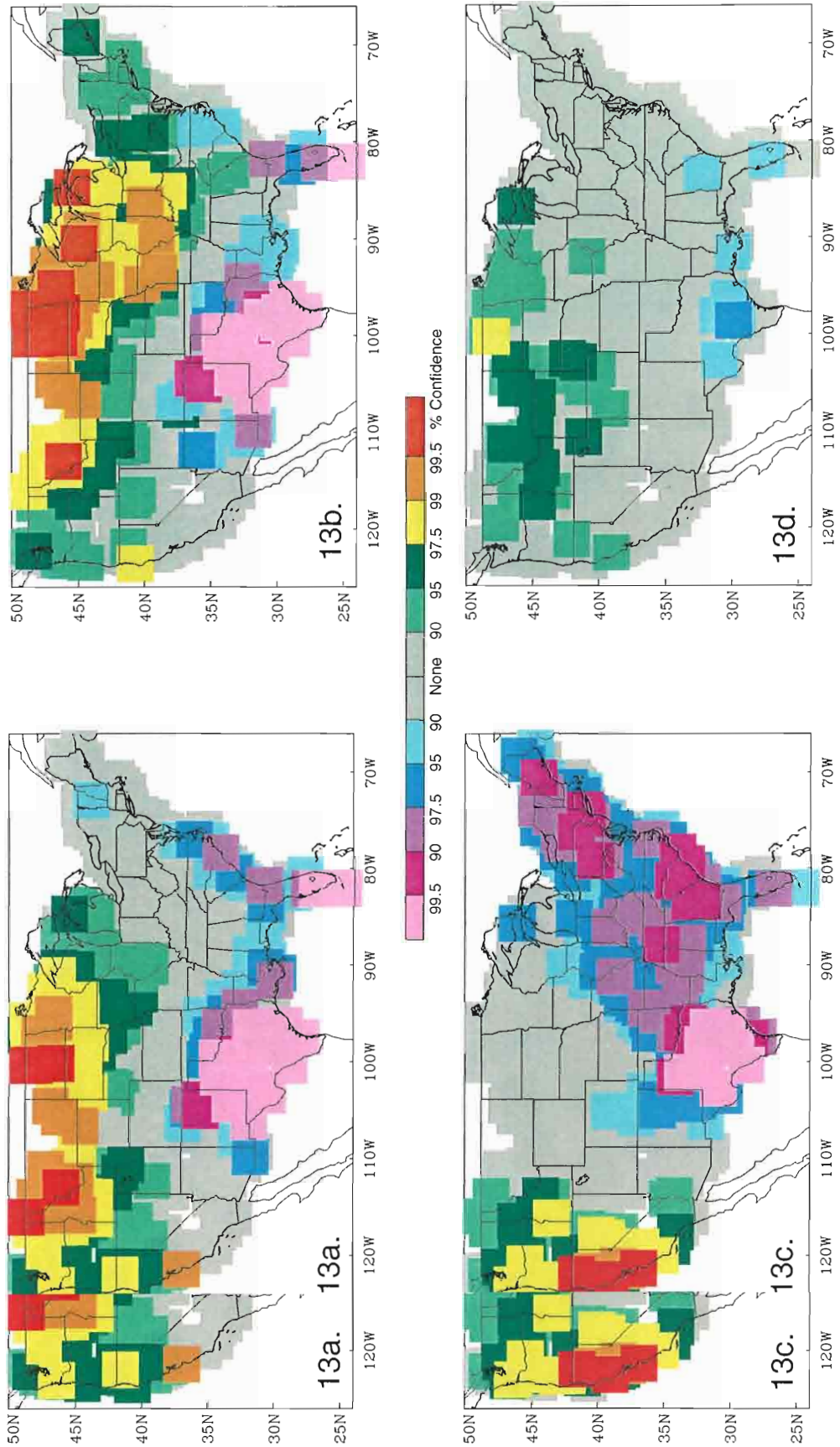


Figure 13. Confidence in (a) AMJ El Niño temperature anomalies, (b) AMJ El Niño(+) temperature anomalies, (c) AMJ El Niño(0) temperature anomalies, (d) AMJ El Niño(-) temperature anomalies. Cool colors indicate regions of cold anomaly predictability above 90%; warm colors indicate regions of warm anomaly predictability above 90%.

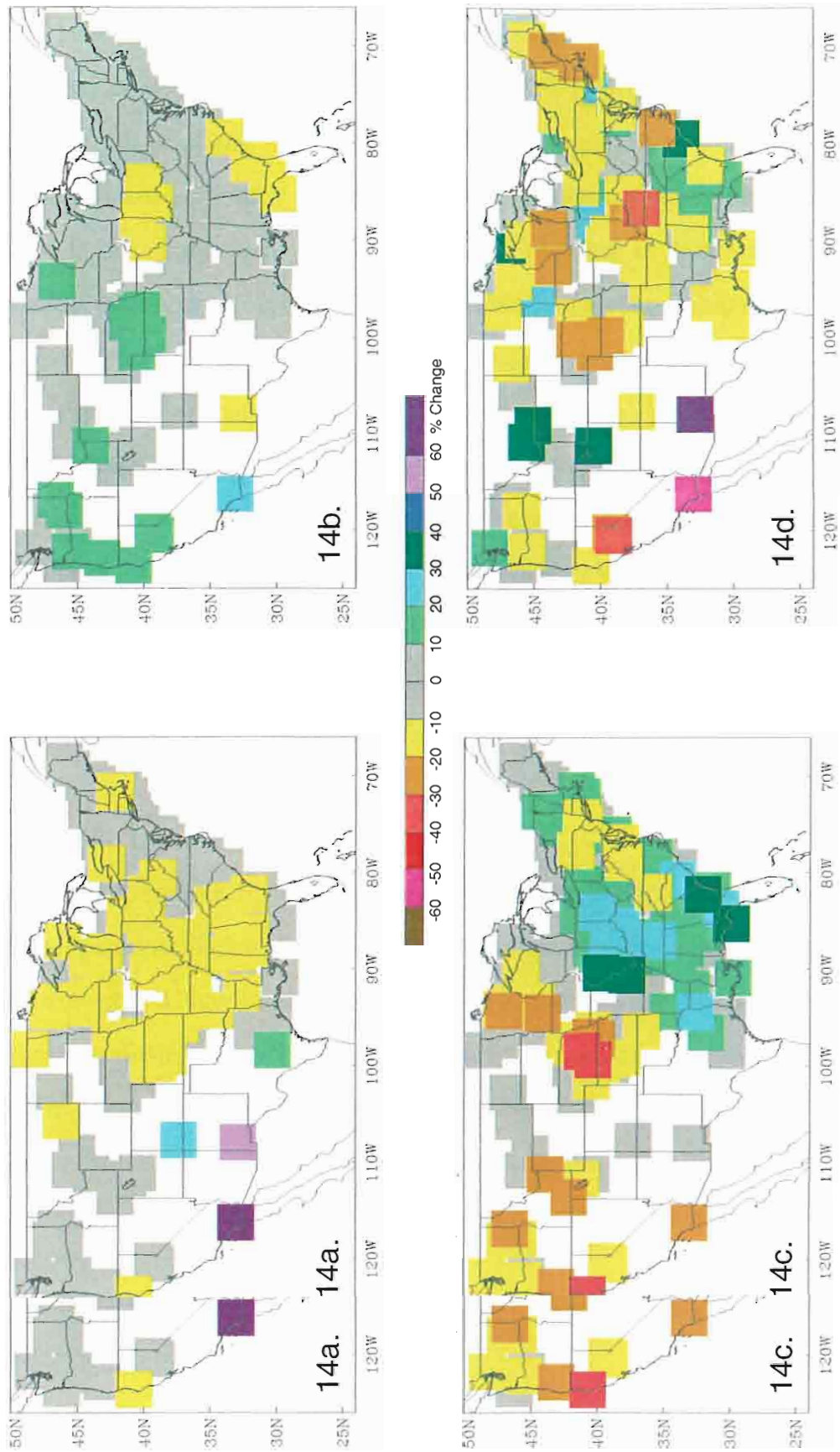


Figure 14a. El Niño precipitation anomalies for AMJ. Difference between AMJ El Niño precipitation anomalies and (b) AMJ El Niño(+ Niño(+)) precipitation anomalies, (c) AMJ El Niño(0) precipitation anomalies, (d) AMJ El Niño(-) precipitation anomalies. Cool colors indicate regions of wet anomalies; warm colors indicate regions of dry anomalies.

negating the wet conditions usually seen during El Niño AMJ.

The broad drier conditions during El Niño AMJ are statistically significant, and in some locations show confidence above 99% (Figure 15a). Two stations in the desert southwest also show significantly wetter conditions. Other regions show no significance. El Niño(+) precipitation anomalies are significant in these regions as well, but significantly wet conditions also appear in Nebraska and the Pacific Northwest (Figure 15b). Overall, the confidence of wet anomalies during El Niño(+) is less than those during El Niño, with confidence intervals typically between 90 and 95 percent. El Niño(0) shows strong confidence in dry conditions from Minnesota to Kansas (Figure 15c). Confidence in this regions can exceed 97.5%. The Pacific Northwest and the Mid-Atlantic states are also significantly dry, but at a lower confidence interval. Areas of the southeast exhibit wet conditions. El Niño(-) AMJ shows a broad area of significantly dry conditions over the central Mississippi valley, with confidence intervals ranging from 80 to 90 percent. No other regions show coherent significance during El Niño(-) AMJ.

4) El Niño JAS Patterns

(i) **Temperature.** By JAS, the winter and spring El Niño anomaly patterns are no longer present (Figure 16a). Summer El Niño patterns include cooling in the desert southwest and New England, as well as a band of warmer temperatures extending from Wisconsin and Michigan southeastward to the Carolinas and Florida. Anomalies in New England are only 0.25 – 0.5°C below normal, while cool anomalies in the southwest can reach 1.0°C in Utah and Arizona. Warm anomalies are strongest in the Ohio Valley and Mid-Atlantic States, with temperatures 1.0°C above neutral ENSO conditions.

in the Ohio Valley and Mid-Atlantic States, with temperatures 1.0°C above neutral ENSO conditions.

El Niño(+) JAS anomalies intensify the El Niño pattern (Figure 16b). Conditions

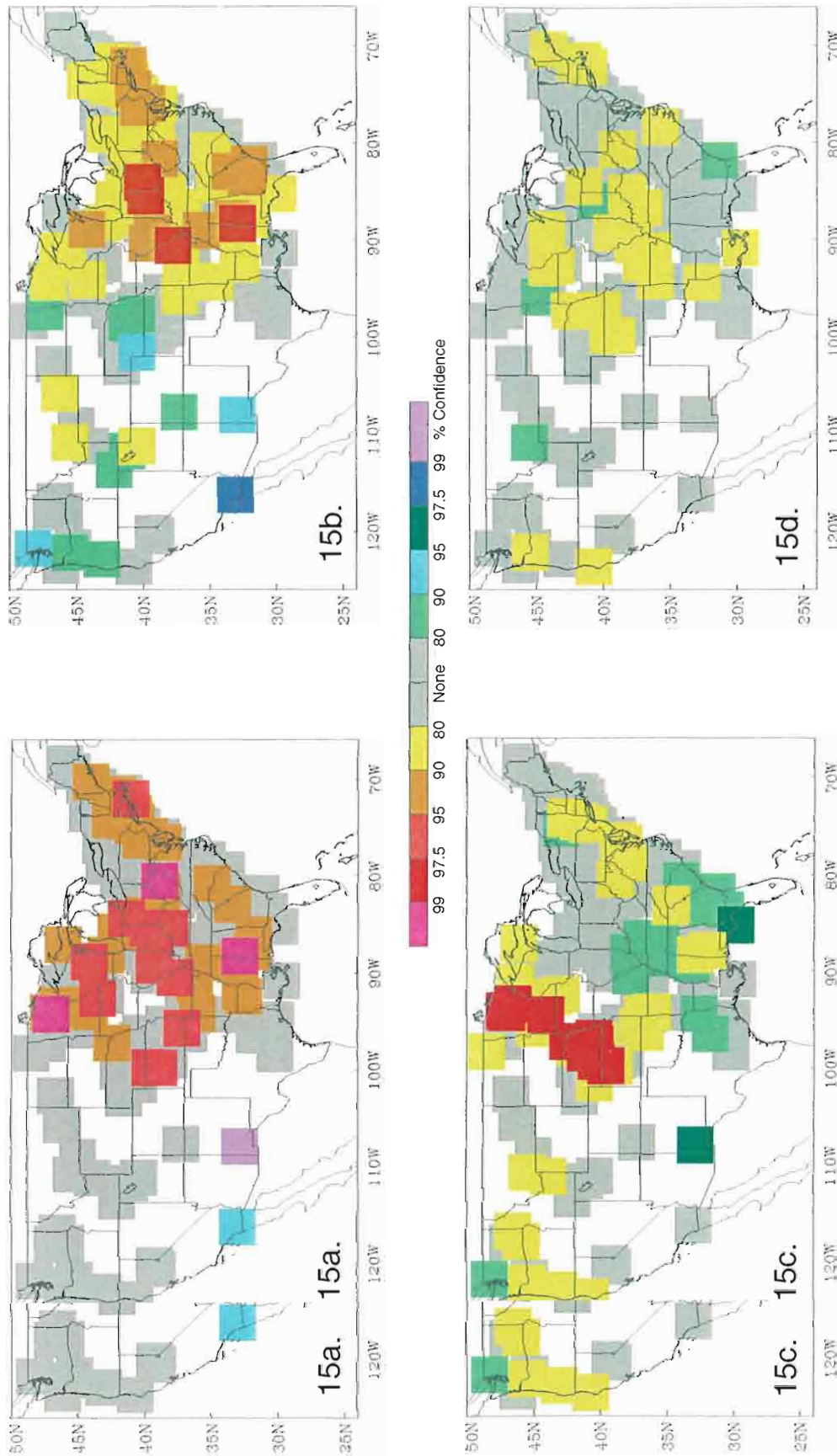


Figure 15. Confidence in (a) AMJ El Niño precipitation anomalies, (b) AMJ El Niño(+) precipitation anomalies, (c) AMJ El Niño(0) precipitation anomalies, (d) AMJ El Niño(-) precipitation anomalies. Cool colors indicate regions of statistically significant wet conditions; warm colors indicate regions of statistically significant dry conditions.

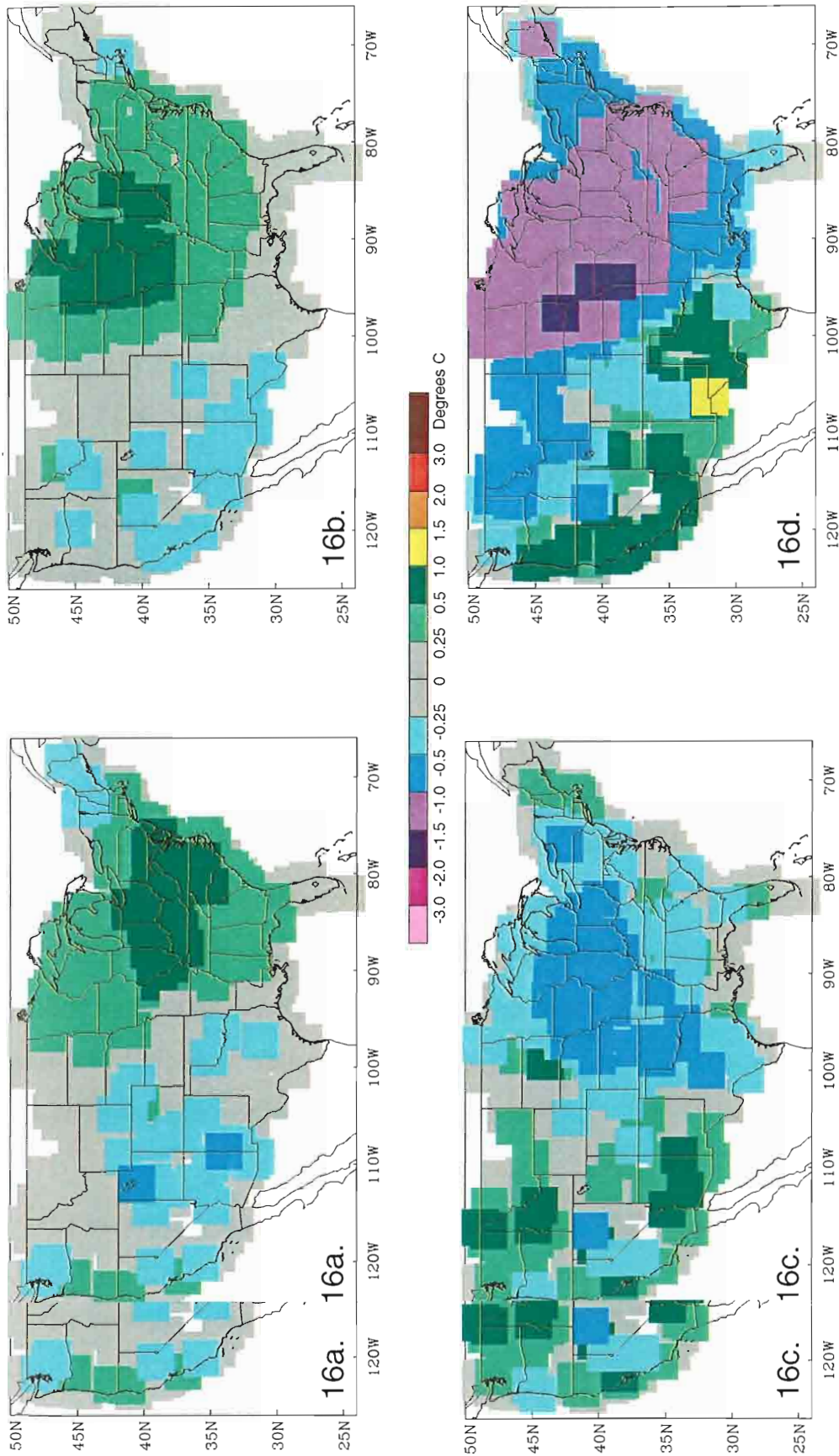


Figure 16a. El Niño temperature anomalies for JAS. Difference between JAS El Niño Temperature anomalies and (b) JAS El Niño(+ Niño(+)) temperature anomalies, (c) JAS El Niño(0) temperature anomalies, (d) JAS El Niño(-) temperature anomalies. Cool colors indicate regions of cold anomalies; warm colors indicate regions of warm anomalies.

are up to 0.5°C cooler in the southwest, while the upper Mississippi Valley is up to 1.0°C warmer than in El Niño. This means that El Niño(+) has the same anomaly pattern, but stronger. El Niño(0) sees cooler conditions in the plains and Ohio valley (Figure 16c). The 1.0°C cooling in the Ohio Valley negates the warming typically seen in El Niño, while the southern plains cool. Anomalies in the western U.S. during El Niño(0) are weak and show no coherent signal. El Niño(-) summers are 1.5°C cooler over much of the eastern United States, which cancel the warm anomalies typically seen during El Niño (Figure 16d). Meanwhile, the southwest is warmer by $0.5 - 1.0^{\circ}\text{C}$, making the region warmer than seen in El Niño.

The warming in the east during El Niño JAS is significant at the 99.5% level in Virginia and the Carolinas, with lesser confidence extending northwest into Wisconsin (Figure 17a). The cool anomalies in the desert southwest also show statistical significance. El Niño(+) sees the confidence of warm temperatures in the east, with the region from Minnesota to South Carolina showing 99.5% confidence of a warming (Figure 17b). Confidence in the southwest spreads westward into California, but the level of confidence does not change. El Niño(0) sees a decrease in the confidence of the warm anomalies in the east, with only the Mid-Atlantic states still showing some confidence above 90% (Figure 17c). No other regions show predictable changes in seasonal temperature during El Niño(0) JAS. In contrast to the El Niño and the other subsets, El Niño(-) JAS shows statistically significant cooling in upper Mississippi Valley (Figure 17d). This region extends southeast in the Tennessee valley, but exhibit weaker confidence.

(ii) Precipitation. JAS El Niño conditions are 10-20% wetter in the Ohio and Mississippi River valleys, and 10% drier along the Atlantic Coast (Figure 18a).

(ii) Precipitation. JAS El Niño conditions are 10-20% wetter in the Ohio and Mississippi River valleys, and 10% drier along the Atlantic Coast (Figure 18a). Areas of the Pacific Northwest are also 10% wetter. California and Oregon are 10%

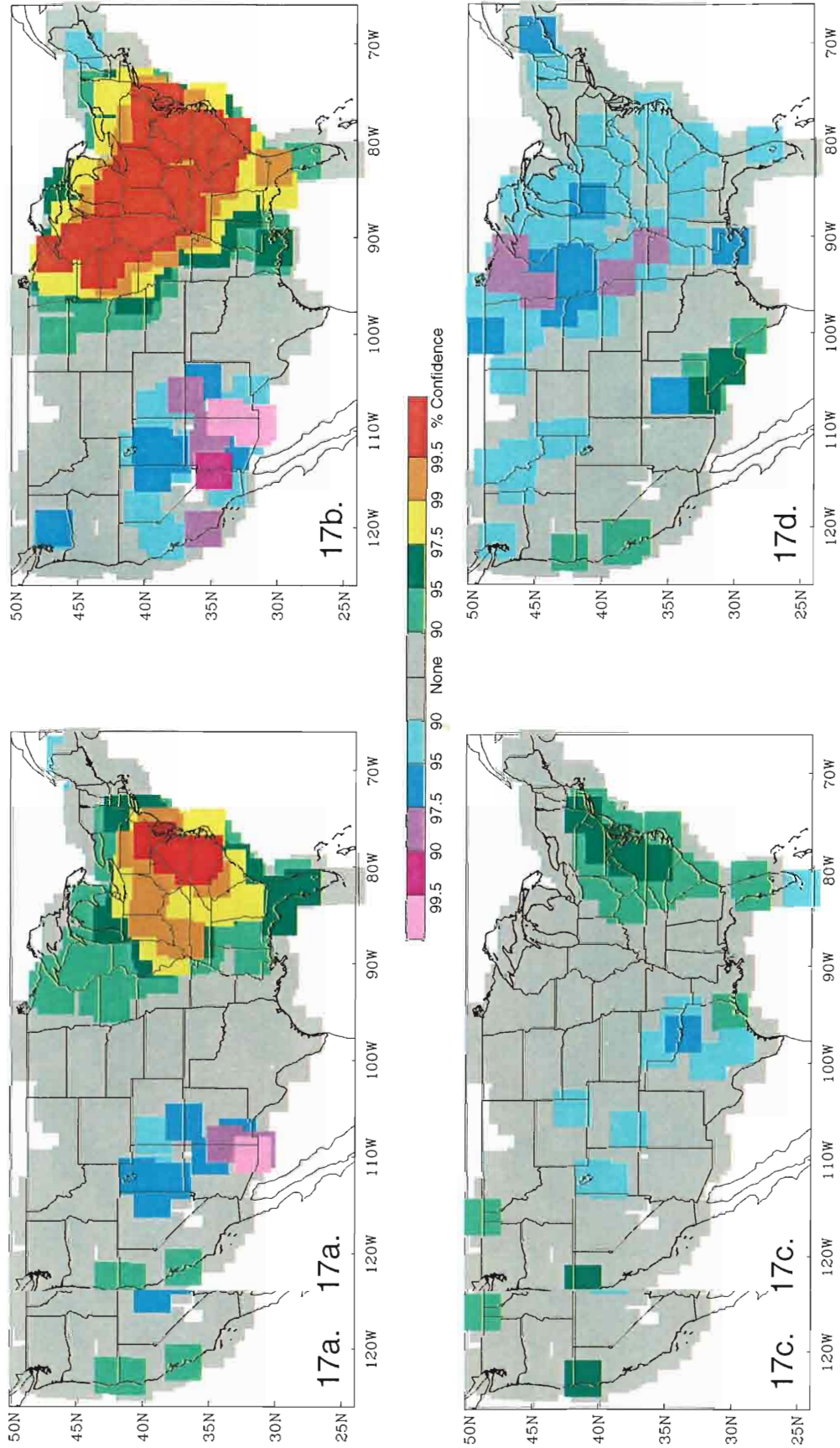


Figure 17. Confidence in (a) JAS El Niño(+) temperature anomalies, (b) JAS El Niño(-) temperature anomalies, (c) JAS temp(0) temperature anomalies, (d) JAS El Niño(-) temperature anomalies. Cool colors indicate regions of cold anomaly predictability above 90%; warm colors indicate regions of warm anomaly predictability above 90%.

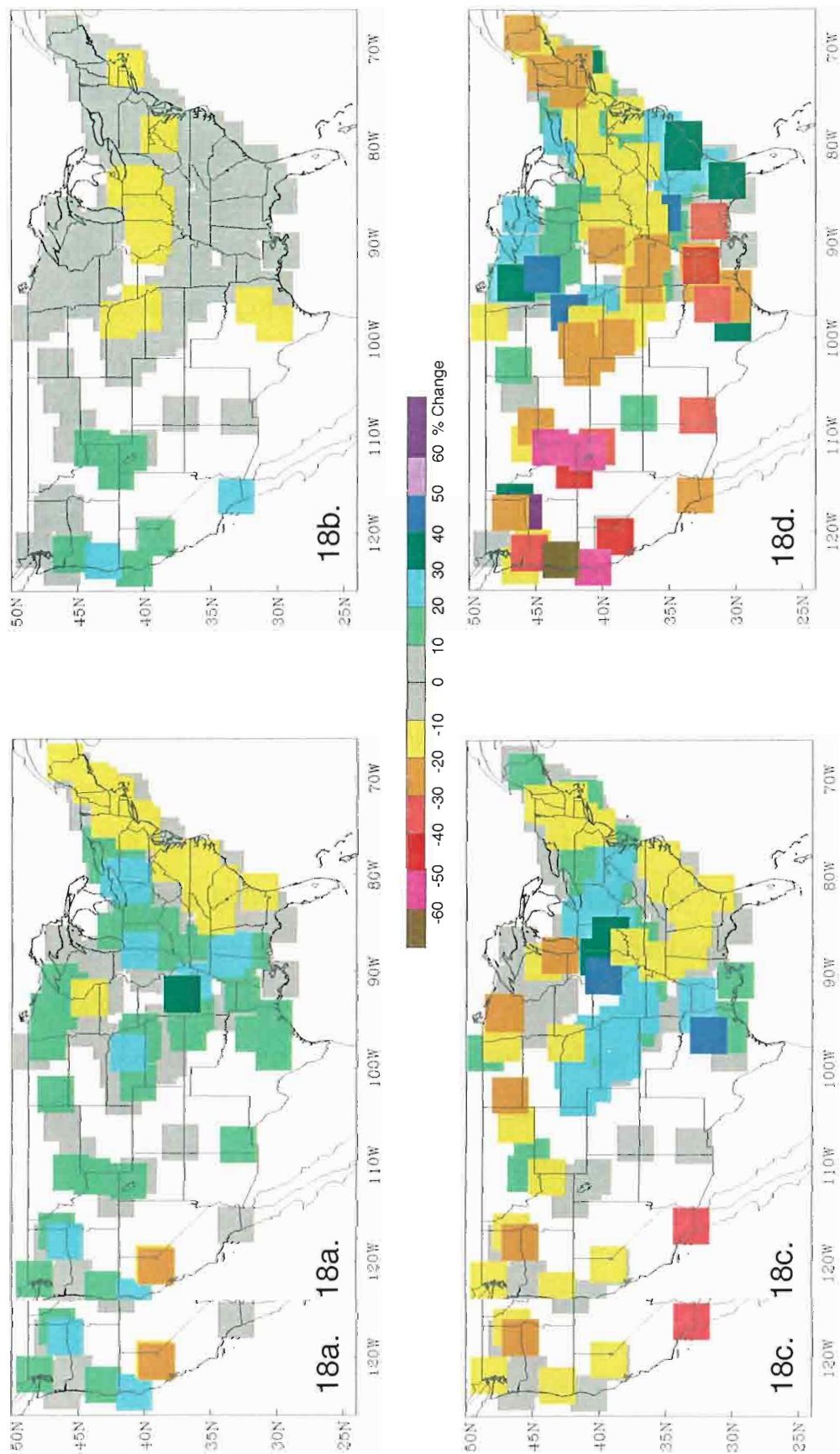


Figure 18a. El Niño precipitation anomalies for JAS. Difference between JAS El Niño precipitation anomalies and (b) JAS El Niño(+ Niño(+)) precipitation anomalies, (c) JAS El Niño(0) precipitation anomalies, (d) JAS El Niño(-) precipitation anomalies. Cool colors indicate regions of wet anomalies; warm colors indicate regions of dry anomalies.

wetter in the El Niño(+) subset, with no coherent changes in precipitation in the east (Figure 18b). El Niño(0) is 10 - 20% drier in the Pacific Northwest, opposite of the El Niño pattern (Figure 18c). The southern plains and Ohio valley are 10 - 20% wetter, intensifying the conditions there. Regions of the eastern seaboard are also 10% drier, bringing intensified condition as well. El Niño(-) sees negating anomalies in many regions, including 30-60% dry conditions in the west (Figure 18d). Other regions seeing opposite anomalies during El Niño(-) are the Ohio and Mississippi Valleys, which are 10 - 30% drier, and the southeast, which is up to 40% wetter.

El Niño JAS precipitation anomalies are significant in two regions (Figure 19a). New England is dry, and the significant anomalies extend southwest into New Jersey, and potentially as far south as Georgia. Meanwhile, significantly wet anomalies dominate the length of the Mississippi River. Confidence of dry anomalies can reach 99%, and wet anomalies can reach 97.5%. El Niño(+) conditions show the same significantly dry pattern along the east coast, but at lower confidence intervals (Figure 19b). Significantly wet conditions can be seen along the Mississippi River, and a region of wet conditions is seen in the northern Rocky Mountains as well. Confidence in these wet anomalies range from 80 to 90 percent. El Niño(0) shows the same patterns as El Niño(+), except for the wet conditions in the Rocky Mountains (Figure 19c). Confidence in the wet conditions along the Mississippi is greater, while confidence in the dry conditions along the east coast is reduced. El Niño(-) shows marginally significant dry conditions in New England and marginally significant wet conditions in the northern plains (Figure 19d). No other regions during El Niño(-) exhibit any coherence.

during El Niño(-) exhibit any coherence.

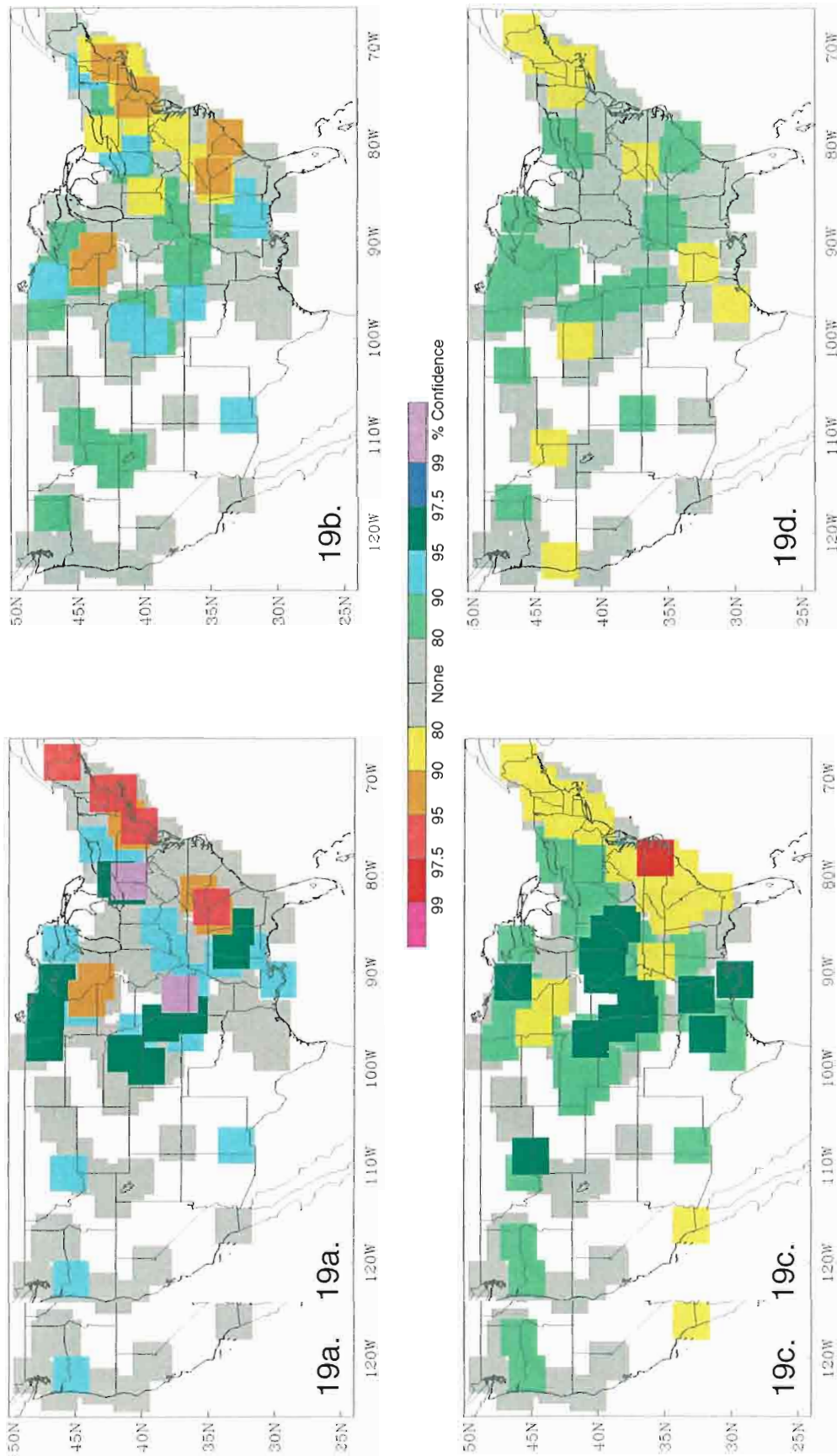


Figure 19. Confidence in (a) JAS El Niño precipitation anomalies, (b) JAS El Niño(+) precipitation anomalies, (c) JAS El Niño(0) precipitation anomalies, (d) JAS El Niño(-) precipitation anomalies. Cool colors indicate regions of statistically significant wet conditions; warm colors indicate regions of statistically significant dry conditions.

5) La Niña OND Patterns

(i) **Temperature.** The temperature anomalies associated with La Niña winters start to appear during fall (Figure 20a). A band of warm anomalies, ranging from 0.25 to 1.0°C above normal, extend from Texas north to southeastern Minnesota and Michigan. The Pacific states and the intermountain west are colder, with temperatures up to -1.0°C below normal.

OND temperatures are up to 1.0°C warmer than La Niña conditions in the Pacific Northwest during La Niña(+), and 1.0°C cooler in the Ohio Valley and Northeast (Figure 20b). These changes make the southern plains warmer by 0.5°C and the east cooler by up to 1.5°C than in La Niña. La Niña(0) OND sees temperatures 0.5 to 1.5°C in the northern Rocky mountains and plains, and the east coast warmer by 0.25 to 0.5°C (Figure 20c). This results in the typical La Niña warming extending eastward, while the cold anomalies in the west deepening by 1.0°C and extending northeastward. The north central plains and northeast are up to 1.0°C warmer during La Niña(-) OND (Figure 20d). This results in the northern plains and northeast 1.0°C warmer during La Niña(-) than seen in the La Niña climatology. There is little change during La Niña(-) and La Niña in the western U.S.

The cool anomalies along the Pacific coast and the warm anomalies in the southern plains during La Niña OND show confidence above 90% (Figure 21a). La Niña(+) OND also exhibits statistical significance of cool anomalies in California, but not the Pacific Northwest (Figure 21b). The confidence of the warm anomalies in the southern plains is weakened, while the cold anomalies in the northeast, seen only in La Niña(+), are significant at the 90% level. Confidence of the cool western anomalies remains the same during La Niña(0), while confidence in the warm anomalies in the southern plains is diminished (Figure 21c). La Niña(-) OND shows less confidence remains the same during La Niña(0), while confidence in the warm anomalies in the southern plains is diminished (Figure 21c). La Niña(-) OND shows less confidence in the cool western anomalies, while confidence of warm anomalies in the

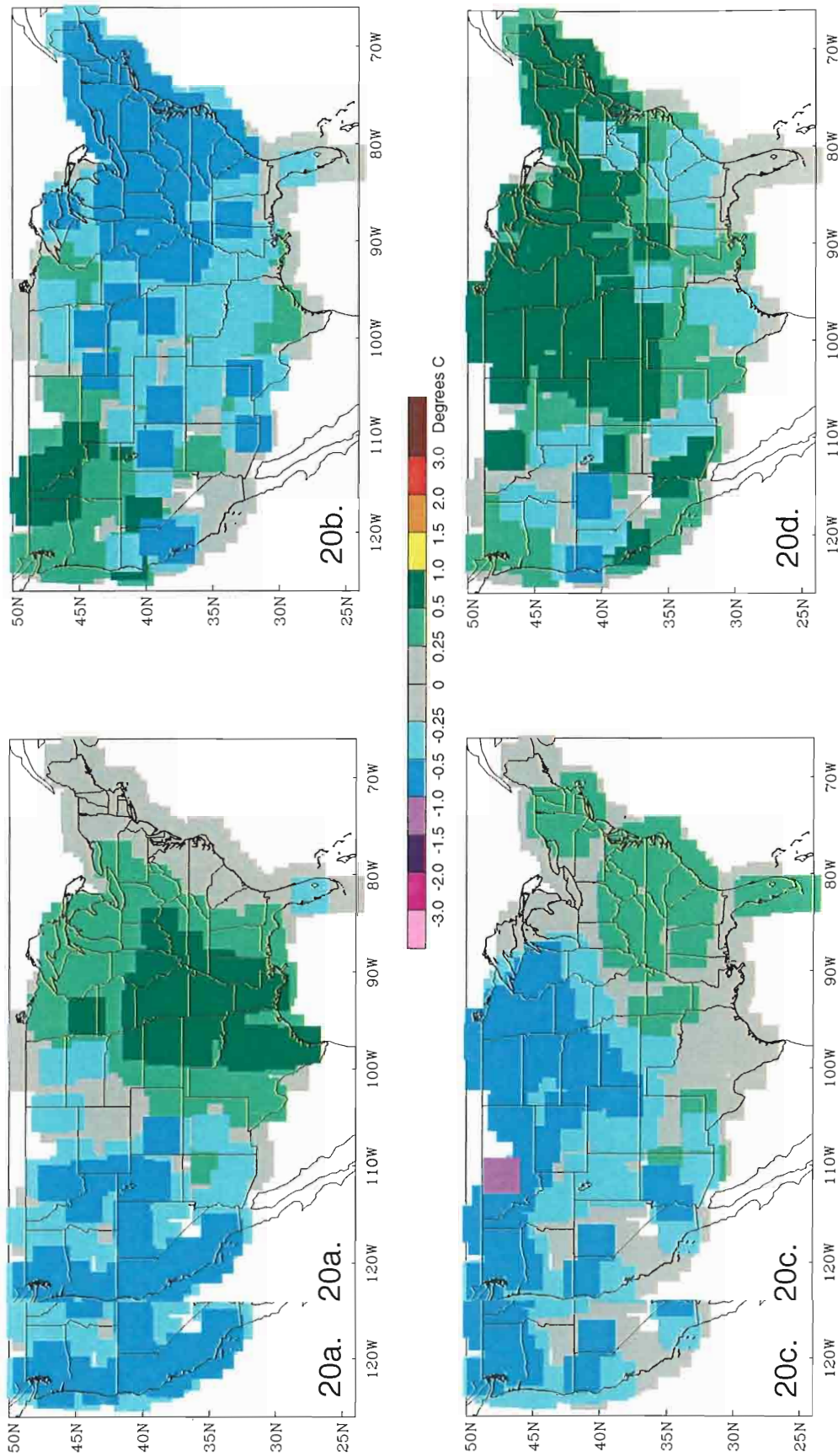


Figure 20a. La Niña temperature anomalies for OND. Difference between OND La Niña Temperature anomalies and (b) OND La Niña(+) temperature anomalies, (c) OND La Niña(0) temperature anomalies, (d) OND La Niña(-) temperature anomalies. Cool colors indicate regions of cold anomalies; warm colors indicate regions of warm

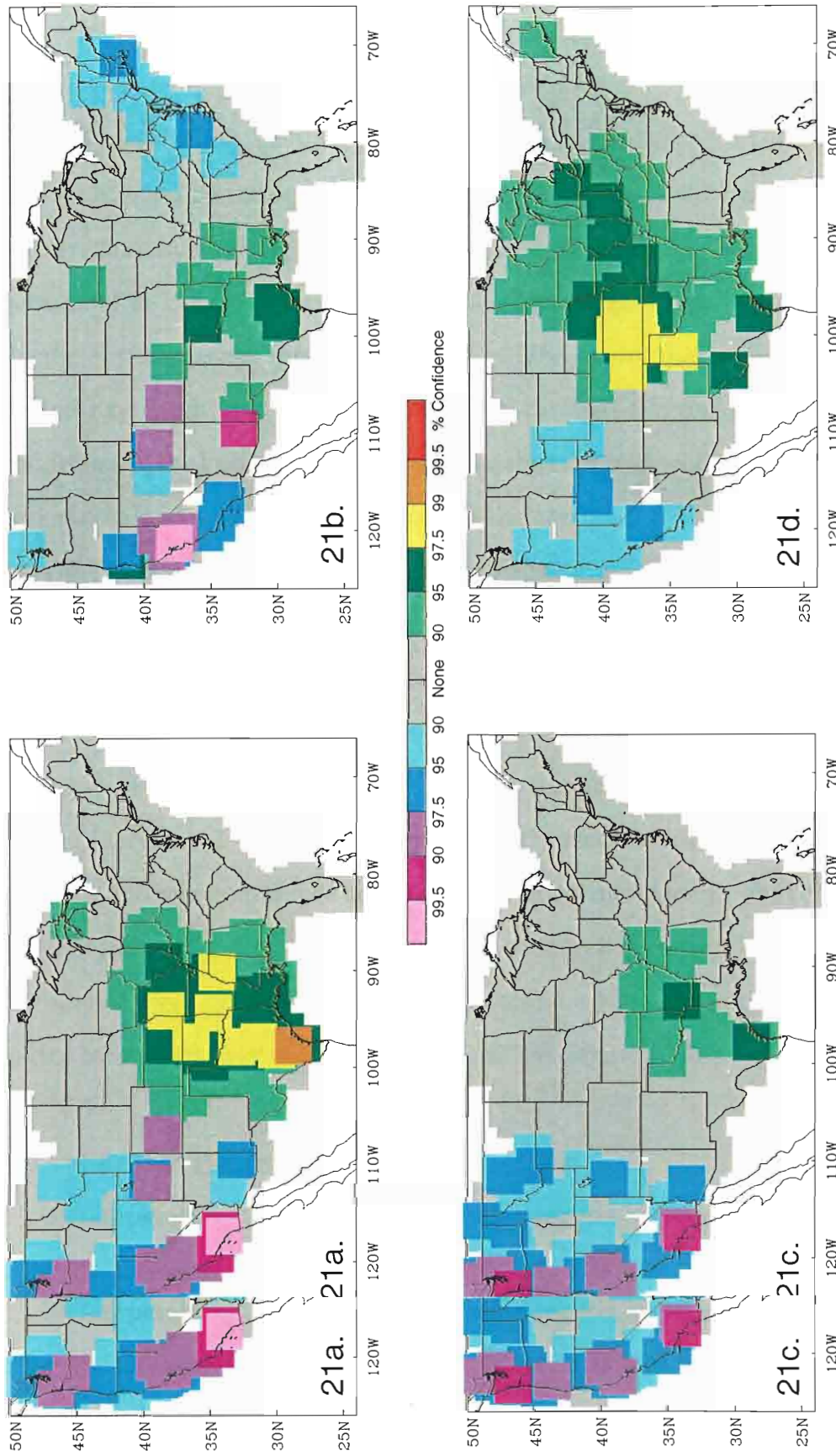


Figure 21. Cor21. Confidence in (a) OND La Niña temperature anomalies, (b) OND La Niña(+) temperature anomalies, (c) OND La Niña(0) temperature anomalies, (d) OND La Niña(-) temperature anomalies. Cool colors indicate regions of cold anomaly predictability above 90%; warm colors indicate regions of warm anomaly predictability above 90%.

central U.S. extends north to the western Great Lakes (Figure 21d). This is a result of warmer temperatures across this region during La Niña(-).

(ii) Precipitation. La Niña OND sees the eastern third of the United States drier by 10 - 20%, while the northern Rocky Mountains are 10-20% wetter (Figure 22a). The dry anomalies along the east coast are intensified by 10 - 20% in the La Niña(+) subset, while Nebraska is up to 30% wetter (Figure 22b). The wet conditions in the Pacific Northwest are intensified by up to 30% during La Niña(0) fall, while expected dry conditions in the southeast are negated (Figure 22c). La Niña(-) dry conditions in the Pacific Northwest weaken the expected wet anomalies there, while wet anomalies weaken dry conditions in the northeast (Figure 22d).

The Deep South and New England are significantly dry during La Niña OND, while the northern Rocky Mountains are significantly wet (Figure 23a). Confidence in these regions can exceed 97.5%. Confidence in the dry anomalies in New England during La Niña(+) increases, while confidence in the Deep South dry anomalies weakens. No coherent regions of confidence are seen in the Rocky Mountains during La Niña(+). However, the significantly wet conditions there appear in La Niña(0), and the confidence in those conditions increases to above 99% (Figure 23c). Significantly dry conditions are still seen in the eastern U.S., but at a lower confidence level, particularly in New England. La Niña(-) shows weak confidence in dry conditions over most of the eastern U.S. (Figure 23d).

6) La Niña JFM Patterns

(i) Temperature. During winter (Figure 24a), the warm anomalies in the south intensify and extend from New Mexico to Florida, as well as northward to the Ohio

(i) Temperature. During winter (Figure 24a), the warm anomalies in the south intensify and extend from New Mexico to Florida, as well as northward to the Ohio Valley. The Deep South sees the warmest anomalies, reaching 1.5°C above the neu-

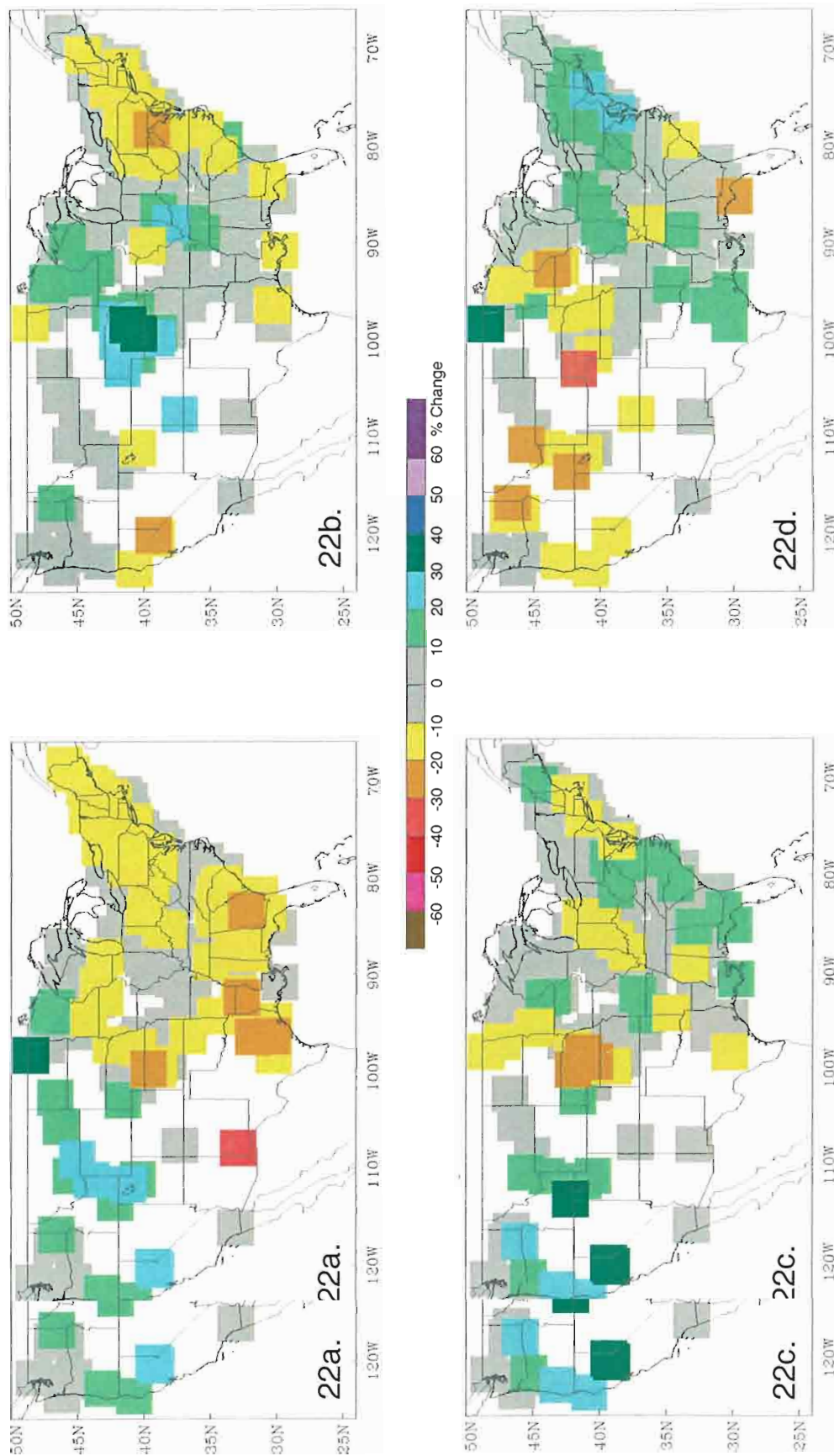


Figure 22a. La Niña precipitation anomalies for OND. Difference between OND La Niña precipitation anomalies and (b) OND La Niña(+ Niña(+)) precipitation anomalies, (c) OND La Niña(0) precipitation anomalies, (d) OND La Niña(-) precipitation anomalies. Cool colors indicate regions of wet anomalies; warm colors indicate regions of dry anomalies.

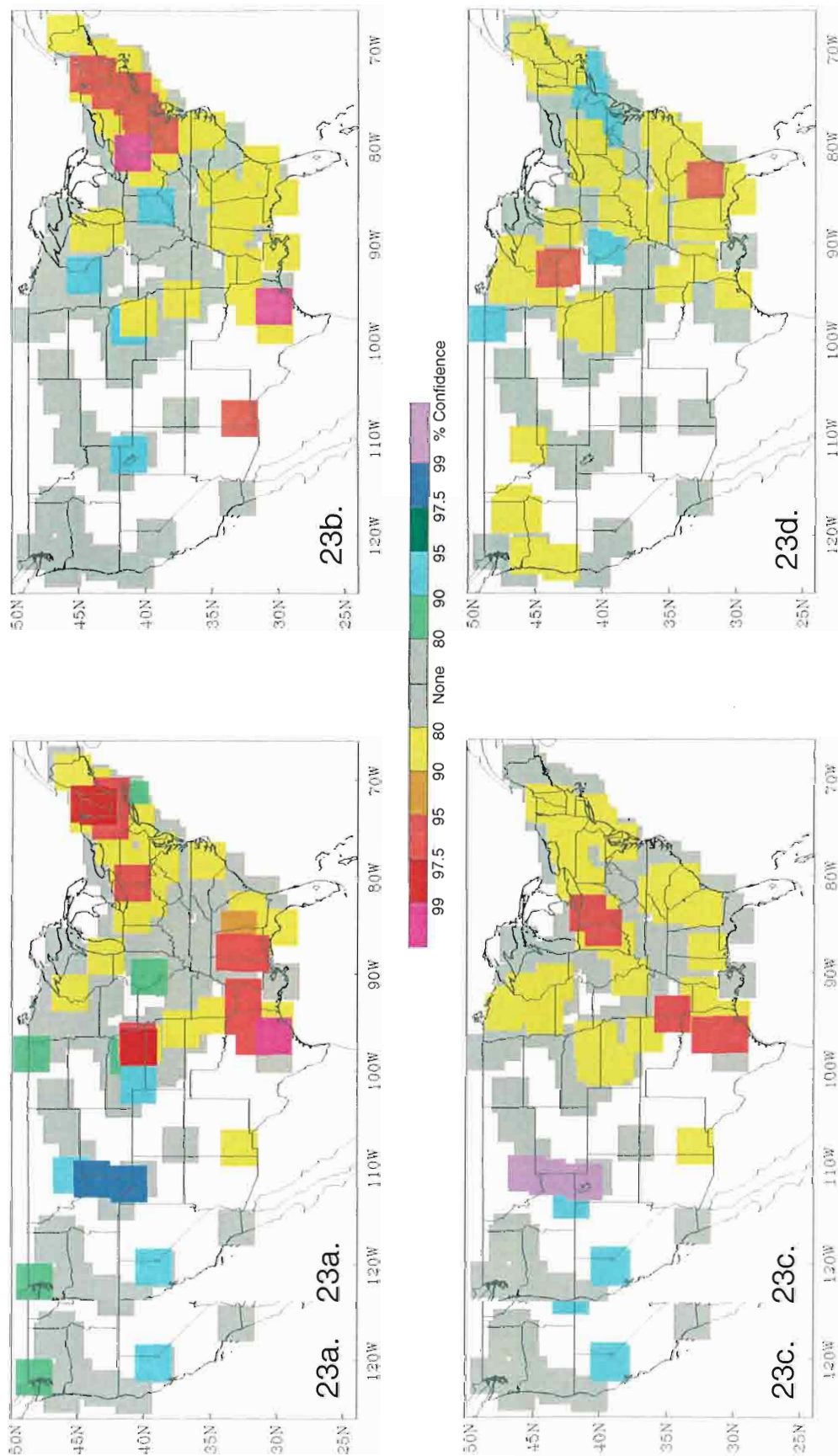


Figure 23. Confidence in (a) OND La Niña precipitation anomalies, (b) OND La Niña(+) precipitation anomalies, (c) OND La Niña(0) precipitation anomalies, (d) OND La Niña(-) precipitation anomalies. Cool colors indicate regions of statistically significant wet conditions; warm colors indicate regions of statistically significant dry conditions.

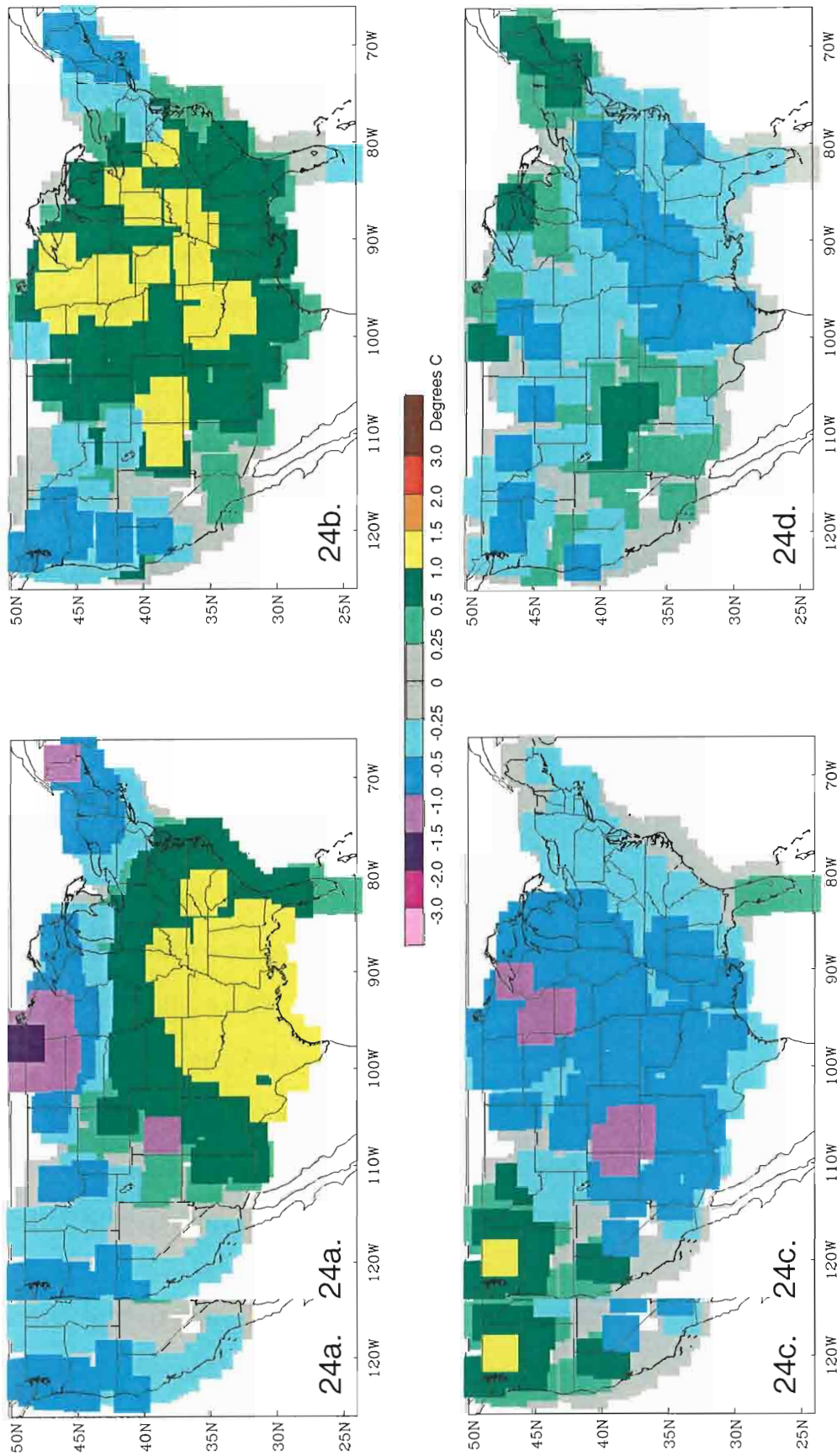


Figure 24a. La Niña temperature anomalies for JFM. Difference between JFM La Niña Temperature anomalies and (b) JFM La Niña(+ Niña(+)) temperature anomalies, (c) JFM La Niña(0) temperature anomalies, (d) JFM La Niña(-) temperature anomalies. Cool colors indicate regions of cold anomalies; warm colors indicate regions of warm anomalies.

tral ENSO conditions. The intermountain west returns to normal conditions, while the Pacific states remain about 0.5°C below normal. Winter also sees New England and the high plains becoming colder than normal, with seasonal temperatures up to 1.5°C colder in New England and 2°C degrees colder in North Dakota and Minnesota.

La Niña(+) sees an intensification of the warm anomalies seen in the south and east (Figure 24b). Temperatures in the region are $1.0 - 1.5^{\circ}\text{C}$ warmer and encompass most of the United States, except for New England and the Pacific Coast, where conditions are up to 1.0°C cooler. These changes intensify that expected La Niña pattern in all regions except the northern plains, there the cool anomalies are diminished in magnitude. While La Niña(+) mostly intensifies expected La Niña anomalies, La Niña(0) tends to weaken them (Figure 24c). Conditions in the central plains are cooler by $1.0 - 1.5^{\circ}\text{C}$, weakening the warm anomalies typically seen. These cool anomalies reach the Canadian border, where they intensify the cool anomalies seen during La Niña. Meanwhile, the Pacific Northwest is 1.0°C warmer in La Niña(0), which weakens expected cold anomalies there. The southeastern La Niña JFM warm anomalies are also weakened by the $0.5 - 1.0^{\circ}\text{C}$ cooler conditions seen in La Niña(-) (Figure 24d). Cooler conditions in the Pacific Northwest intensify conditions there, while warmer temperatures weaken the cold anomalies present in New England. Finally, a 0.5°C warming in the desert southwest extends La Niña warm anomalies west into Arizona.

The warming in the southeast during La Niña JFM is significant above the 90% level from Illinois south, with much of Texas and the gulf coast seeing confidence above 99.5% (Figure 25a). New England, the northern plains, and the Pacific coast, which all see cooler conditions during this time, are also statistically significant above 99.5% (Figure 25a). New England, the northern plains, and the Pacific coast, which all see cooler conditions during this time, are also statistically significant above 90%. La Niña(+) sees an increase in confidence of the warm anomalies in the

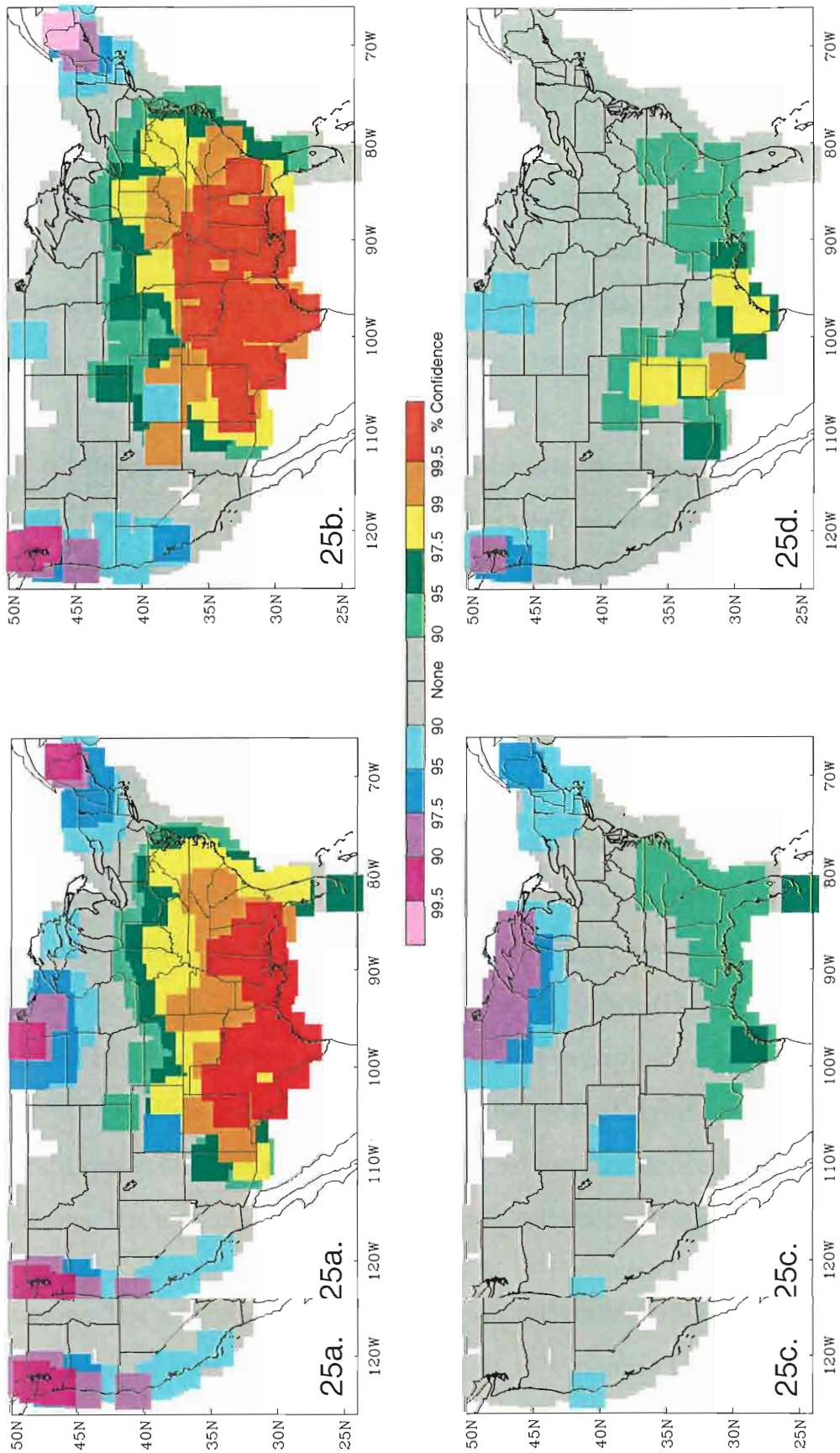


Figure 25. Confidence in (a) JFM La Niña(+) temperature anomalies, (b) JFM La Niña(0) temperature anomalies, (c) JFM La Niña(-) temperature anomalies, (d) JFM La Niña(0) terra(0) temperature anomalies. Cool colors indicate regions of cold anomaly predictability above 90%; warm colors indicate regions of warm anomaly predictability above 90%.

southeast, but no increased spatial coverage of confidence (Figure 25b). The Pacific Coast and New England see confidence similar to La Niña, while confidence of cold anomalies in the northern plains disappears, due to the reduced cooling in the region. The warm anomalies in the south and cool anomalies in New England show less confidence during La Niña(0) JFM, while confidence in cool anomalies expands in the western Great Lakes (Figure 25c). Only the confidence of cool anomalies in the Pacific Northwest remain unchanged from La Niña JFM levels in the La Niña(-) subset (Figure 25d). All other regions show weaker or no confidence.

(ii) Precipitation. La Niña JFM precipitation anomalies exhibit a banding pattern across the eastern half of the United States (Figure 26a). The central plains are up to 50% drier from Oklahoma to South Dakota. East of there, a band of 10-20% wetter anomalies extends from Tennessee to New York. Finally, another dry band of weather sits in along the eastern coast, from Florida to New Jersey. In the west, Oregon sees 10-20% wetter conditions.

The La Niña(+) subset sees conditions 20% wetter in the southwest, and the Deep South 10-20% drier (Figure 26b). The banding pattern seen in La Niña is reversed in La Niña(0), essentially negating any precipitation anomalies seen during La Niña JFM (Figure 26c). The La Niña banding is intensified during La Niña(-), however, with La Niña anomalies increased by 10-20% (Figure 26d).

The banding patterns seen in La Niña JFM precipitation anomaly patterns are also statistically significant (Figure 27a). The greatest significance lies with the dry conditions in Nebraska and the southeast, where confidence exceeds 99% at many stations. The wet conditions in Washington and the band extending from Maine to Tennessee generally are significant at the 80 to 95 percent levels, though some locations. The wet conditions in Washington and the band extending from Maine to Tennessee generally are significant at the 80 to 95 percent levels, though some locations within those regions exhibit greater confidence. Similar significantly dry con-

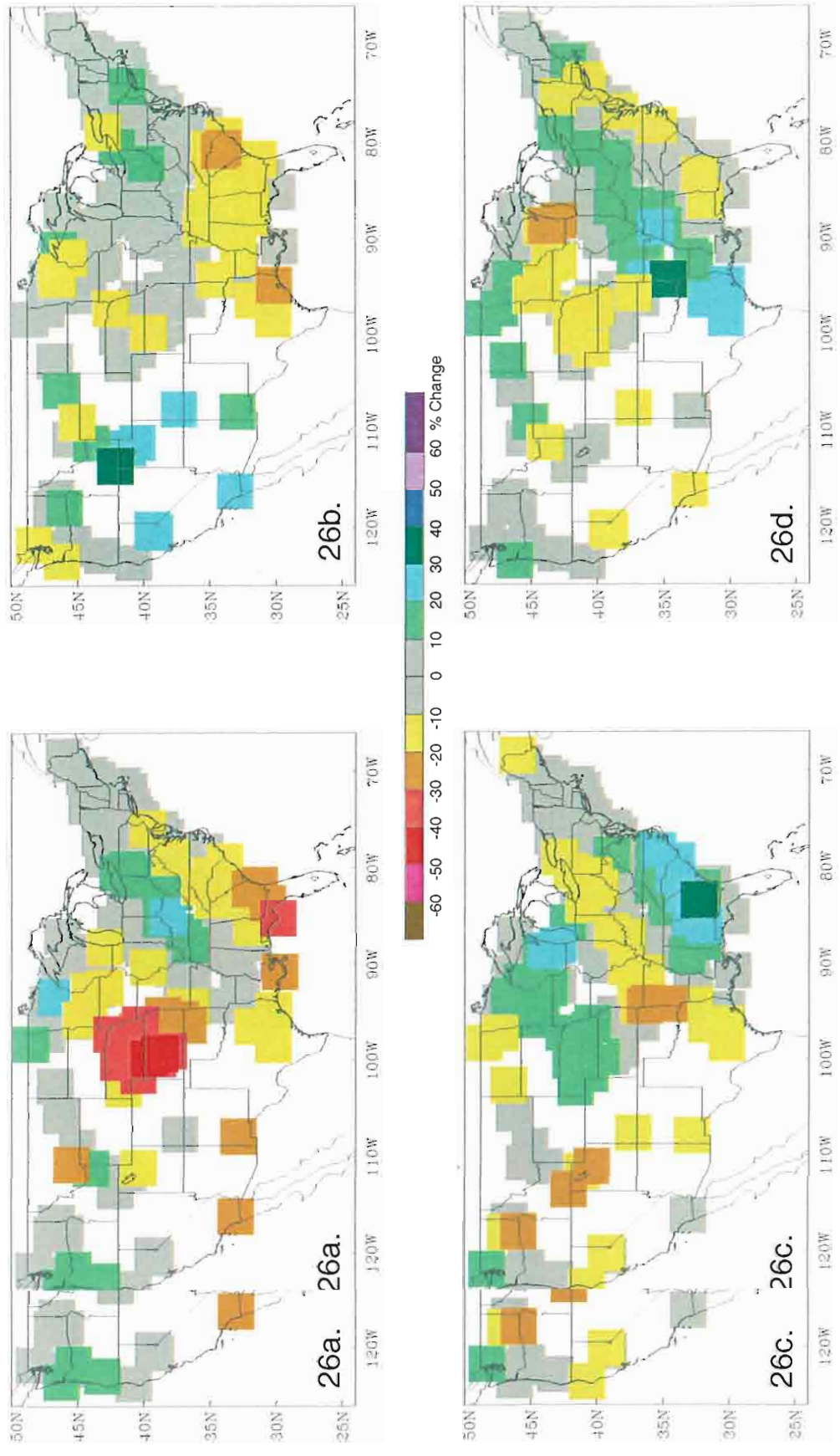


Figure 26a. La Niña precipitation anomalies for JFM. Difference between JFM La Niña precipitation anomalies and (b) JFM La Niña(+ Niña(+)) precipitation anomalies, (c) JFM La Niña(0) precipitation anomalies, (d) JFM La Niña(-) precipitation anomalies. Cool colors indicate regions of wet anomalies; warm colors indicate regions of dry anomalies.

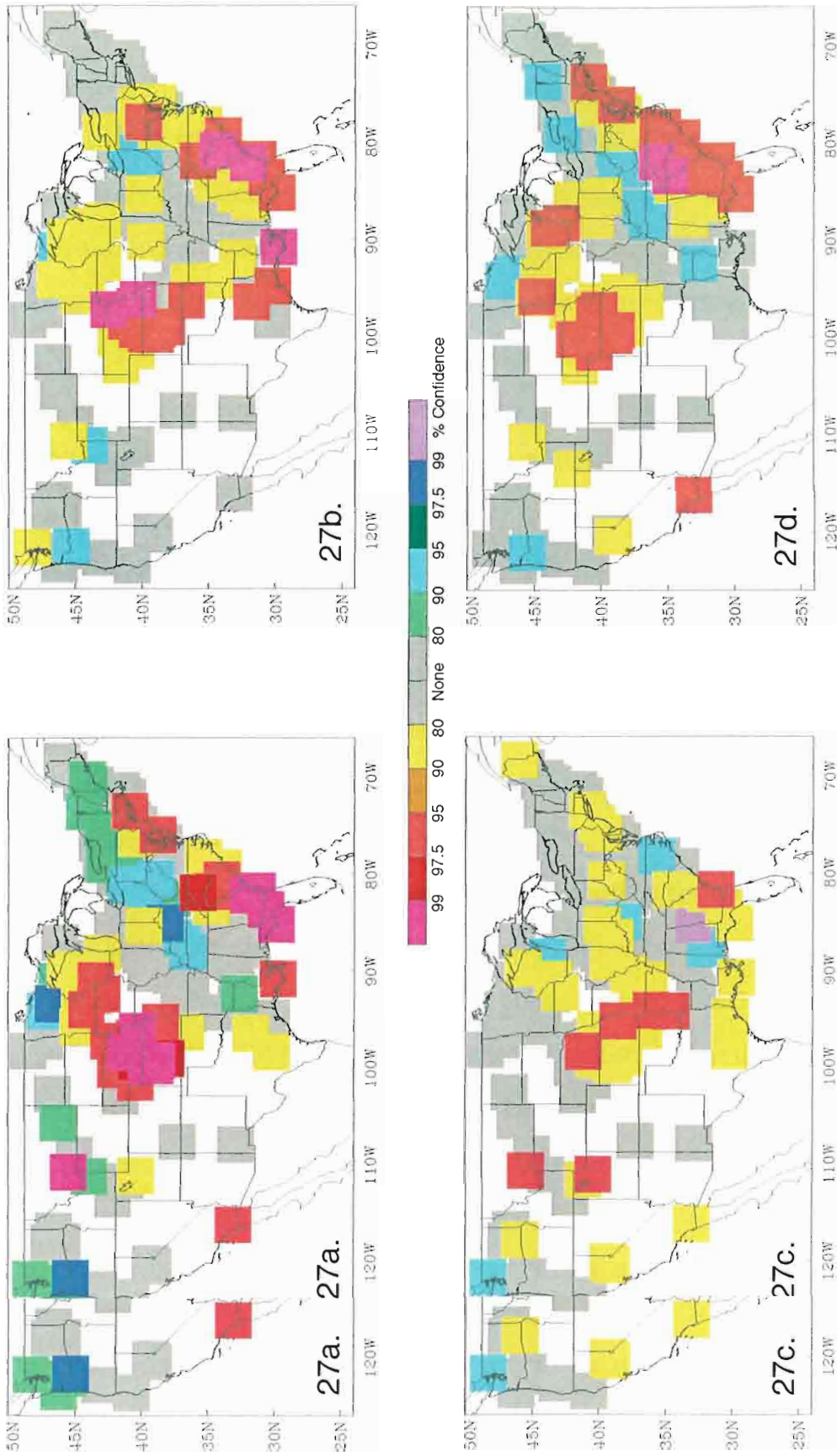


Figure 27. Confidence in (a) JFM La Niña precipitation anomalies, (b) JFM La Niña(+) precipitation anomalies, (c) JFM La Niña(0) precipitation anomalies, (d) JFM La Niña(-) precipitation anomalies. Cool colors indicate regions of statistically significant wet conditions; warm colors indicate regions of statistically significant dry conditions.

ditions are seen during La Niña(+), with stronger confidence in Texas and lesser confidence in the upper Mississippi valley (Figure 27b). Coherent regions of significantly wet conditions are not seen in the La Niña(+) subset. Large areas of significantly wet conditions are not seen during La Niña(0) as well (Figure 27c). The significantly dry conditions are still present, but at a lower confidence interval. La Niña(-) shows an expanded regions of significantly dry conditions in the southeast (as compared to the other 3 cases), while conditions in Nebraska are comparable to La Niña and La Niña(+); (Figure 27d). Significantly wet conditions occur in the same band from Tennessee to Vermont as seen in the La Niña confidence plot (Figure 27a), but the confidence level during La Niña(-) is less than during La Niña.

7) La Niña AMJ Patterns

(i) **Temperature.** By AMJ, the deep warm and cold anomalies seen during La Niña winter are replaced by cooler conditions over most of the United States (Figure 28a). Temperatures changes average 0.25–0.5°C cooler over most of the country, excluding Texas and New Mexico. A region of deeper cooling extends over the Appalachians with maximum anomalies of 1.0°C.

The cooling over the Appalachians is more intense in the La Niña(+) subset and extends further southwest, into Texas (Figure 28b), increasing the cool anomalies seen during La Niña by 1.0°C. The Pacific states also see a further cooling of 0.5°C as well. The La Niña(0) AMJ once again shows conditions that interfere with the La Niña pattern (Figure 28c). The dominant La Niña(0) pattern is warming of 0.25–1.0°C across the Plains and east to the Mid-Atlantic states. This results in warm anomalies across the plains, where slightly cooler conditions are typically expected. Cool anomalies are limited to the northeast, where cooler La Niña(0) temperature anomalies across the plains, where slightly cooler conditions are typically expected. Cool anomalies are limited to the northeast, where cooler La Niña(0) temperature intensify the La Niña anomalies by 0.5°C. The anomaly patterns in the west are

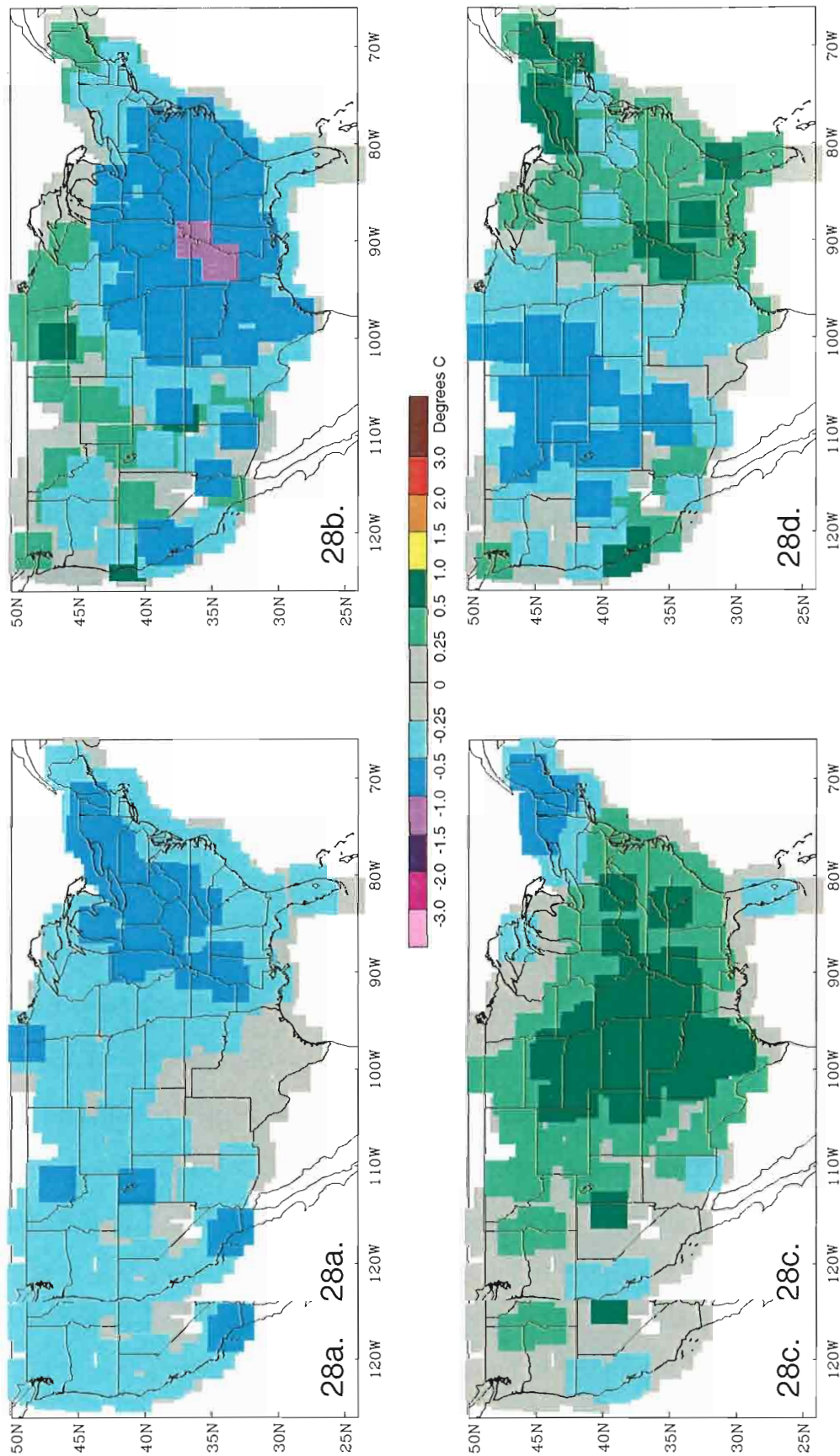


Figure 28a. La Niña temperature anomalies for AMJ. Difference between AMJ La Niña Temperature anomalies and (b) AMJ La Niña(+ Niña(+)) temperature anomalies, (c) AMJ La Niña(0) temperature anomalies, (d) AMJ La Niña(-) temperature anomalies. Cool colors indicate regions of cold anomalies; warm colors indicate regions of warm anomalies.

similar in both La Niña(0) and La Niña. Finally, La Niña(-) AMJ patterns indicate cooler conditions in the Rocky Mountains and northern Plains and a warming in the east (Figure 28d). The cooling of 0.5 - 1.0°C makes the Rocky Mountains and northern plains colder than in La Niña, while the 0.5-1.0°C warming in the east diminishes the expected cool anomalies there.

Confidence in La Niña AMJ anomalies are seen east of the Mississippi and in the Pacific Northwest (Figure 29a). La Niña(+) shows the same confidence of cool anomalies in the west, but shows an increase in statistical significance for the cool anomalies in the east (Figure 29b). Most of the Deep South sees cool anomalies predictable at the 99.5% level during La Niña(+) AMJ. The confidence of La Niña(0) AMJ anomalies are weaker in all regions except New England, where the confidence of cool anomalies increases (Figure 29c). The cooling in the west and the majority of the east disappears, due to warmer conditions in the region. This warming even shows some confidence in the southern plains above the 90% level. La Niña(-) anomalies are most significant in the northern Rocky Mountains, due to increased cooling in the region (Figure 29d). The cooling in other regions show no coherent confidence pattern.

(ii) Precipitation. La Niña precipitation anomalies weaken by AMJ (Figure 30a). Conditions are 10% dry along the northeastern coast and the upper Mississippi River. The Tennessee River valley is marginally wet, which intensifies by 20% during La Niña(+) (Figure 30b). These wet anomalies also extend and over most of the Deep South. The dry conditions in the upper Mississippi River intensify by 10 - 20% as well. La Niña(0) and La Niña(-) both show opposite patterns, with dry conditions in the southeast and wet conditions in the upper Mississippi Valley (Figure 20% as well. La Niña(0) and La Niña(-) both show opposite patterns, with dry conditions in the southeast and wet conditions in the upper Mississippi Valley (Fig-

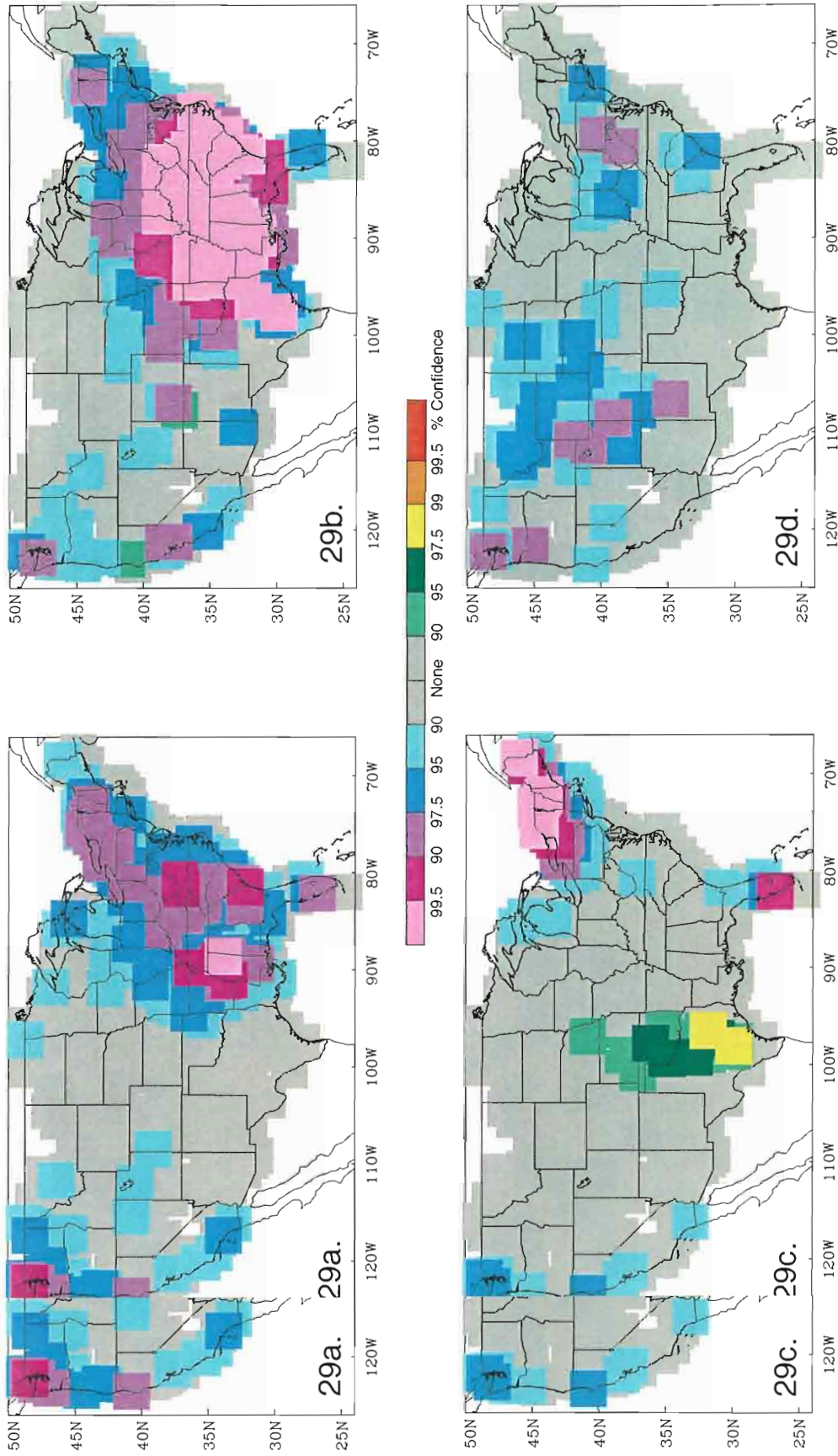


Figure 29. Confidence in (a) AMJ La Niña temperature anomalies, (b) AMJ La Niña(+) temperature anomalies, (c) AMJ La Niña(-) temperature anomalies, (d) AMJ La Niña(0) temperature anomalies. Cool colors indicate regions of cold anomaly predictability above 90%; warm colors indicate regions of warm anomaly predictability above 90%.

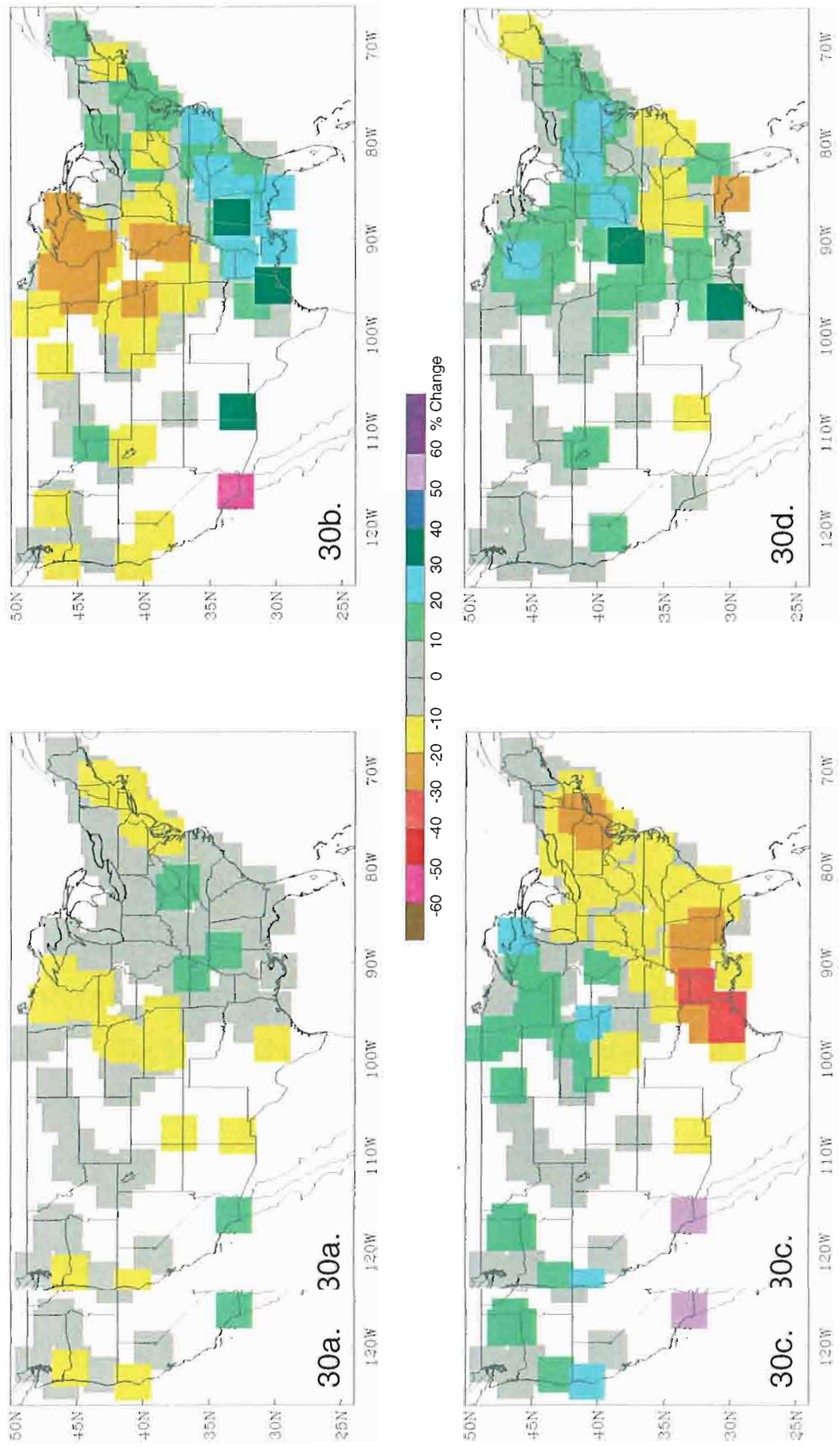


Figure 30a. La Niña precipitation anomalies for AMJ. Difference between AMJ La Niña precipitation anomalies and (b) AMJ La Niña(+ Niña(+)) precipitation anomalies, (c) AMJ La Niña(0) precipitation anomalies, (d) AMJ La Niña(-) precipitation anomalies. Cool colors indicate regions of wet anomalies; warm colors indicate regions of dry anomalies.

ures 30c&d). The two subset's anomalies differ in the northeast; La Niña(0) is dry, La Niña(-) is wet.

The dry conditions on southern New England during La Niña AMJ are significant at the 99% level (Figure 31a). The upper Mississippi valley and the Mid-Atlantic states also see significantly dry conditions, but at lower confidence intervals. The Ohio valley is significantly wet, with a confidence interval of 80 to 95 percent. The significantly dry anomalies in the upper Mississippi valley exhibit stronger confidence during La Niña(+), with some locations exceeding the 99% threshold (Figure 31b). New England remains significantly dry, while regions of the Columbia River are dry as well. Spotty areas of the deep south see significantly wet conditions. The La Niña(0) AMJ subset show that no regions which are significantly wet (Figure 31c). New England remains significantly dry, with confidence levels above 95% spreading south into Maryland and Virginia. The deep south and Kansas also show significantly dry conditions. La Niña(-) also shows dry conditions in New England, but at an overall lower confidence interval (Figure 31d). La Niña(-) also shows the Ohio Valley is significantly wet at a confidence level of 90 to 50 percent.

8) La Niña JAS Patterns

(i) **Temperature.** The general cool pattern seen in La Niña AMJ persists in the northern states during JAS, but the southern U.S. returns to normal conditions (Figure 32g). The largest changes are found in the northern plains and desert southwest, with anomalies ranging from 0.25 - 1.0°C below neutral JAS conditions.

The cooling seen in La Niña JAS is stronger in the La Niña(+) subset, with cool anomalies dominating much of the country (Figure 32b). While most of the U.S. is only 0.25 - 0.5°C colder during La Niña(+), the Pacific states can be up to 1.5°C anomalies dominating much of the country (Figure 32b). While most of the U.S. is only 0.25 - 0.5°C colder during La Niña(+), the Pacific states can be up to 1.5°C colder. Only Texas exhibits warm anomalies, which shows no temperature anoma-

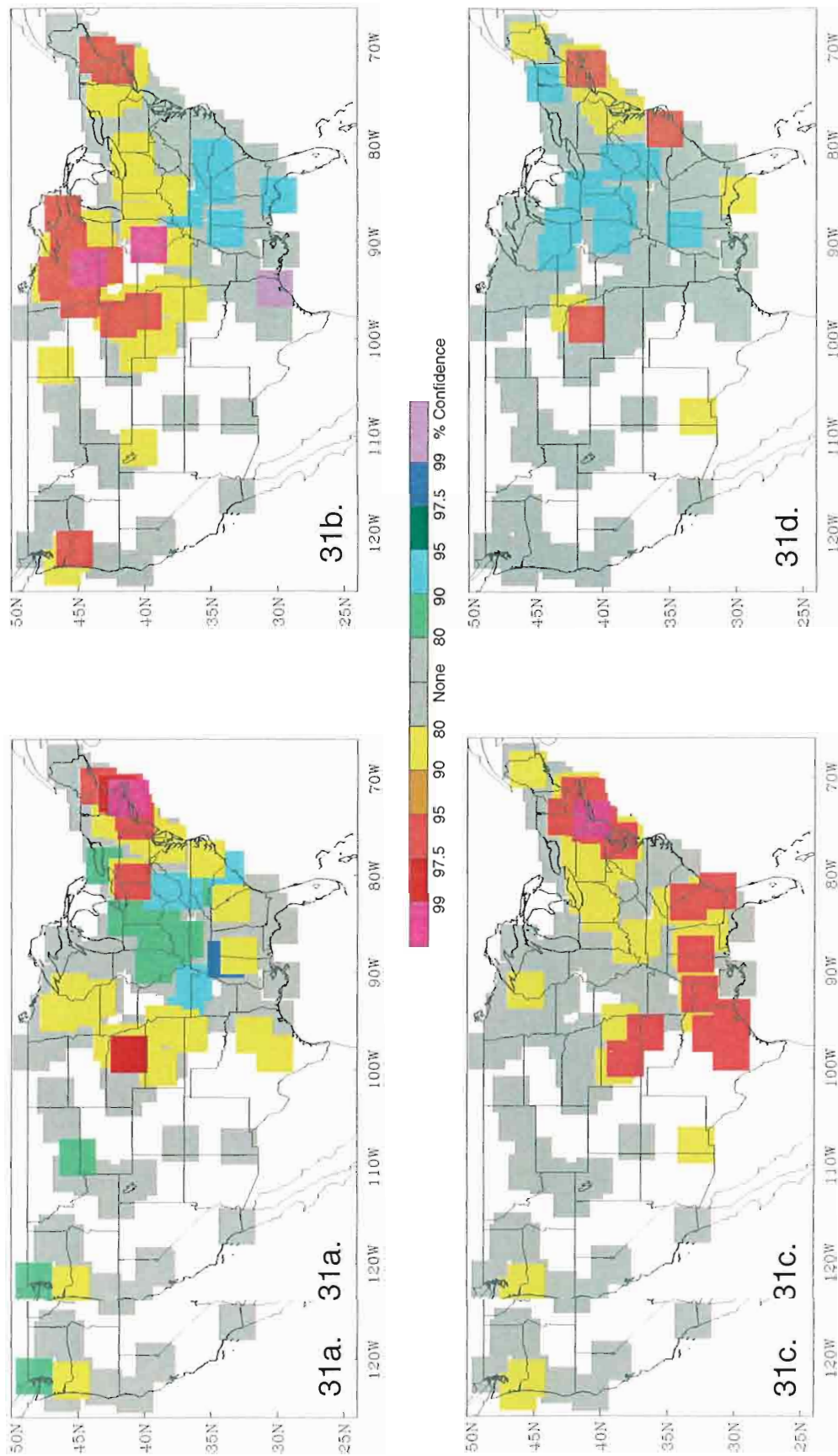


Figure 31. Confidence in (a) AMJ La Niña precipitation anomalies, (b) AMJ La Niña(+) precipitation anomalies, (c) AMJ La Niña(0) precipitation anomalies, (d) AMJ La Niña(-) precipitation anomalies. Cool colors indicate regions of statistically significant wet conditions; warm colors indicate regions of statistically significant dry conditions.

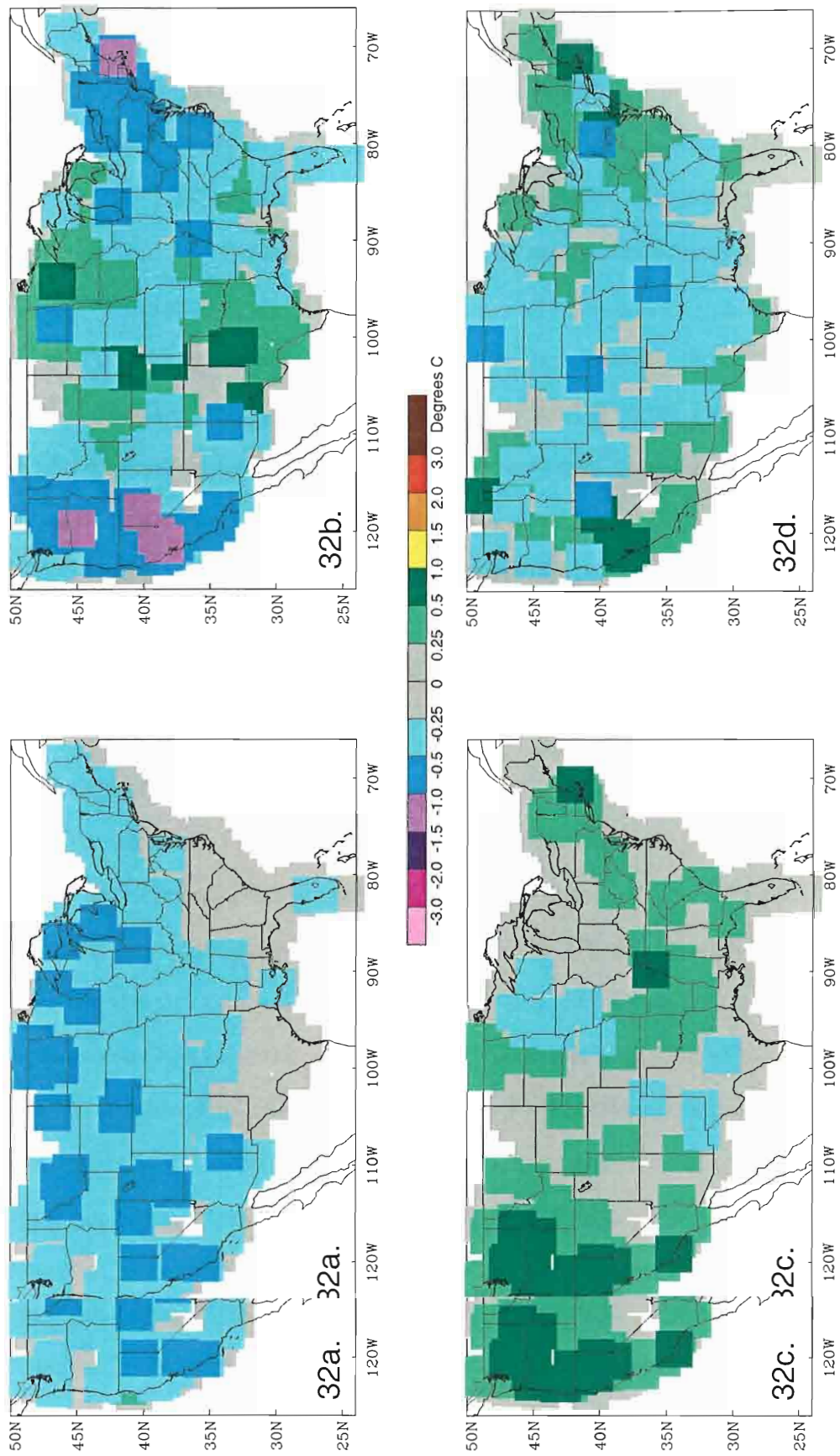


Figure 32a. La Niña temperature anomalies for JAS. Difference between JAS La Niña Temperature anomalies and (b) JAS La Niña(+) temperature anomalies, (c) JAS La Niña(0) temperature anomalies, (d) JAS La Niña(-) temperature anomalies. Cool colors indicate regions of cold anomalies; warm colors indicate regions of warm anomalies.

lies in the La Niña climatology. Warm conditions over the Pacific States during La Niña(0) JAS negate the cool anomalies typically seen there (Figure 32c). In fact, the Pacific Northwest becomes warm during La Niña(0), when the region is typically cooler by 0.25°C. Other La Niña(0) JAS anomalies lack spatial coherence. La Niña(-) JAS is 0.25-0.5°C cooler than La Niña over much of the country (Figure 32d). The cooling intensifies the La Niña pattern over much of the country, particularly in the Rocky Mountains.

The continued cooling during La Niña JAS remains significant over the 90% level in the southwest, north, and New England (Figure 33a). La Niña(+) shows increased confidence over La Niña in the west and New England, but confidence in the northern anomalies are not seen (Figure 33b). In contrast, La Niña(0) shows no coherent predictable anomaly patterns during JAS (Figure 33c). La Niña(-) shows confidence in the cool anomalies in the intermountain west, but the confidence levels are less than La Niña JAS.

(ii) Precipitation. New England is 10-20% drier during La Niña JAS than in ENSO neutral conditions (Figure 34a). Wet conditions are present in the Tennessee Valley and central pacific states. All three subsets of La Niña JAS show spotty anomaly difference patterns. La Niña(+) JAS is 20% wetter in New England, counteracting the dry conditions there (Figure 34b). The Ohio valley is 10% wetter, but the western Gulf states become drier. La Niña(0) is highlighted by 20% drier conditions in Washington, the central plains, and Mid-Atlantic states (Figure 34c). Also present are wet conditions along the western Gulf, intensifying La Niña conditions there. La Niña(-) JAS is characterized by New England and California being 10% drier, while Washington and Minnesota are 10% wetter (Figure 34d). there. La Niña(-) JAS is characterized by New England and California being 10% drier, while Washington and Minnesota are 10% wetter (Figure 34d).

New England once again is significantly dry during La Niña JAS, while the

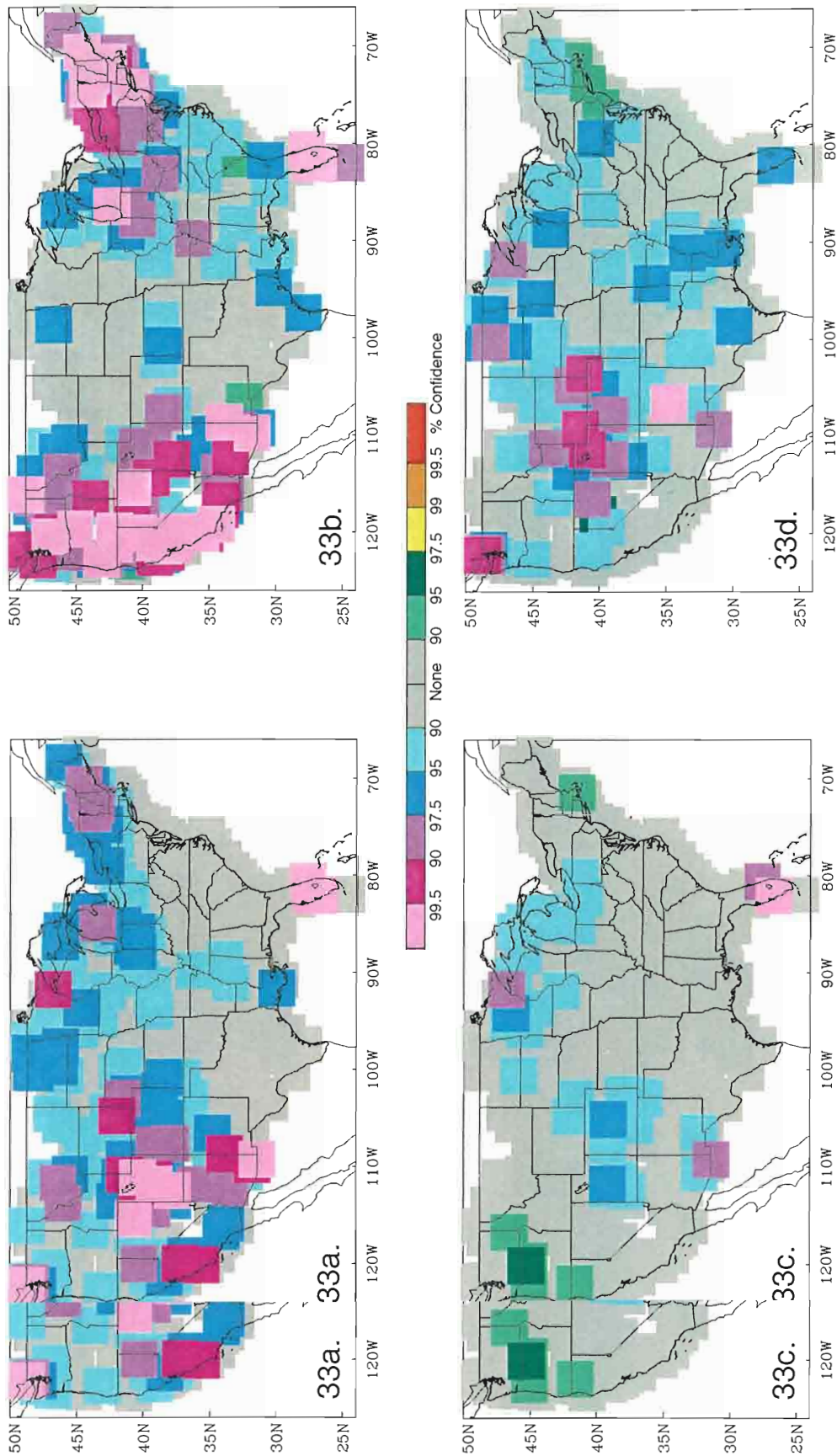


Figure 33. Confidence in (a) JAS La Niña temperature anomalies, (b) JAS La Niña(+) temperature anomalies, (c) JAS La Niña(0) temperature anomalies, (d) JAS La Niña(-) temperature anomalies. Cool colors indicate regions of cold anomaly predictability above 90%; warm colors indicate regions of warm anomaly predictability above 90%.

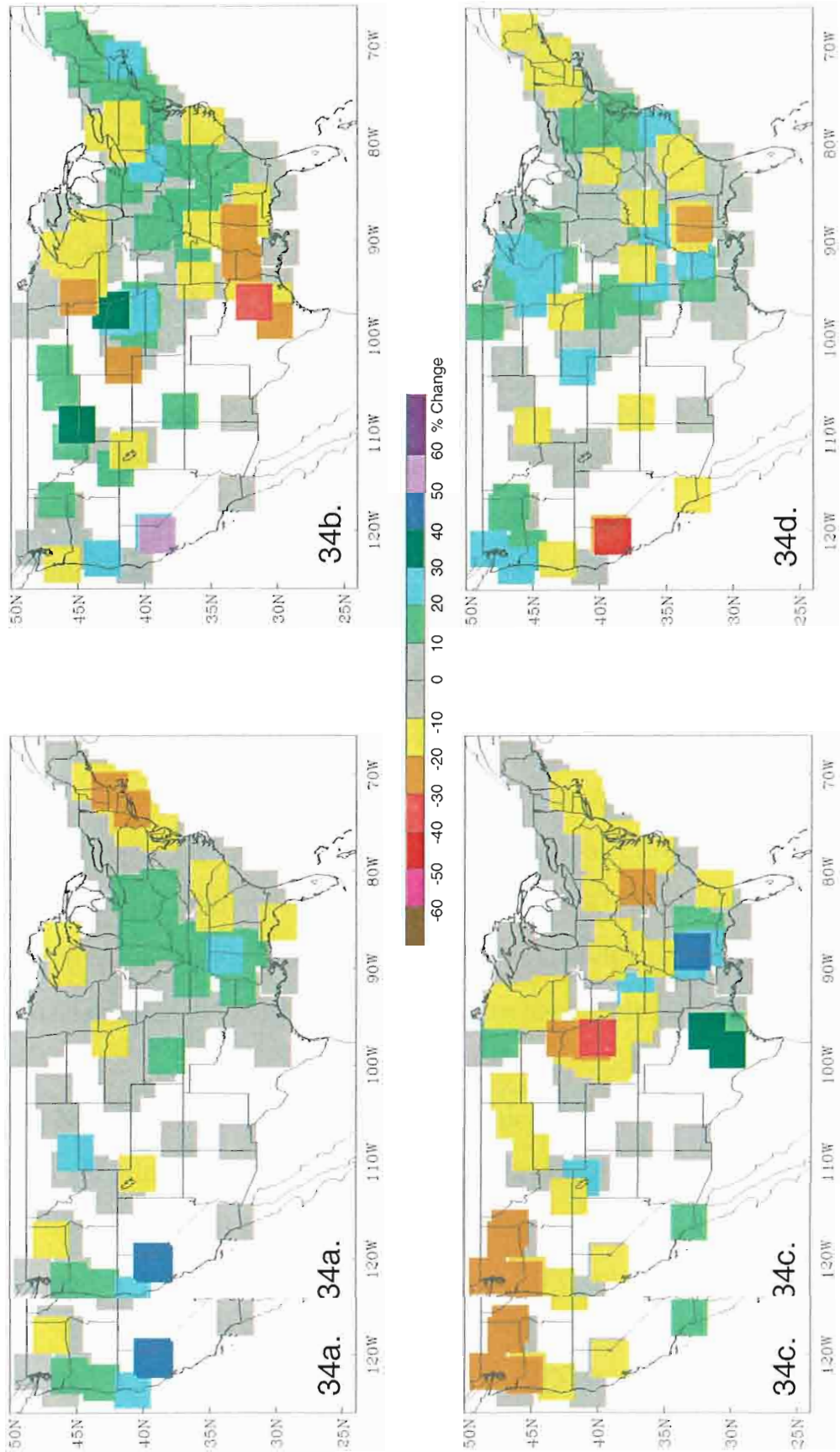


Figure 34a. La Niña precipitation anomalies for JAS. Difference between JAS La Niña precipitation anomalies and (b) JAS La Niña(+ Niña(+)) precipitation anomalies, (c) JAS La Niña(0) precipitation anomalies, (d) JAS La Niña(-) precipitation anomalies. Cool colors indicate regions of wet anomalies; warm colors indicate regions of dry anomalies.

Ohio and Tennessee are significantly wet (Figure 35a). Confidence levels can exceed 97.5% in New England, while some stations in the Ohio and Tennessee river valleys can exceed 99%. Confidence in La Niña(+) precipitation anomalies are generally spotty and scattered (Figure 35b). Two regions that do show some coherence are the Mid-Atlantic States and the upper Mississippi valley, which both exhibit significantly dry conditions. La Niña(0) JAS is dominated by significantly dry conditions from Nebraska east to Maine (Figure 35c). Maximum significance in these dry patterns is in Nebraska and southern New England, with confidence levels between 97.5 and 99 percent. Significant precipitation anomalies are very spotty and statistically weak during La Niña(-), with only coherent regions of dry conditions in the southeast and New England (Figure 35d). Confidences in these dry conditions are typically 80 to 90 percent. Spotty significance in wet conditions is seen elsewhere, but lack coherence.

b. JFM Cumulative Probability Distributions

Inverse cumulative probability distributions of representative stations are given only for JFM, due to the strength of the ENSO/PDO signal during this time, as well as for brevity. Distributions in regions showing temperature and precipitation changes in different ENSO/PDO states behave similarly in other seasons.

1) El Niño/PDO Temperature Distributions

El Niño temperature anomalies in Florida during JFM are typically 1.0 to 1.5°C below neutral ENSO temperatures. The conditions are relatively unchanged during El Niño(+), but conditions are up to 1.0°C colder during El Niño(0) and up to 1.5°C below neutral ENSO temperatures. The conditions are relatively unchanged during El Niño(+), but conditions are up to 1.0°C colder during El Niño(0) and up to 1.5°C during El Niño(-). A representative station showing these changes is Fort

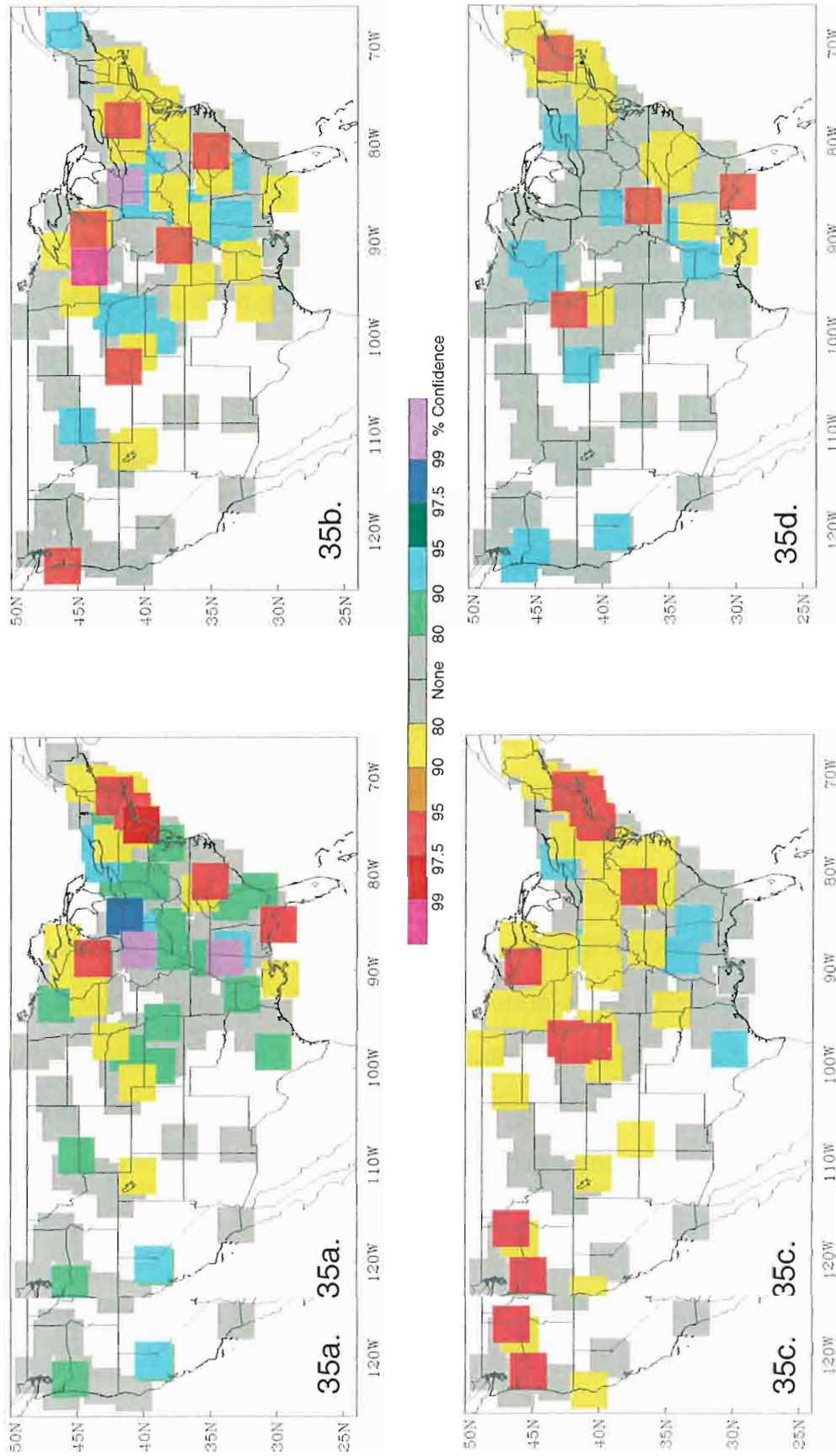


Figure 35. Confidence in (a) JAS La Niña(+) precipitation anomalies, (b) JAS La Niña(0) precipitation anomalies, (c) JAS La Niña(-) precipitation anomalies, (d) JAS La Niña(-) precipitation anomalies. Cool colors indicate regions of statistically significant wet conditions; warm colors indicate regions of statistically significant dry conditions.

Myers, FL (Figure 36). During El Niño(+) there is a 50% probability that your average seasonal temperature will be 18.5°C or more. In comparison, the probability of the seasonal temperature being at least 18.5°C during El Niño(0) and El Niño(-) are 0% and 100%, respectively. Alternatively, we can also examine other probability thresholds. For example the JFM average temperature exceeds 17.0°C 90% of the time. This seasonal temperature is exceeded 65% of the time during El Niño(0), 80% of the time during El Niño(+) and 100% of the time during El Niño(-). At the other end of the distribution curve, El Niño JFM seasonal temperatures exceed 19.5°C 10% of the time. In the available bootstrapped data, El Niño(0) JFM seasonal temperatures never exceed 19.5°C. El Niño(+) also exceeds this temperature 10% of the time, and El Niño(-) exceeds 19.5°C up to 40% of the time. Examining these distributions at different levels indicates that El Niño(0) phases in Florida are typically colder than the other two ENSO or ENSO-PDO phases, while El Niño(-) is warmer than the other phases.

To demonstrate that the distributions seen in Fort Myers, Florida, are representative of the JFM El Niño/PDO distributions in the entire region, we also examine conditions at Fernandina Beach, Florida (Figure 37). Here, the JFM seasonal temperature exceeds 12.0°C 50% of the time during El Niño. This temperature is surpassed during El Niño(0) only 20% of the time, 40% of the time during El Niño(+), and always during El Niño(-). This distribution, at the 50% level and other levels, is similar to those seen in Fort Myers, indicating that there is spatial continuity to the patterns.

California is another location seeing distribution changes in the ENSO/PDO subsets. California is typically 0.5 to 1.0°C warmer during El Niño. Changes to these conditions during the El Niño(+) and El Niño(0) are marginal, with warming subsets. California is typically 0.5 to 1.0°C warmer during El Niño. Changes to these conditions during the El Niño(+) and El Niño(0) are marginal, with warming of less than 1.0°C in each. However, El Niño(-) brings larger distribution changes,

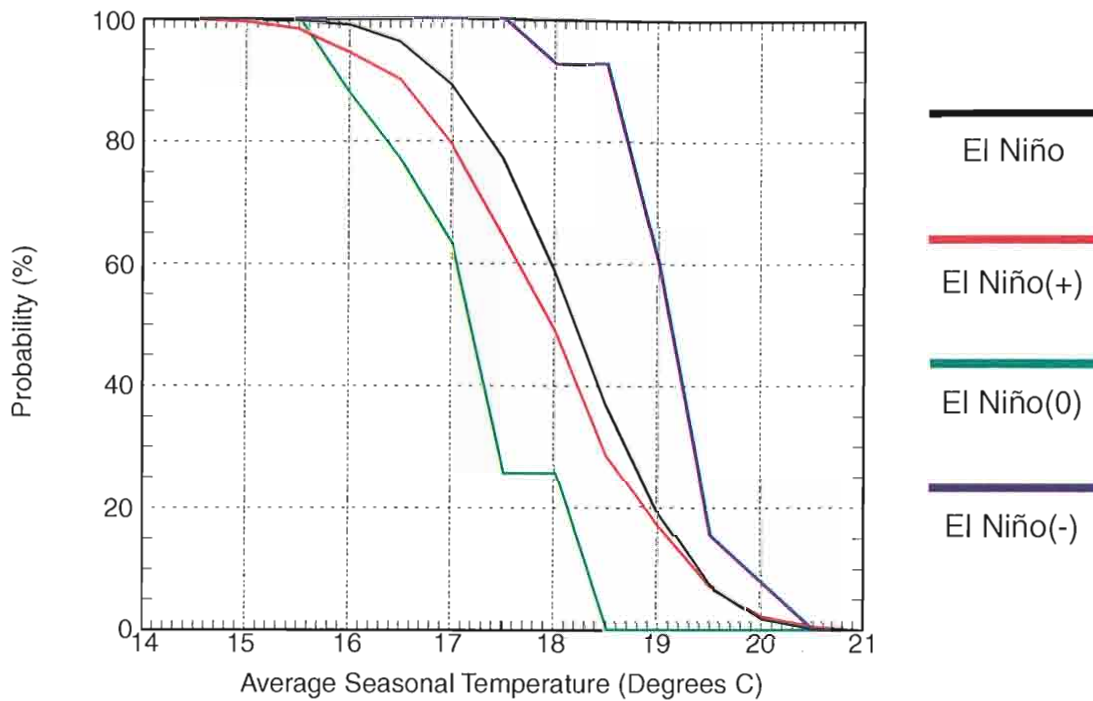


Figure 36. Inverse cumulative probability distributions of JFM seasonal temperatures in Fort Myers, Florida. Vertical axis indicates the probability of seasonal values reaching or exceeding a certain temperature.

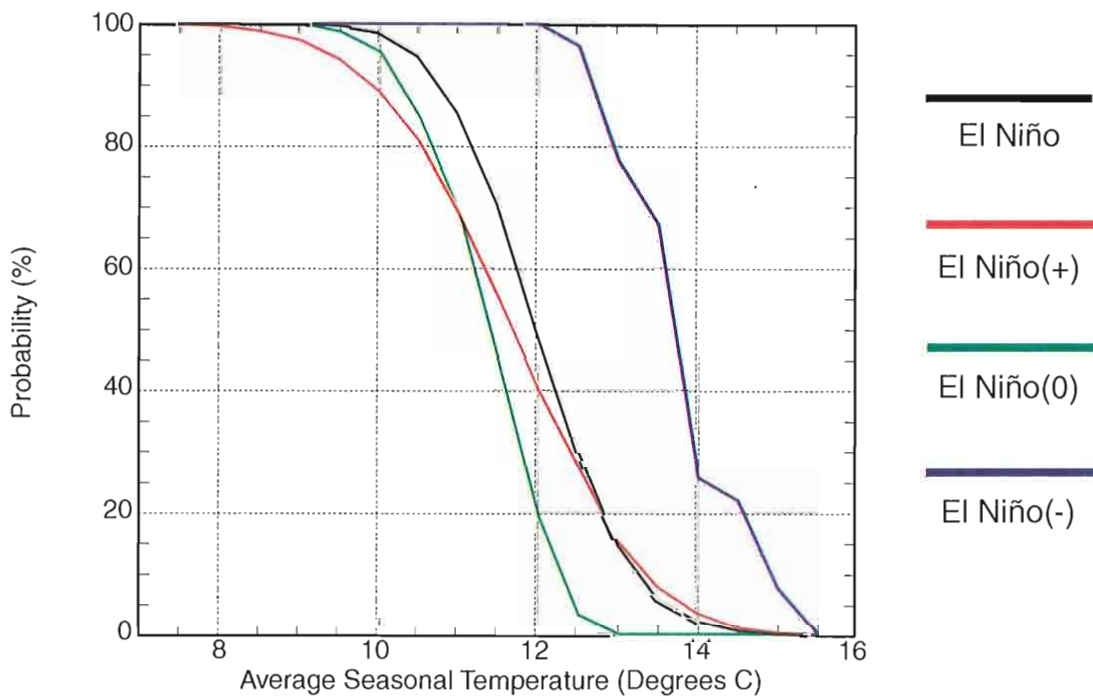


Figure 37. Inverse cumulative probability distributions of JFM seasonal temperatures in Fernandina Beach, Florida. Vertical axis indicates the probability of seasonal values reaching or exceeding a certain temperature.

with conditions 1.5 to 2.0°C colder. A good example of this is Cuyamaca (Figure 38). JFM seasonal temperatures exceed 5.0°C 50% of the time during El Niño. The El Niño(+) and El Niño(0) distributions, which are warmer, surpass this temperature 80% and 75% of the time, respectively. Meanwhile, the El Niño(-) only exceeds 5.0°C 15% of the time, indicative of the cooler conditions. Looking at the tails of the probability curves, it can be determined that JFM seasonal temperatures exceed 3.5°C 90% of the time in Cuyamaca. This temperature is always surpassed during El Niño(+), and exceeded 97% of the time during El Niño(0), but is only reached 70% of the time during El Niño(-). At the other end, El Niño JFM seasonal temperatures exceed 6.5°C 10% of the time. El Niño(+) and El Niño(0) reach this temperature 20% of the time, while El Niño(-) seasonal temperatures, given the available bootstrapped data, never reaches 6.5°C.

New England and Utah are another regions where El Niño(-) probability distribution differs from the other phases. During El Niño, the JFM average temperature exceeds 0.5°C 50% of the time in Provincetown, Massachusetts (Figure 39). The probability of El Niño(-) JFM seasonal temperatures exceeding 0.5°C is 100%. At the high end of the temperature distribution, the JFM average in Provincetown is above 1.5°C 10% of the time. El Niño(-) seasonal temperatures surpass 1.5°C 50% of the time. In Utah, El Niño(-) is cooler than El Niño. In Modena (Figure 40), seasonal temperatures exceed 0.5°C 50% of the time during El Niño, but only 12% of the time during El Niño(-). At a greater extreme, temperatures exceed 1.5°C 10% of the time in Modena during El Niño, but, given the available bootstrapped data, never occurs during El Niño(-).

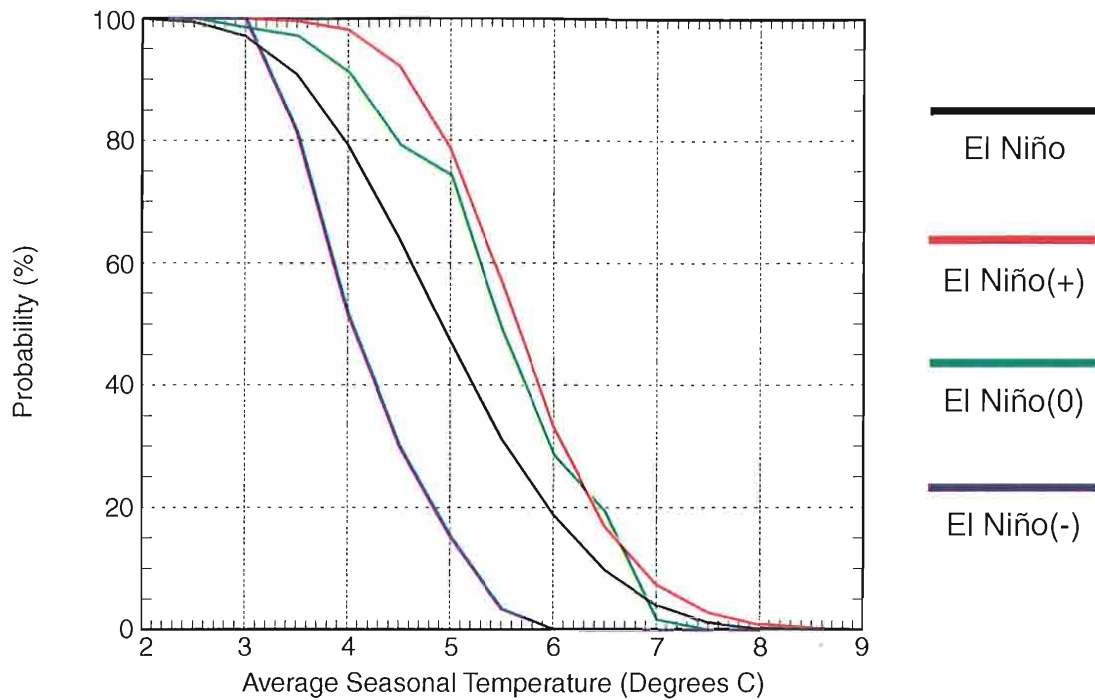


Figure 38. Inverse cumulative probability distributions of JFM seasonal temperatures in Cuyamaca, California. Vertical axis indicates the probability of seasonal values reaching or exceeding a certain temperature.

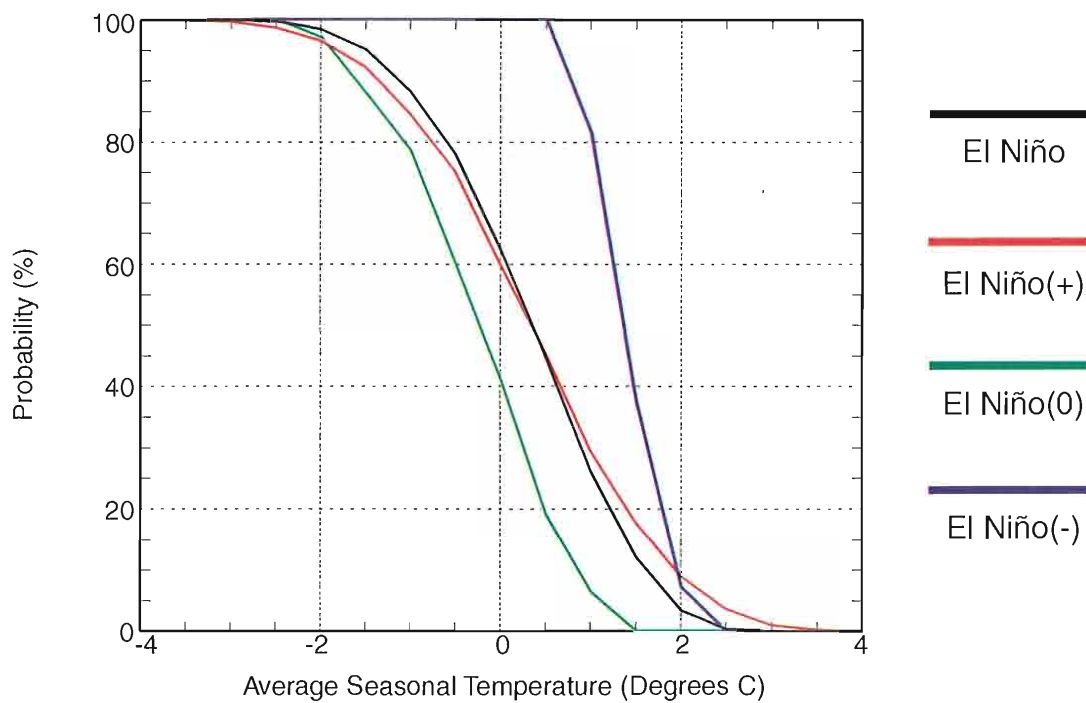


Figure 39. Inverse cumulative probability distributions of JFM seasonal Average Seasonal Temperature (Degrees C)

Figure 39. Inverse cumulative probability distributions of JFM seasonal temperatures in Provincetown, Massachusetts. Vertical axis indicates the probability of seasonal values reaching or exceeding a certain temperature.

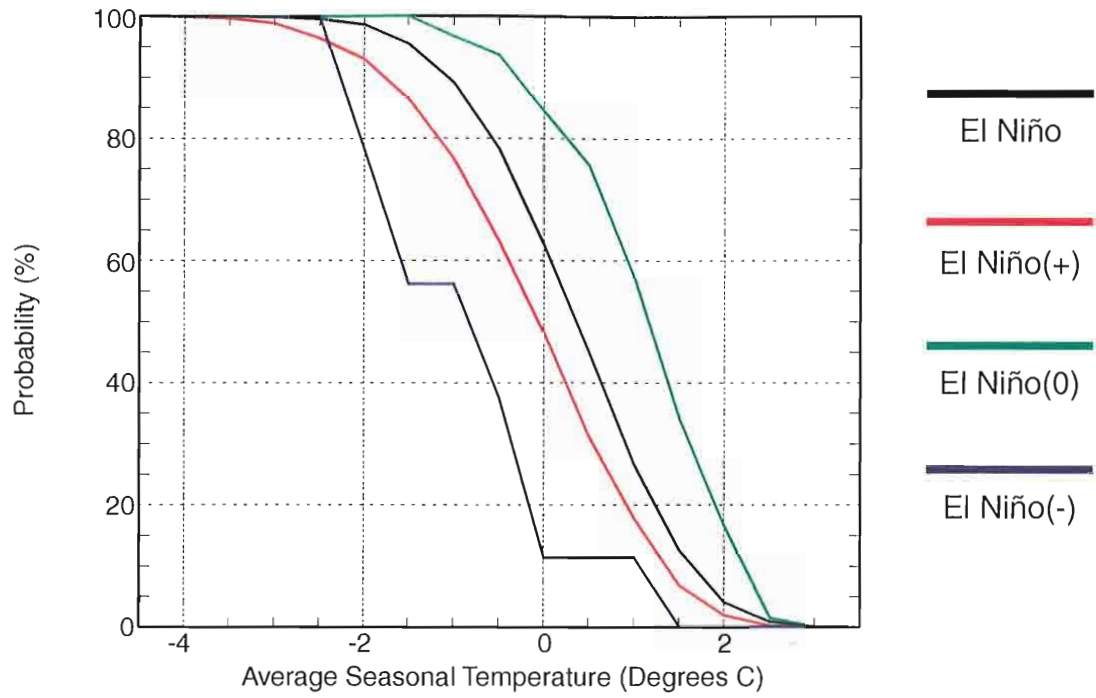


Figure 40. Inverse cumulative probability distributions of JFM seasonal temperatures in Modena, Utah. Vertical axis indicates the probability of seasonal values reaching or exceeding a certain temperature.

2) El Niño/PDO Precipitation Distributions

Georgia is expected to be 10% to 30% wetter during El Niño JFM. Conditions in Georgia are up to 20% drier in the El Niño(+) subset, while the wet conditions are intensified during El Niño(0) and El Niño(-). The changes can be seen in precipitation distributions in Eastman, Georgia (Figure 41). Eastman averages more than 12cm of precipitation during El Niño JFM 50% of the time. The probability of receiving more precipitation than this average is only 40% during El Niño(+), but 68% during El Niño(0), and 75% during El Niño(-). For larger average precipitation, the probabilities lessen. Eastman sees a seasonal precipitation average of 17cm during 10% of El Niño events. El Niño(+) only exceeds this average 4% of the time, but El Niño(0) and El Niño(-) JFM precipitation exceed 17cm 18% and 35% of the time, respectively.

Further north, Ohio is up to 40% drier during El Niño than during ENSO neutral conditions. Examining the El Niño/PDO subsets, we find no change during El Niño(+), drier conditions during El Niño(0), and wetter conditions during El Niño(-). Precipitation distributions seen at Findlay, Ohio, are typical of these shifts (Figure 42). For example, JFM monthly precipitation in Findlay exceeds 4cm in half of the bootstrapped El Niño events. The El Niño(+) distribution exceeds 4cm 46% of the time, but only 25% of the time during El Niño(0). However, JFM average monthly precipitation always exceeds 4 cm during El Niño(-). Also, Findlay sees an average monthly precipitation of 6.5cm less than 10% of the time during El Niño, El Niño(+) and El Niño(0), but sees at least 6.5cm in 70% of El Niño(-) phases.

The wet conditions expected in Nebraska during El Niño JFM are intensified slightly during El Niño(+), but weakened during El Niño(0) and El Niño(-). An example of these changes can be seen in the precipitation distributions in Purdum, Nebraska (Figure 43). Most precipitation in Nebraska during JFM is frozen, and

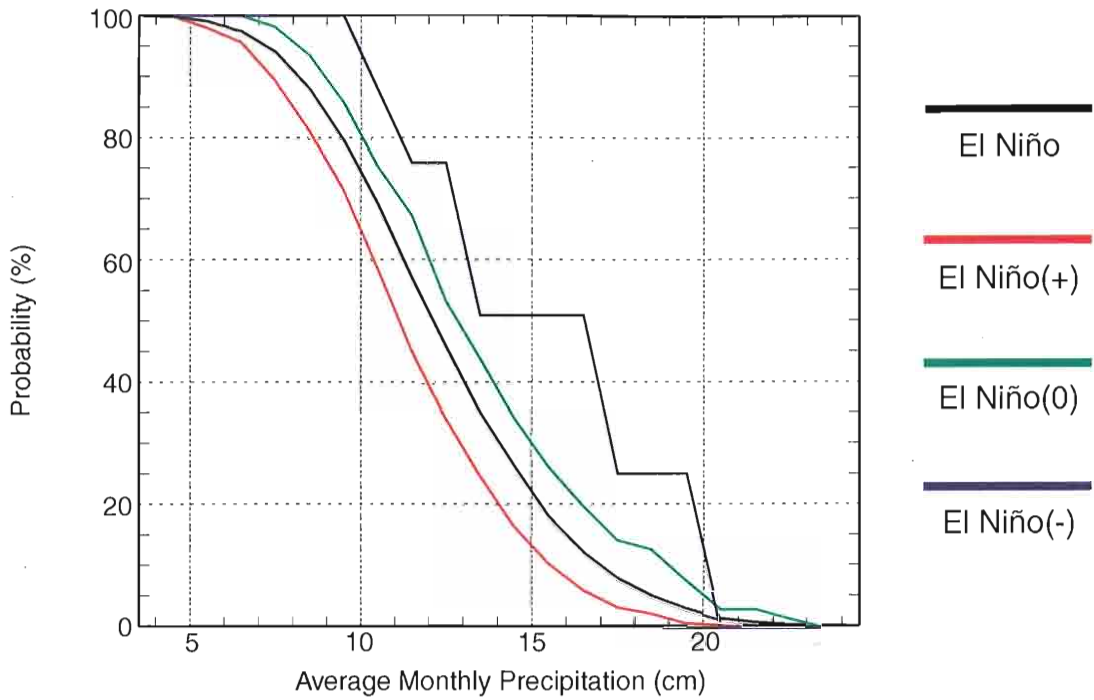


Figure 41. Inverse cumulative probability distributions of JFM monthly precipitation in Eastman, Georgia. Vertical axis indicates the probability of monthly values reaching or exceeding a certain precipitation amount.

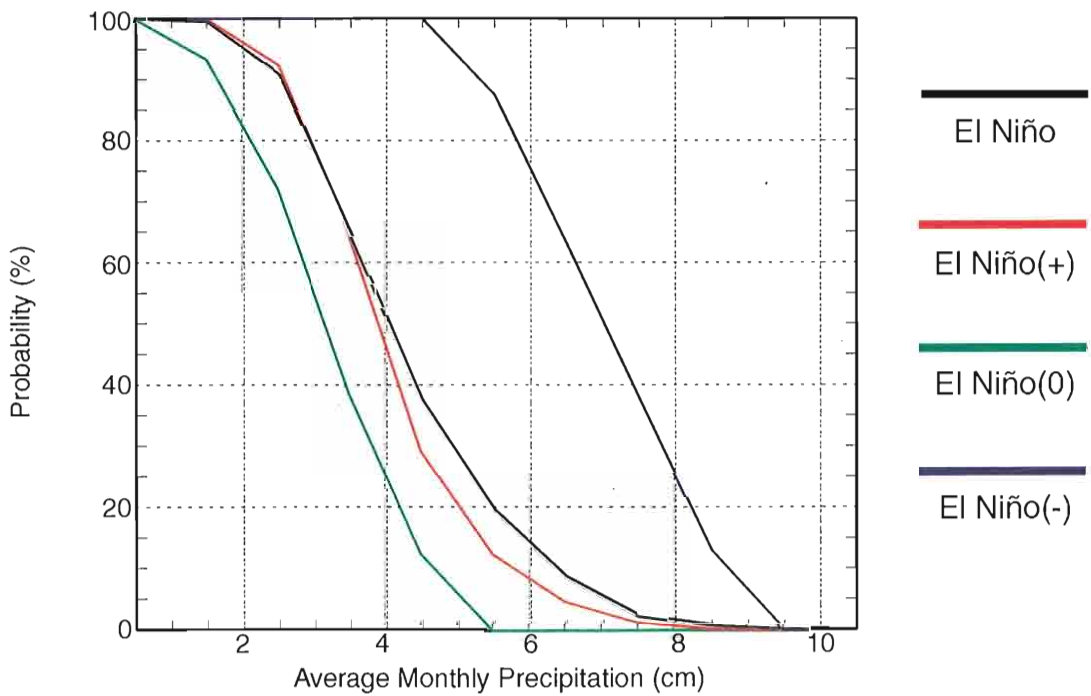


Figure 42. Inverse cumulative probability distributions of JFM monthly precipitation in Findlay, Ohio. Vertical axis indicates the probability of monthly values reaching or exceeding a certain precipitation amount.

Figure 42. Inverse cumulative probability distributions of JFM monthly precipitation in Findlay, Ohio. Vertical axis indicates the probability of monthly values reaching or exceeding a certain precipitation amount.

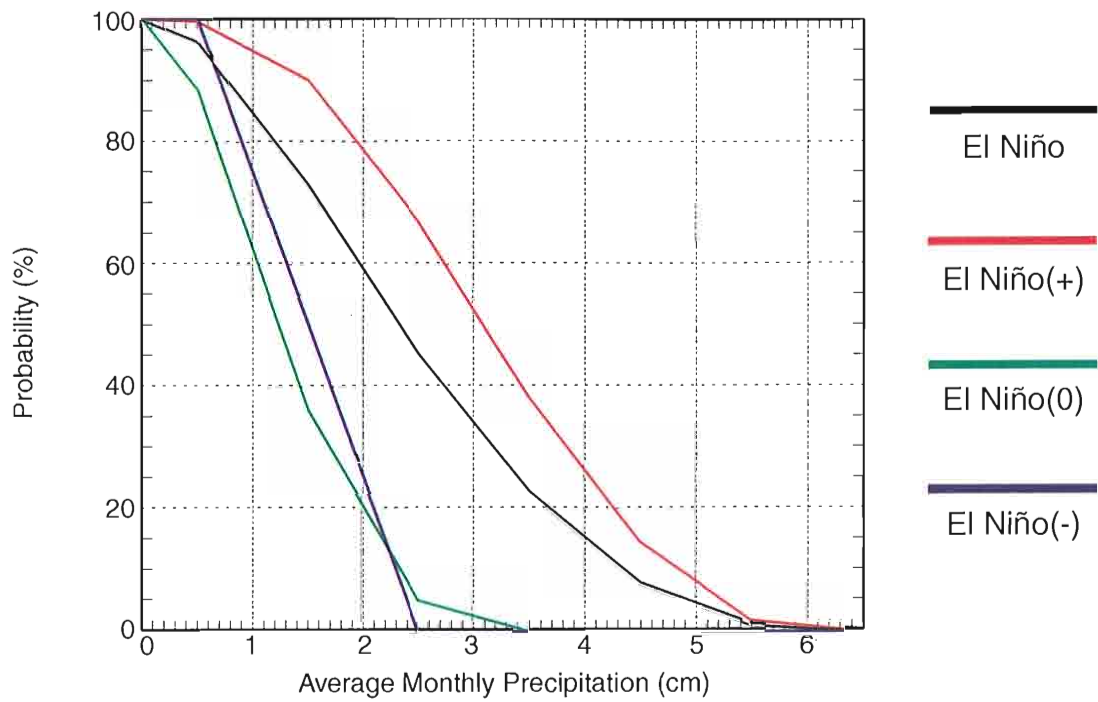


Figure 43. Inverse cumulative probability distributions of JFM monthly precipitation in Purdum, Nebraska. Vertical axis indicates the probability of monthly values reaching or exceeding a certain precipitation amount.

average monthly precipitation amounts are correspondingly low. Purdum exceeds 2.5cm of average monthly JFM precipitation only 50% of the time. The wetter El Niño(+) subset exceeds this amount 70% of the time, while the drier El Niño(0) only exceed 2.5cm in 5% of the bootstrapped data. El Niño(-) average monthly precipitation during JFM never exceeds 2.5cm. In fact, only El Niño and the El Niño(+) subset include seasons that exceed a monthly seasonal average precipitation of 3.5cm, and can see as much as 6cm a month during JFM.

3) La Niña/PDO Temperature Distributions

The Deep South is expected to be 1.0°C to 1.5°C warmer during La Niña JFM. This warming is intensified during La Niña(+) but weakened in La Niña(0) and La Niña(-). A good example of these alterations of the La Niña pattern is seen in Corning, Arkansas (Figure 44). The average JFM temperature in Corning exceeds 6.8°C half of the time. This seasonal temperature is reached at least 82% of the time during La Niña(+), but only 35% and 25% of the time in La Niña(0) and La Niña(-), respectively. At the warm end of the distribution, JFM seasonal temperatures exceed 8.5°C 10% of the time. La Niña(+) exceeds this temperature 30% of the time, while La Niña(0) and La Niña(-) only exceed 8.5°C in 5% and 3% of the bootstrapped occurrences.

The extra warming seen in the La Niña(+) subset in the southern United States also reaches into Minnesota, where typical La Niña temperatures can be up to 2.0°C colder than neutral ENSO temperatures. In the other PDO subsets, La Niña(0) causes a further cooling of Minnesota, while La Niña(-) brings little or no change to the expected La Niña conditions. The temperature distributions at Park Rapids, Minnesota, are representative of these changes (Figure 45). La Niña JFM change to the expected La Niña conditions. The temperature distributions at Park Rapids, Minnesota, are representative of these changes (Figure 45). La Niña JFM seasonal temperatures are at or above -11.5°C in half of the bootstrapped data. La

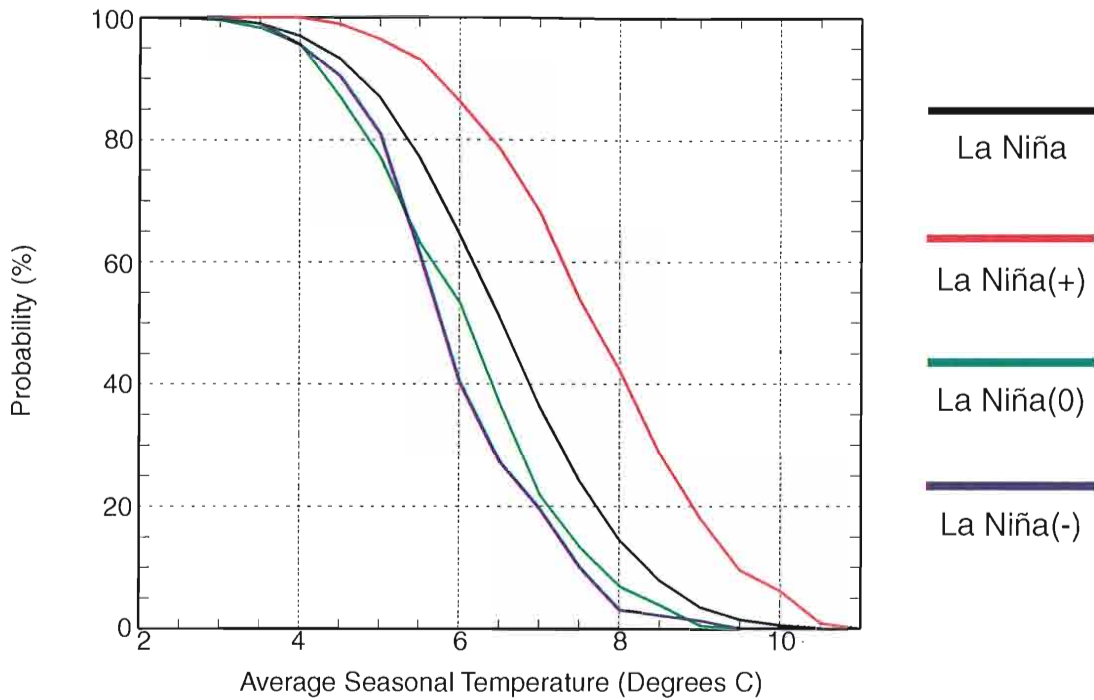


Figure 44. Inverse cumulative probability distributions of JFM seasonal temperatures in Corning, Arkansas. Vertical axis indicates the probability of seasonal values reaching or exceeding a certain temperature.

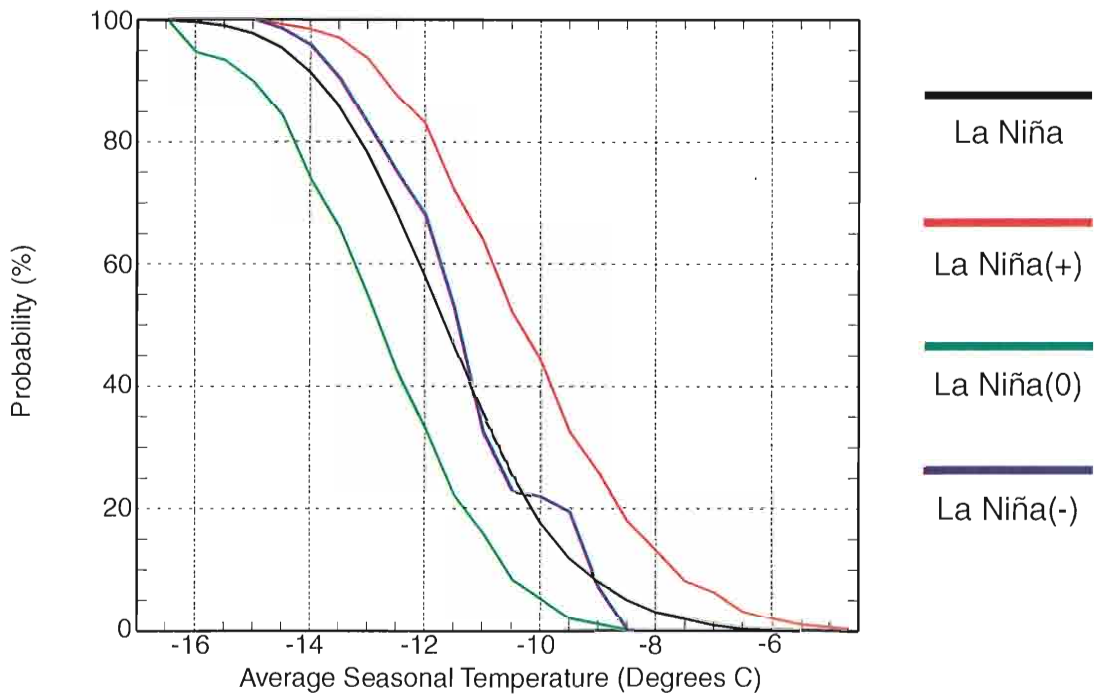


Figure 45. Inverse cumulative probability distributions of JFM seasonal temperatures in Park Rapids, Minnesota. Vertical axis indicates the probability of seasonal values reaching or exceeding a certain temperature.

Niña(+), seasonal temperatures exceed -11.5°C 80% of the time, but La Niña(0) only exceeds this temperature 23% of the time. There is little change in probability seen between La Niña and La Niña(-). At the warm tail of the distribution, La Niña JFM seasonal temperatures exceed -9.0°C 10% of the time. This temperature is surpassed in the La Niña(+) data 35% of the time, but only 2% of the time in La Niña(0). Once again, there is little change between La Niña and La Niña(-).

Two regions that experience smaller distribution shifts due to different PDO phases are New England and the Pacific Northwest. Both regions, on average, are 0.5°C to 1.0°C colder during La Niña than in ENSO neutral conditions. However, New England sees warmer conditions during La Niña(-), and the Pacific Northwest sees warming during La Niña(0), both on the order of 0.5°C to 1.0°C . The other PDO phases see marginal cooling in both locations. Temperature distributions Pomeroy, Washington are typical of the changes in the Pacific Northwest (Figure 46). JFM seasonal temperatures exceed 2.2°C in Pomeroy 50% of the time during La Niña. Meanwhile, this temperature is surpassed 75% of the time during La Niña(0) and 35% of bootstrapped La Niña(+) seasons. At the cold tail of the distribution, La Niña seasonal temperatures exceed 0°C 90% of the time. This temperature is surpassed in 99% of La Niña(0) events, 88% of La Niña(+) events, and 80% of La Niña(-) events. A similar distribution is seen at the warm tail.

The temperature distributions at Acadia National Park, Maine, are representative of the changes in New England (Figure 47). JFM seasonal temperatures are at or above -5.0°C in 50% of La Niña, La Niña(+), and La Niña(0) events. However, La Niña(-) surpasses -5.0°C 70% of the time. At the warm tail, La Niña and La Niña(+) exceed -3.5°C 10% of the time. During La Niña(-), -3.5°C is surpassed 22% of the time, and surpassed 4% of the time in La Niña(0). The La Niña(-) is always warmer than the other distributions, while the other three are very similar, except

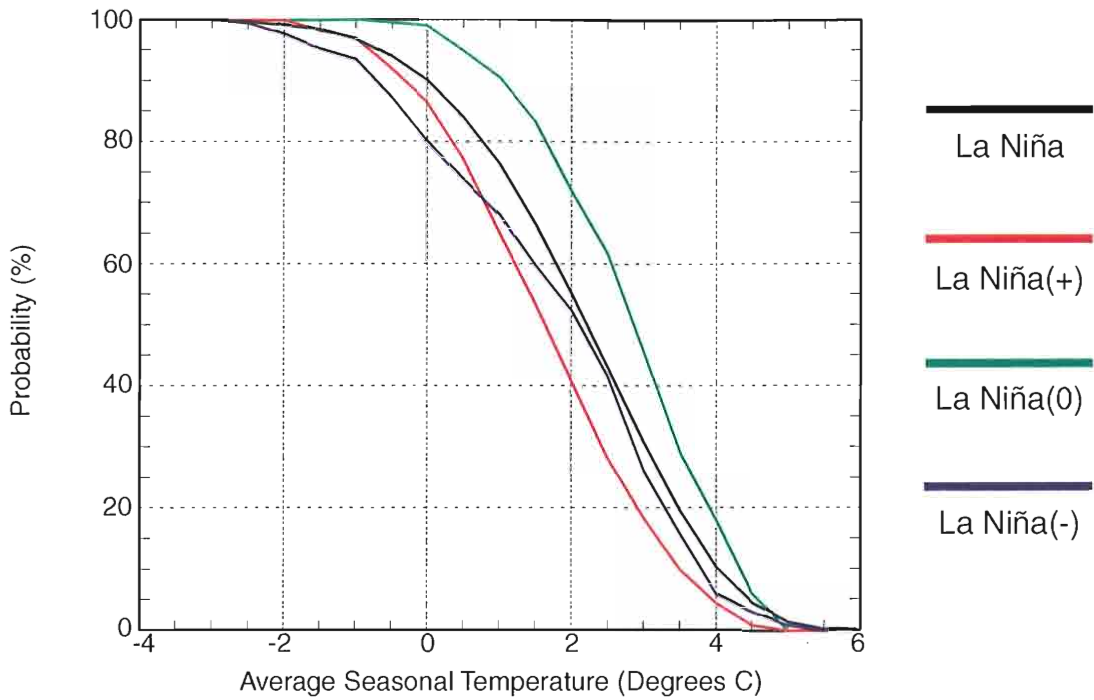


Figure 46. Inverse cumulative probability distributions of JFM seasonal temperatures in Pomeroy, Washington. Vertical axis indicates the probability of seasonal values reaching or exceeding a certain temperature.

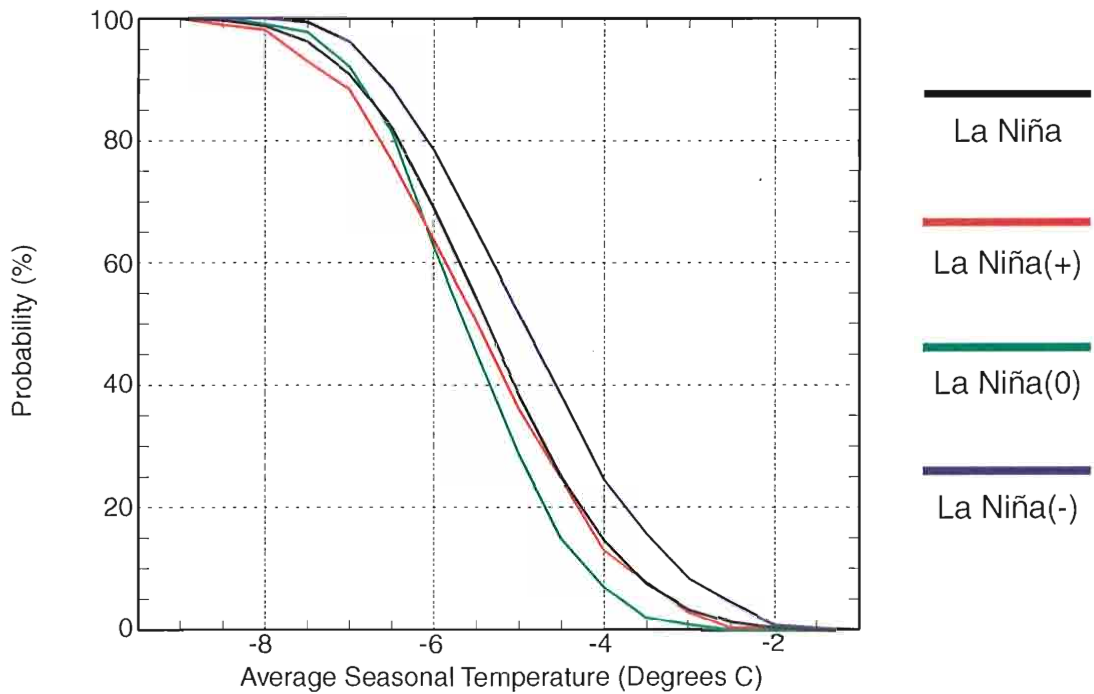


Figure 47. Inverse cumulative probability distributions of JFM seasonal temperatures in Acadia National Park, Maine. Vertical axis indicates the probability of seasonal values reaching or exceeding a certain temperature.

for La Niña(0), which has a lower probability to reach warmer temperatures than La Niña or La Niña(+).

4) La Niña/PDO Precipitation Distributions

La Niña dry conditions in Georgia are intensified in the La Niña(+) and La Niña(-) subsets, but weakened in La Niña(0) subset. A representative station showing these changes is Eastman, Georgia (Figure 48). Monthly JFM precipitation in Eastman exceeds 13cm in half of the bootstrapped seasons. The La Niña(+) and La Niña(-) subsets only reach 13cm 30% of the time, but La Niña(0) JFM average monthly precipitation surpasses 13cm in 85% of its bootstrapped seasons. La Niña(+) and La Niña(-) never see JFM average precipitation of over 18cm per month. However, there is still a 10% chance to see that amount during La Niña and a 35% probability during La Niña(0).

Reverse conditions from those in Georgia are seen in Ohio during La Niña JFM and its corresponding PDO subsets. Ohio is wet during La Niña JFM, and conditions are wetter in the La Niña(+) and La Niña(-) subsets. Meanwhile, La Niña(0) JFM in Ohio is drier by up to 20%. Warren, Ohio, is a good example of these precipitation shifts (Figure 49). JFM monthly precipitation exceeds 6.5cm in 50% of the La Niña bootstrapped seasons. The precipitation amount is surpassed 65% of the time in both La Niña(+) and La Niña(-), but only exceeded in 25% of the bootstrapped samples in the La Niña(0) subset. Examining a larger precipitation amount reveals that La Niña JFM monthly precipitation exceeds 9cm in 10% of the bootstrapped seasons. This amount is only exceeded in 2% of La Niña(0) seasons, but surpassed in La Niña(+) and La Niña(-) 15% and 25% of the time, respectively.

The trend of positive and negative PDO intensifying La Niña conditions but surpassed in La Niña(+) and La Niña(-) 15% and 25% of the time, respectively.

The trend of positive and negative PDO intensifying La Niña conditions and neutral PDO weakening La Niña conditions is also seen in Nebraska. Precipi-

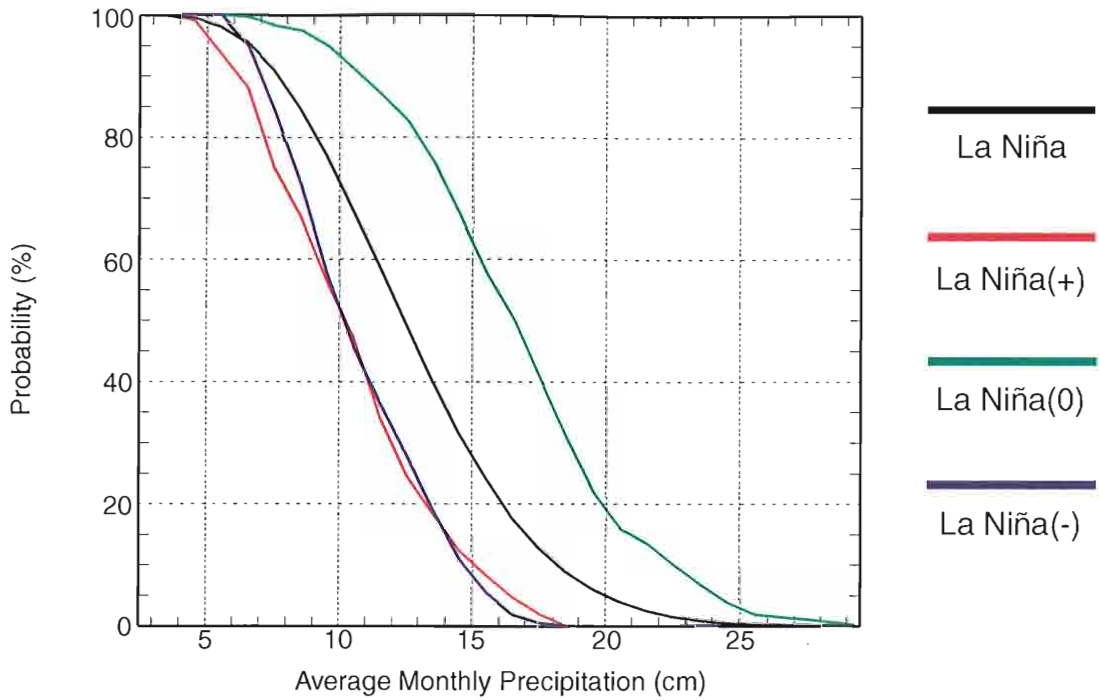


Figure 48. Inverse cumulative probability distributions of JFM monthly precipitation in West Point, Georgia. Vertical axis indicates the probability of monthly values reaching or exceeding a certain precipitation amount.

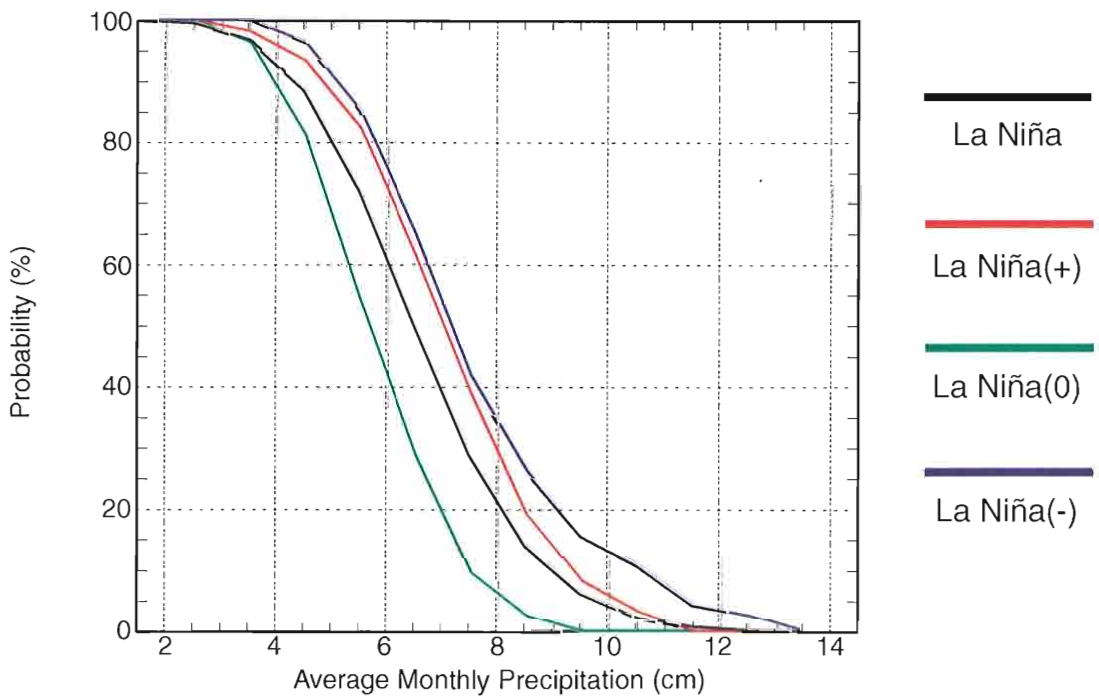


Figure 49. Inverse cumulative probability distributions of JFM monthly precipitation in Warren, Ohio. Vertical axis indicates the probability of monthly values reaching or exceeding a certain precipitation amount.

tation distributions in Oakdale, Nebraska show that La Niña JFM monthly precipitation is greater than 1.3cm in half of the bootstrapped seasons (Figure 50). There is no change of probability in the La Niña(+) subset, but the probability of seeing more than 1.3cm in La Niña(-) is 40%. La Niña(0) is wetter, with a probability of 70% that JFM monthly precipitation in Oakdale will exceed 1.3cm. At a higher precipitation value, it can be determined that La Niña JFM monthly precipitation only exceeds 2.5 cm in 10% of bootstrapped seasons. The percentage is less for both La Niña(+) and La Niña(-), but double for La Niña(0).

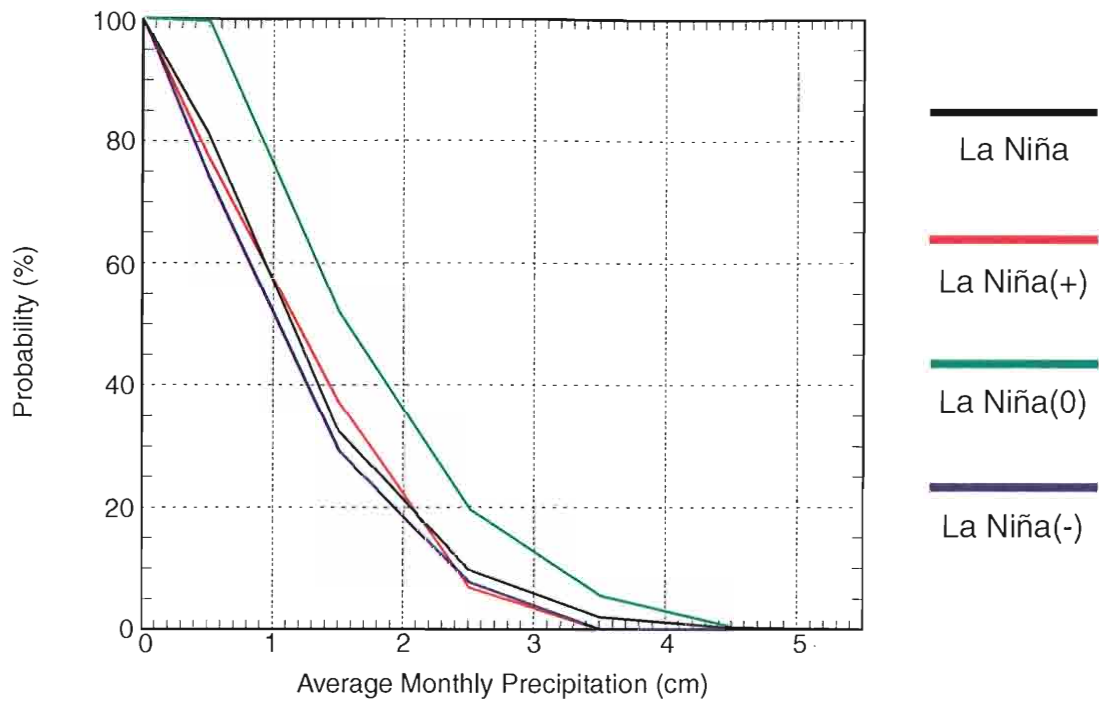


Figure 50. Inverse cumulative probability distributions of JFM monthly precipitation in Oakdale, Nebraska. Vertical axis indicates the probability of monthly values reaching or exceeding a certain precipitation amount.

5. DISCUSSION

a. Summary of Results

The El Niño(+) subset comprises 60% of the El Niño data, therefore changes between El Niño and El Niño(+) patterns are expectedly small. Most temperature differences are less than 1.0°C. However, examining statistically significant temperature shifts reveals that regions of significant El Niño(+) temperature anomalies are generally stronger and cover more area than seen in El Niño (Figures 5, 9, 13, and 17). Some areas, like New England, see a significant cooling during El Niño(+) JFM, but not in El Niño. The only location that sees reduced confidence or spatial coverage during El Niño(+) is the JFM warming in the northern Plains. Meanwhile, the only location with a significant reversal of temperature anomalies is California during JAS, which goes from being significantly warm in El Niño to significantly cold during El Niño(+).

Significant regions of precipitation shifts during El Niño(+) expand spatially, but confidence in these shifts are weaker at many stations (Figures 7, 11, 15, and 19). Regions which show statistical significance in precipitation shifts in during El Niño(+) but not in El Niño include dry conditions in New England during OND and dry conditions in the Pacific Northwest during AMJ.

Areas of significant temperature shifts during El Niño(0) can either resemble or vastly differ from El Niño patterns, depending on the season (Figures 5, 9, 13, and

Areas of significant temperature shifts during El Niño(0) can either resemble or vastly differ from El Niño patterns, depending on the season (Figures 5, 9, 13, and 17). If significant El Niño and El Niño(0) temperature anomalies are spatially com-

parable, the confidence in the El Niño(0) anomalies is typically weaker, (potentially due to small sample size). Areas that are statistically significant during El Niño but are not significant in El Niño(0) include the desert southwest cooling during OND and JAS and the warming in the northern Plains during JFM and AMJ. Regions which exhibit confidence in temperature shifts during El Niño(0) but not in El Niño include cool conditions in California and the Ohio River valley during OND, and cool conditions in the Mississippi and Ohio River valleys, as well as New England, during AMJ.

Significant shifts in precipitation during El Niño(0) include the expected El Niño patterns, but areas of confidence not seen in El Niño are also present (Figures 7, 11, 15, and 19). Once again, where anomalies are spatially comparable, the confidence in the El Niño(0) shifts is weaker. However, increased spatial coverage of significant anomalies is common during El Niño(0). Areas of significant precipitation shifts during El Niño(0) that are not seen in El Niño include wet conditions in the U.S. east of the Mississippi River during OND, northern New England during JFM, and the southeast during AMJ.

Patterns of temperature anomalies in El Niño and El Niño(-) differ greatly. The anomalies in the El Niño(-) often offset the expected El Niño anomaly pattern. The large differences are primarily the result of small sample size, which allows for little confidence in El Niño(-) anomalies (Figures 7, 11, 15, and 19). Significant El Niño(-) temperature patterns resemble El Niño in the southwest during JFM, in AMJ (but much weaker), and California during JAS. Significant temperature shifts, seen in El Niño(-) and not in El Niño, include the upper and middle Mississippi River valleys during JFM. Confidence in temperature shifts reverse in from Minnesota southeast to the Carolinas. This regions is significantly cool during El Niño(-), River valleys during JFM. Confidence in temperature shifts reverse in from Minnesota southeast to the Carolinas. This regions is significantly cool during El Niño(-), but significantly warm during El Niño. Areas of significant precipitation during El

Niño(-) are generally weak (80% to 90% confidence) and spotty (Figures 7, 11, 15, and 19).

Spatial coverage of statistically significant temperature shifts in La Niña and La Niña(+) closely resemble each other (Figures 21, 25, 29, and 33). Significant La Niña temperature anomalies are stronger in confidence and spatial coverage during OND, while La Niña(+) anomalies are typically stronger and cover more area during JFM, AMJ, and JAS. Exceptions to this pattern are the cool patterns in the northern Plains and New England during JFM and the Pacific Northwest during AMJ. All areas exhibiting statistically significant shifts in temperature during La Niña are present in La Niña(+), except for the cooling in the northern Plains during JAS.

Significant precipitation anomalies occur in the same locations in La Niña and La Niña(+), but differences in confidence vary by location instead of season (Figures 23, 27, 31, and 35). For example, dry anomalies are stronger during La Niña than in La Niña(+) in the southeast during OND, but in the Mid-Atlantic states, La Niña(+) shows more confidence in dry conditions than seen in La Niña. Regions showing statistically significant precipitation in La Niña but not La Niña(+) are wet conditions in the northern Rocky Mountains during OND and the Ohio valley in JFM and AMJ. A region seeing significant shifts in precipitation in La Niña(+) but not in La Niña are dry conditions in the southeast during AMJ.

Regions of statistically significant temperature shifts in the La Niña(0) subset retain some resemblance to significant La Niña anomalies during OND, JFM and AMJ, but differs greatly during JAS (Figures 21, 25, 29, and 33). Significant La Niña temperature anomalies that do not appear in the La Niña(0) subset include cool conditions in the Pacific Northwest during JFM, Virginia and the Carolinas during AMJ, and the northeast and California during JAS. La Niña(0) shows significant conditions in the Pacific Northwest during JFM, Virginia and the Carolinas during AMJ, and the northeast and California during JAS. La Niña(0) shows significant warming in the southern Plains during AMJ and warming in Oregon during JAS,

both of which do not appear in the La Niña climatology. Of the spatial anomaly patterns seen in both cases, La Niña(0) patterns are weaker in the southern Plains during OND, the southeast and New England during JFM, along the Pacific coast during AMJ, and the southwest and Great Lakes in JAS. La Niña(0) anomalies show more confidence in cool conditions in the Pacific Northwest during OND, a larger area of spatial coverage in significantly cool anomalies over the northern Plains during JFM, and greater confidence in a colder New England during AMJ. Significantly dry anomalies show more confidence during La Niña, except for the deep South during La Niña(0) AMJ (Figures 23, 27, 31, and 35). Significantly wet anomalies seen in the eastern half of the United States during La Niña do not appear in La Niña(0).

Significant temperature shifts are present in the same locations in La Niña(-) and La Niña, but less confidence is seen in the La Niña(-) anomaly subset (Figures 21, 25, 29, and 33). The only exception is the southern Plains during OND. Significant anomalies seen in La Niña but not in La Niña(-) include cooling the New England, and cooling in California during JFM, AMJ, and JAS. One Region where significant anomalies are seen in La Niña(-) but not in La Niña is the intermountain west during AMJ. Significance in precipitation shifts are similar in both cases, but with less confidence in the La Niña(-) subset (Figures 23, 27, 31, and 35). Large differences between the two cases only occur in the expectedly wet northern Rocky Mountains during OND and Ohio River valley during JAS.

In general, positive PDO tends to enhance ENSO anomalies while the other two phases create weaker ENSO anomaly patterns or negate them entirely. However, PDO influence on ENSO anomalies is not uniform. That is, given a specific PDO and ENSO state, some regions will see intensification of ENSO conditions, while PDO influence on ENSO anomalies is not uniform. That is, given a specific PDO and ENSO state, some regions will see intensification of ENSO conditions, while other regions see a weakening of (or no change in) ENSO conditions. For instance,

the warm temperature anomalies over the central United States during La Niña are intensified during La Niña(+), as well as the cold temperature anomalies over New England and the Pacific Northwest. However, the cold anomalies seen in La Niña over the northern Plains are not intensified during La Niña(+).

b. Physical Mechanisms

Mantua et al. (1997) states that atmospheric responses to the PDO occur within the Aleutian Low. Positive PDO deepens the Aleutian Low, while negative PDO weakens the Aleutian Low. Also, Smith et al. (1998) indicated that El Niño events intensify the Aleutian Low, while La Niña events weaken the Low. Gershunov and Barnett (1998) apply these modulations of the Aleutian Low intensity to ENSO anomaly patterns, hypothesizing that ENSO extrema anomaly patterns are altered due to intensification or weakening of the Aleutian Low from both ENSO and the PDO.

From these hypotheses, it is then likely that the strongest, most stable (longwave patterns remain unchanged for long periods of time) Aleutian Low occurs during El Niño(+), since both El Niño and positive PDO enhance the Low (Gershunov and Barnett 1998). In other cases, both constructive and destructive patterns influencing the Aleutian Low (i.e., La Niña(+) and El Niño(-)), have two destructive patterns affecting it (i.e. La Niña(-)), or only one pattern influencing the Aleutian Low (neutral PDO cases). Thus, El Niño(+), due to a stabilized longwave pattern, sees the most enhanced ENSO signal. El Niño(-) and La Niña(+) longwave patterns are less stable, while La Niña(-) has a very unstable longwave pattern associated with the Aleutian Low.

less stable, while La Niña(-) has a very unstable longwave pattern associated with the Aleutian Low.

ENSO extreme phases during neutral PDO conditions exhibit characteristics of

both positive and negative PDO phases. When ENSO extrema are strongest, neutral PDO anomalies tend to resemble expected ENSO patterns, but are less intense than in El Niño(+) and La Niña(+). However, in seasons where ENSO influence is weaker, the anomaly patterns associated with ENSO/neutral PDO couplings are less distinct, and more closely resemble the incoherent or previously unseen anomaly patterns found in the negative PDO cases.

The PDO is not the sole cause of variability of ENSO climate anomalies. Other influences on variability of ENSO climate anomalies include the strength of the ENSO event, the North Atlantic Oscillation, and the natural variability in the atmosphere (e.g., Hurrell 1995; Kumar and Hoerling 1997). It does appear, however, that the PDO itself has sufficient influence on U.S. ENSO anomaly patterns to have the potential to be predictable and useful in forecasting.

c. Comparison to Previous Works

The only previous work closely resembling this paper is 'PDO modulation of U.S. ENSO Teleconnections' by Gershunov and Barnett (1998). This work concluded that the states of El Niño(+) and La Niña(-) are more stable and intense than El Niño(-) and La Niña(+). Their results for El Niño(+) agree with the findings of this paper, but their findings on La Niña(-) do not.

To determine why the findings on La Niña(+) and La Niña(-) do not agree, the differences in classifying ENSO and PDO extreme phases in each study should be examined. Gershunov and Barnett (1998) investigated the years from 1933-1993. By determining if SSTs in the Niño 3.4 region are above 0.8 standard deviations from the long term mean, 15 years are classified as El Niño and 12 are classified as La Niña. By determining if SSTs in the Niño 3.4 region are below 0.8 standard deviations from the long term mean, 15 years are classified as El Niño and 12 are classified as La Niña. In this work, ENSO events are classified by the JMA index (Section 2.b.1).

These two methods of determining ENSO extreme phases of identify different years as ENSO extrema, particularly if an ENSO extreme phase is weak. For example, 5 out of the 15 El Niño years identified in Gershunov and Barnett (1998) are considered neutral by the JMA index.

Next, the Gershunov and Barnett (1998) applied a different definition of positive or negative PDO. Since Gershunov and Barnett only consider PDO interdecadal variability, the PDO phase of each ENSO extreme is determined by the PDO epoch it occurred in. Thus, all ENSO extreme phases occurring between 1933–1946 and 1977–1993 are identified as positive PDO, while all ENSO extreme phases occurring between 1947–1976 are identified as negative PDO. In this paper (Section 2.b.2.ii), PDO events are identified from the running two-year SST anomaly within the selected PDO region. This methodology takes into account the interannual variability in the PDO, and identifies PDO extreme phases by the PDO conditions present at a given time, and not based on the interdecadal PDO pattern. For example, ENSO year 1991 would be considered El Niño(+) when just examining the interdecadal variation of the PDO. However, including interannual variability in the PDO classification makes ENSO year 1991 El Niño(-). Thus, due to the different classifications of ENSO and PDO events, accurate comparison of the work works can not be made, so discrepancies between the two works are expected.

d. Future Applications

Further research, via statistics or modeling, should be conducted on the impacts of ENSO and the PDO on U.S. climate anomalies. Improved understanding of the physical mechanisms behind ENSO, the PDO, and their teleconnections will

pacts of ENSO and the PDO on U.S. climate anomalies. Improved understanding of the physical mechanisms behind ENSO, the PDO, and their teleconnections will lead to improved understanding and forecasting ability. Other natural interdecadal

variability, like the NAO, should also be investigated for joint U.S. impacts with either ENSO or the PDO. Further, other atmospheric parameters other than sea level pressures and geopotential heights should be examined for ENSO/PDO response. By examining many variables, an improved understanding of the influence of these two phenomena will result.

6. CONCLUSIONS

The influence of the PDO on U.S. ENSO temperature and precipitation anomalies are quantified and tested for statistical significance. If the PDO is in its positive phase, U.S. climate anomalies associated with ENSO are typically intensified and more stable. If PDO conditions are neutral or negative, U.S. ENSO climate anomalies are significantly weakened.

Knowledge of PDO conditions can be used operationally to fine-tune seasonal climate forecasts. If the PDO is positive, ENSO extreme phases will be more stable, improving the accuracy of El Niño and La Niña forecasts. If the PDO is neutral, typical ENSO anomaly patterns can be expected when anticipated while the ENSO phases are strong. However, when the ENSO phase weakens, so will the anomaly patterns associated with them. If the PDO is negative, anomaly patterns associated with ENSO will be very weak. PDO conditions should be applied to modify ENSO seasonal forecasts accordingly, thus improving the accuracy of the ENSO forecast.

ENSO events can be very destructive to property, industry, and agriculture in the United States, and can cause billions of dollars in damages. However, since the development of ENSO events can be observed months in advance, careful planning and preparation can mitigate some damages. Use of the PDO phase to estimate the strength of ENSO events will increase the success of mitigation efforts, potentially saving the U.S. millions of dollars in damages for each event.

REFERENCES

- Barnett, T. P., D. W. Pierce, R. Saravanan, N. Schneider, D. Dommengot, and M. Latif, 1999: Climate Studies - Origins of the midlatitude Pacific decadal variability. *Geophys. Res. Lett.*, **26**, 1453-1460.
- _____, _____, M. Latif, D. Dommengot, and R. Saravanan, 1999: Interdecadal interactions between the tropics and midlatitudes in the Pacific basin. *Geophys. Res. Lett.*, **26**, 615-618.
- Bhattacharyya, G. K., and R. A. Johnson, 1977: Statistical Concepts and Methods. Wiley and Sons, New York, 639 pp.
- Bjerknes, J., 1969: Atmospheric teleconnections from the equatorial Pacific. *Mon. Wea. Rev.*, **97**, 163-172.
- Bove, M. C., J. B. Elsner, C. W. Landsea, X. Niu, and J. J. O'Brien, 1998: Effect of El Niño on U.S. Landfalling Hurricanes, Revisited. *Bull. Amer. Meteor. Soc.*, **79**, 2477-2482.
- Buell, C. E., 1971: Integral equation representation for factor analysis. *J. Atmos. Sci.*, **28**, 1502-1505.
- CDIAC, cited 2000: United States Historical Climatology Network. [Available online from <http://cdiac.esd.ornl.gov/epubs/ndp019/ndp019.html>.]
- Chen, T.-C., J.-M. Chen, and C. K. White, 1996: Interdecadal variation in U.S. Pacific coast precipitation over the past four decades. *Bull. Amer. Meteor. Soc.*, **77**, 1197-1205.
- Dettinger, M. D., D. R. Cayan, H. F. Diaz, and D. M. Meko, 1998: North-South Precipitation Patterns in Western North America on Interannual-to-Decadal Timescales. *J. Climate*, **11**, 3095-3111.
- Downton, M. W., and K. A. Miller, 1993: The freeze risk to Florida citrus, Part II: Temperature variability and circulation patterns. *J. Climate*, **6**, 364-372.
- Downton, M. W., and K. A. Miller, 1993: The freeze risk to Florida citrus, Part II: Temperature variability and circulation patterns. *J. Climate*, **6**, 364-372.

- Draconis, P., and B. Efron, 1983: Computer-intensive methods in statistics. *Sci. Amer.*, **248**, 116-130.
- Enfield, D. B., and J. S. Allen, 1980: On the structure and dynamics of monthly mean sea level anomalies along the Pacific coast of North and South America. *J. Phys. Oceanogr.*, **10**, 557-578.
- Gershunov, A., 1998: ENSO Influence on Intreseasonal Extreme Rainfall and Temperature Frequencies in the Contiguous United States: Implications for Long-range Predictability. *J. Climate*, **11**, 3192-3203.
- _____, and T. P. Barnett, 1998: Interdecadal Modulation of ENSO Teleconnections. *Bull. Amer. Meteor. Soc.*, **79**, 2715-2725.
- _____, _____, and D. R. Cayan, 1999: North Pacific Interdecadal Oscillation Seen as Factor in ENSO-Related North American Climate Anomalies. *Eos, Trans. Amer. Geophys. Union*, **80**, 25, 29-30.
- Glantz, M. H., 1996: *Currents of Change: El Niño's Impact of Climate and Society*. Cambridge University Press, 194 pp.
- Green, P. 1996: Regional Analysis of Canadian, Alaskan, and Mexican precipitation and temperature for ENSO impact. COAPS Technical Report 96-3. [Available from the Center for Ocean-Atmospheric Prediction Studies, The Florida State University, Tallahassee, FL 32306-2840].
- Hall, C. T., 2000: Ocean data suggest shift in weather winter patterns could change for 20 years. *San Francisco Chronicle*, 20 January, p. A1.
- Higgins, W., 2000: Towards Improved Predictions of the US Precipitation and Surface Air Temperature. *The Climate Report*, **1**, 6-9.
- Horel, J. D., and J. M. Wallace, 1981: Planetary-scale atmospheric phenomena associated with the Southern Oscillation. *Mon. Wea. Rev.*, **109**, 813-829.
- Hurrell, J. W., 1995: Decadal Trends in the North Atlantic Oscillation: Regional temperatures and precipitation. *Science*, **269**, 676-679.
- Jin, F. F., 1997: A Theory of Interdecadal Climate Variability of the North Pacific Ocean-Atmospheric System. *J. Climate*, **10**, 1821-1835.
- JPL, cited 2000: Pacific Decadal Oscillation (PDO). [Available on-line from Ocean-Atmospheric System. *J. Climate*, **10**, 1821-1835.
- JPL, cited 2000: Pacific Decadal Oscillation (PDO). [Available on-line from <http://topex-www.jpl.nasa.gov/discover/PDO.html>.]

- Kumar, A., and M. P. Hoerling, 1997: Interpretation and Implications of the observed Inter-El Niño Variability. *J. Climate*, **10**, 83-91.
- Legler, David M., 1983: Empirical Orthogonal Function Analysis of Wind Vectors over the Tropical Pacific Region. *Bull. Amer. Meteor. Soc.*, **64**, 234-241.
- Mantua, N. J., S. R. Hare, Y. Zhang, J. M. Wallace, and R. C. Francis, 1997: A Pacific Interdecadal Climate Oscillation with Impacts on Salmon Production. *Bull. Amer. Meteor. Soc.*, **78**, 1069-1079.
- Mantua, N. J., 2000: How Does The Pacific Decadal Oscillation Impact Our Climate? *The Climate Report*, **1**, 10-13.
- Marine Department, the Japan Meteorological Agency, 1991: Climate charts of sea surface temperature of the western north Pacific and the global ocean. 51 pp.
- Meyers, S.D., J.J. O'Brien and E. Thelin, 1997: Reconstruction of monthly SST in the Tropical Pacific Ocean during 1868 - 1993 using adaptive climate basis functions, *Mon. Wea. Rev.*, **127**(7), 1599-1612, July 1999.
- Minobe, S., 1997: A 50-70 year climatic oscillation over the North Pacific and North America. *Geophys. Res. Lett.*, **24**, 683-686
- ___, and N. Mantua, 1999: Interdecadal modulation of Interannual atmospheric and Oceanic Variability Over the North Pacific. *Prog. In Oceano.*, **43**, 163-192.
- Nakamura, H., 1996: Year-to-year and interdecadal variability in the activity of intraseasonal fluctuations in the Northern Hemisphere wintertime circulation. *Theor. Appl. Climatol.*, **55**, 19-32.
- ___, G. Lin, and T. Yamagata, 1997: Decadal Climate Variability in the North Pacific during the Recent Decades. *Bull. Amer. Meteor. Soc.*, **78**, 2215-2225.
- Namias, J., 1976: Negative ocean-air feedback systems over the North Pacific in the transition from warm to cold seasons. *Mon. Wea. Rev.*, **104**, 1107-1121.
- North, G. R., T. L. Bell, and R. F. Cahalan, 1982: Sampling Errors in the Estimation of Empirical Orthogonal Functions. *Mon. Wea. Rev.*, **110**, 699-706.
- North, G. R., T. L. Bell, and R. F. Cahalan, 1982: Sampling Errors in the Estimation of Empirical Orthogonal Functions. *Mon. Wea. Rev.*, **110**, 699-706.
- Parker, D. E., C. K. Folland, and M. Jackson, 1995: Marine Surface Temperature:

- Observed Variations and Data Requirements. *Climate Change*, **31**, 559-600.
- Rasmusson, E. M., and J. M. Wallace, 1983. Meteorological aspects of the El Niño/Southern Oscillation. *Science*, **222**, 1195-1202.
- Rayner, N.A., E. B. Horton, D. E. Parker, C. K. Folland, and R. B. Hackett, 1996: Versions 2.2 of the Global sea-Ice and Sea Surface Temperature data set, 1903-1994. Available from the Hadley Centre for Climate Prediction and Research, Meteorological Office, London Road, Bracknell, Berkshire RG12 2SY.
- Schneider, N., S. Venzke, A. J. Miller, D. W. Pierce, T. P. Barnett, D. Deser, and M. Latif, 1999: Pacific thermocline bridge revisited. *Geophys. Res. Lett.*, **26**, 1329-1332.
- Servain, J., and D. M. Legler, 1986: Empirical Orthogonal Function Analyses of Tropical Atlantic Sea Surface Temperature and Wind Stress. *J. Geophys. Res.*, **91**, No. C12, 14,181-14,191.
- Sittel, M. C., 1994: Differences in the means of ENSO extremes for maximum Temperature and precipitation in the United States. COAPS Tech. Rep. 94-2, 50 pp. [Available from Center for Ocean-Atmospheric Prediction Studies, The Florida State University, Tallahassee, FL 32306-2840.]
- Smith, S. R., P. M. Green, A. P. Leonardi, and J. J. O'Brien, 1998: Role of Multiple-Level Tropospheric Circulations in Forcing ENSO Winter Precipitation Anomalies. *Mon. Wea. Rev.*, **126**, 3102-3116.
- _____, D. M. Legler, M. J. Remigio, and J. J. O'Brien, 1999: Comparison of 1997-98 U.S. Temperature and Precipitation Anomalies to historical ENSO warm phases. *J. Climate*, **12**, 3507-3515.
- Spiegel, M. R., 1961: Small Sampling Theory. *Theory and Problems of Statistics*, Schaum, 188-200.
- Trenberth, K. E., and J. W. Hurrell, 1994: Decadal atmosphere-ocean variations in the Pacific. *Climate Dyn.*, **9**, 303-319.
- _____, 1997: The Definition of El Niño. *Bull. Amer. Meteor. Soc.*, **78**, 2771-2777.
- Zhang, Y., J. M. Wallace, and D. S. Battisti, 1997: ENSO-like Interdecadal Variability: 1900-93. *J. Climate*, **10**, 1004-1020.

BIOGRAPHICAL SKETCH

Mark Christopher Bove was born on May 25, 1975 in Newburgh, New York. He lived with his parents in Lincoln Park, New Jersey until 1987, when they moved to Cape Coral, Florida. He attended North Fort Myers High School, graduating eighth in a class of 320.

Mark started undergraduate work in Meteorology at The Florida State University in 1993 and finished his Bachelor of Science degree in 1997. During this time, he began work as an undergraduate research assistant at the Center for Ocean-Atmospheric Prediction Studies (COAPS) under the tutelage of Dr. James J. O'Brien. After graduation, Mark continued at Florida State University and COAPS to pursue his Masters degree in the same field.

During his stay at Florida State and COAPS, he has conducted research into ENSO impacts on hurricanes, tornadoes, temperatures, and precipitation. In 1998, Mark received the Father James B. Macelwane award in meteorology for outstanding undergraduate research from the American Meteorological Society, for his research on the influence of ENSO on U.S. tornadic activity.